The Use of Zeolites Synthesized from Fly Ash in Adsorption Chiller

Tarikul Hasan

Thesis to obtain the Master of Science Degree in

Energy Engineering and Management

Supervisors: Dr. Inz. Karol Sztekler
Prof. Moisés Luzia Gonçalves Pinto

Examination Committee

Chairperson: Prof. Francisco Manuel da Silva Lemos

Supervisor: Dr. Inz. Karol Sztekler

Member of the Committee: Prof. Maria Cristina de Carvalho Silva Fernandes

June 2021

Special Acknowledgement

I would like to thank InnoEnergy Master's School for providing me the opportunity to study the MSc program in Energy Transition. It includes MSc in Chemical Technology and Master's in Energy Engineering and Management. InnoEnergy provided financial support as well. I received full tuition fee waiver and monthly financial support from InnoEnergy. I gratefully appreciate it.

Acknowledgement

I would like to start by thanking the Almighty for keeping me in good health and for all other blessings.

I am really grateful to my thesis supervisors **Prof. Dr. Inz. Karol Sztekler** and **Prof. Dr. Moisés Luzia Pinto** for their immense support, precise guidance and encouragement throughout my thesis work.

I am also thankful to **Prof. Dr. Konrad Świerczek** and **Mr. Marcin Sowa** for their technical support.

Special thanks to **Prof. Dr. Fatima Montemor** and **Prof. Dr. Edgar Caetano Fernandes** for their helpful attitude on different occasions.

I also would like to thank **Mrs. Ewa Figorska, Mrs. Rossela Leitao** and **Mrs. Marta Abrantes** for their continuous support from the beginning of the program.

Last but not least, thanks go to my family, teachers, and friends for their immense support throughout the journey.

Abstract

Adsorption chiller can produce cold energy, using the waste heat from the industries and the energy from the sun, thus reducing the energy consumption. A major waste, fly ash, can be converted to zeolite and used in adsorption chiller as adsorbent. In this thesis research, three different types of zeolites were synthesised from fly ash (power plant) via a hydrothermal reaction in an alkaline solution (NaOH). Later the samples (Na-A zeolites) were modified with K_2CO_3 to increase the adsorption capacity of these samples. XRD analysis suggests that desired zeolites formed properly, but other crystalline phases also exist. The determined specific surface area for Na-A zeolite (12 h) and Na-A zeolite (24 h) are 45 m^2/g and 185 m^2/g respectively, while the specific surface area for synthesized 13X zeolite is almost negligible. Water-isotherm for each of these samples had been produced with the data obtained from DVS Vacuum-Surface Measurement System. Equilibrium adsorption at lower pressure steps was almost reached in less than 25 minutes for 13-X zeolite and less than 20 minutes for Na-A zeolites, which is almost similar/better than silica gel and suitable for adsorption refrigeration system. At usual operating conditions for adsorption chiller during adsorption and desorption, available water vapor for evaporation for the synthesized samples is also very low, 1.73% and 1.27% for first and second operating conditions respectively for synthesized 13-X zeolite, whereas no water vapor is available for evaporation for Na-A zeolite (12 h) and Na-A zeolite (24 h). This analysis implies that among the synthesized materials only 13-X zeolite has some potential to produce cold energy in adsorption refrigeration system, but it cannot replace silica gel. Other two samples have no potential to produce any cold energy.

Key Words : Adsorption Chiller, Fly Ash, Zeolite, XRD, Specific Surface Area, Water Adsorption.

Resumo

Refrigeradores de adsorção podem produzir energia fria usando o calor residual de indústrias e a energia do sol, reduzindo assim o consumo de energia. Um desperdício, cinzas volantes, pode ser convertido em zeolitos e usado em refrigeradores de adsorção como adsorvente. Na investigação desta tese, foram sintetizados três tipos diferentes de zeolitos a partir de cinzas volantes (de central elétrica) através de uma reação hidrotermal numa solução alcalina (NaOH). Posteriormente, as amostras (zeólito NaA) foram modificadas com K_2CO_3 para aumentar a sua capacidade de adsorção. A análise por XRD sugere que os zeólitos desejados se formaram corretamente, mas outras fases cristalinas também foram identificadas. A área específica determinada para zeólito NaA (12 h) e zeólito NaA (24 h) são de 45 m^2/g e 185 m^2/g, respetivamente, enquanto a área específica para zeólito 13X sintetizado é quase insignificante. A isotérmica de adsorção de água para cada uma destas amostras foi obtida a partir do sistema de medição DVS Vacuum-surface measurement system. A adsorção de equilíbrio em degraus de pressão mais baixas foi quase alcançada em menos de 25 minutos para zeolite de 13-X e menos de 20 minutos para zeolites Na-A, que é quase semelhante/melhor do que o gel de sílica e adequado para o sistema de refrigeração de adsorção. Nas condições normais de funcionamento do refrigerador, durante a adsorção e a desadsorção, o vapor de água disponível para a evaporação das amostras sintetizadas também é muito baixo, 1,73% e 1,27% para as condições de primeira e segunda operações, respetivamente para o zeólito 13X sintetizado, enquanto que para zeólito NaA (12 h) e zeólito NaA (24 h) não está disponível vapor de água para evaporação. Esta análise implica que entre os materiais sintetizados apenas o zeólito 13X tem algum potencial para produzir energia fria num sistema de refrigeração por adsorção, mas não pode substituir o gel de sílica. As outras duas amostras não têm potencial para produzir energia fria.

Palavra-chave: Refrigerador de adsorção, Cinzas volantes, Zeólito, XRD, Área específica, Adsorção de Água.

Table of Contents

Special acknowledgement.....i
Acknowledgement..... ii
Abstract..... iii
Resumo..... iv
Table of Contents..... v
List of Tables.....ix
List of Figures.....x
List of abbreviation.....xiii
1.0.Introduction 1
1.1. Topic Overview and Motivation of the Work 1
1.2. Objectives 2
2.0. Literature Review and State of Art 3
2.1. Physical Adsorption 3
2.2. Chemical Adsorption 3
2.3. Adsorbent 5
2.3.1. Physical Adsorbents 5
2.3.1.1. Activated Carbon and Activated Carbon Fiber 5
2.3.1.2. Silica Gel 6
2.3.1.3. Zeolite 6
2.3.1.4. Novel Porous Materials 8
2.3.1.5. MOFs 9
2.3.2. Chemical Adsorbent 9
2.3.2.1. Metal Chlorides 9
2.3.2.2. Metal Hydrides 9
2.3.2.3. Salt Hydrates 10
2.3.3. Composite Adsorbents 10
2.4. Adsorption Working Pair 10
2.4.1. Physical Adsorption Refrigeration Working Pair 10
2.4.1.1. Activated Carbon-Methanol 11

2.4.1.2. Activated Carbon-Ammonia 11
2.4.1.3. Silica Gel -Water 11
2.4.1.4. Zeolite -Water 11
2.4.2. Chemical Adsorption Refrigeration Working Pair 11
2.4.2.1. Metal Chloride-Ammonia 12
2.4.2.2. Metal Hydrides–Hydrogen 12
2.4.2.3. Metal Oxides-Water and Metal Oxides-Carbon Dioxide 12
2.4.2.4. Salt Hydrates and Water 12
2.5. Adsorption Theories 13
2.5.1. Equilibrium Adsorption Models 13
2.5.1.1. Equilibrium Models for Physical Adsorption 13
2.5.1.2. Equilibrium Models for Chemical Adsorption 14
2.5.1.3. Adsorption Rate Models 14
2.6. Adsorption Isotherm 15
2.6.1. The Langmuir Model 16
2.6.2. The Freundlich Model 16
2.6.3. BET Model 17
2.6.4. Adsorption Isotherm Types 18
2.7. Hysteresis 20
2.8. Adsorption Refrigeration Process 21
2.8.1. The basic adsorption refrigeration cycle 21
2.8.2. Adsorption Refrigeration Using Solar Energy 23
2.8.3. Adsorption Desalinisation 24
2.9. Coefficient of Performance (COP) 25
2.10. Specific Cooling Power 26
2.11. Previous Research Works 26
2.12. Commercialized Adsorption Chillers 29
3.0. Experimental Methods 30

3.1. Sample Preparation Method 30
3.1.1. Na-A Zeolite (12 h) Preparation 30
3.1.2. Na-A Zeolite (24 h) Preparation 30
3.1.3. 13X Zeolite Preparation 31
3.2. XRD Analysis 31
3.3. Surface Area Analysis 31
3.4. Isotherm Determination 31
3.4.1. DVS Vacuum- Surface Measurement System 31
3.4.1.1. Components of DVS Vacuum- System Measurement System 32
3.4.1.2. Working Procedure of DVS Vacuum- System Measurement System 32
4.0. Results and Discussion 34
4.1. Sample Characterization 34
4.1.1. XRD Analysis 34
4.1.1.1 Na - A Zeolite (12 h) 34
4.1.1.2 Na - A Zeolite (24 h) 35
4.1.1.3. 13X Zeolite 36
4.1.2. Surface Area Analysis 37
4.2. Adsorption Isotherm and Potential Use in Adsorption Chiller 38
4.2.1. Silica Gel 38
Temp: 25 ºC 38
Temp: 35 ºC 39
Temp: 45 ºC 40
Temp: 55 ºC 41
Temp 65 ºC 42
4.2.2. Fly Ash 43
Temp: 25 ºC 43
Temp: 65 ºC 44
4.2.3 Synthesized Na – A Zeolite (12 h) 44

Temp: 25 ºC 44
Temp: 35 ºC 45
Temp: 45 ºC 46
Temp: 55 ºC 47
Temp: 65 º C 48
4.2.4 Synthesized Na-A (24 h) Zeolite 51
Temp: 25 ºC 51
Temp: 35 ºC 52
Temp: 45 ºC 53
Temp: 55 ºC 54
Temp: 65 ºC 55
4.2.5 Synthesized 13-X Zeolite 57
Temp: 25 ºC 57
Temp: 35 ºC 59
Temp: 45 ºC 60
Temp: 55 ºC 61
Temp: 65 ºC 62
5.0. Conclusion 65
Reference 66
Appendix 74

List of Tables

Table-1: Difference between Physical Adsorption and Chemical Adsorption 4

Table-2: Different Properties of Working Pair (Physical) [1,9] 13

Table-3: COP-SCP for Different Adsorption Chiller 26

Table 4: Isotherm Data for Silica Gel (25 ^{o}C) 74

Table 5: Isotherm Data for Silica Gel (35 ^{o}C) 74

Table 6: Isotherm Data for Silica Gel (45 ^{o}C) 74

Table 7: Isotherm Data for Silica Gel (55 ^{o}C) 74

Table 8: Isotherm Data for Silica Gel (65 ^{o}C) 75

Table 9: Isotherm Data for Fly Ash (25 ^{o}C) 75

Table 10: Isotherm Data for Fly Ash (65 ^{o}C) 75

Table 11: Isotherm Data for Synthesized Na-A Zeolite (12 h) (25 ^{o}C) 75

Table 12: Isotherm Data for Synthesized Na-A Zeolite (12 h) (35 ^{o}C) 76

Table 13: Isotherm Data for Synthesized Na-A Zeolite (12 h) (45 ^{o}C) 76

Table 14: Isotherm Data for Synthesized Na-A Zeolite (12 h) (55 ^{o}C) 76

Table 15: Isotherm Data for Synthesized Na-A Zeolite (12 h) (65 ^{o}C) 76

Table 16: Isotherm Data for Synthesized Na-A Zeolite (24 h) (25 ^{o}C) 77

Table 17: Isotherm Data for Synthesized Na-A Zeolite (24 h) (35 ^{o}C) 77

Table 18: Isotherm Data for Synthesized Na-A Zeolite (24 h) (45 ^{o}C) 77

Table 19: Isotherm Data for Synthesized Na-A Zeolite (24 h) (55 ^{o}C) 77

Table 20: Isotherm Data for Synthesized Na-A Zeolite (24 h) (65 ^{o}C) 78

Table 21: Isotherm Data for Synthesized 13-X Zeolite (25 ^{o}C) 78

Table 22: Isotherm Data for Synthesized 13-X Zeolite (35 ^{o}C) 78

Table 23: Isotherm Data for Synthesized 13-X Zeolite (45 ^{o}C) 78

Table 24: Isotherm Data for Synthesized 13-X Zeolite (55 ^{o}C) 79

Table 25: Isotherm Data for Synthesized 13-X Zeolite (65 ^{o}C) 79

List of Figures

Figure-1: Structure of Activated Carbon 5

Figure-2: Silica Gel Structure 6

Figure-3: Tetrahedral arrangement of the SiO_4 and AlO_4 7

Figure-4: A two-dimensional representation of the framework structure of zeolites 7

Figure-5: Framework of Na-A (LTA) and Na-X (FAU) Zeolite 8

Figure-6: Structure of MOF 9

Figure-7: Adsorption curves of strontium chloride–ammonia 14

Figure-8: Langmuir's kinetic model of adsorption 16

Figure-9: Determination of the constant from the logarithmic form of Freundlich isotherm. 17

Figure-10: Schematic of the adsorption of gas molecules onto the surface of a sample showing (a) the monolayer adsorption model assumed by the Langmuir theory and (b) s the multilayer adsorption model assumed by the BET theory. 17

Figure-11: Determination of the constants of the BET adsorption isotherm. 18

Figure-12: Type I Adsorption Isotherm [42] 18

Figure-13: Type II Adsorption Isotherm [42] 19

Figure-14: Type III Adsorption Isotherm [42] 19

Figure-15: Type IV Adsorption Isotherm [42] 20

Figure-16: Type V Adsorption Isotherm [42] 20

Figure-17: Type VI Adsorption Isotherm 20

Figure-18: IUPAC Classification of Hysteresis Loops 21

Figure-19: Basic adsorption cooling system under one complete cycle. 22

Figure-20: Clapeyron diagram of an ideal adsorption refrigeration cycle. 22

Figure-23: The p-T diagram of adsorption refrigeration cycle 24

Figure-24: Two Bed Desalination System 25

Figure-25: DVS Vacuum Schematic 32

Figure-26: XRD Result Comparison, (a) Commercial Na-A Zeolite (b) Synthesized Na-A Zeolite (12 h) 34

Figure-27: XRD Result Comparison, (a) Commercial Na-A Zeolite (b) Synthesized Na-A Zeolite (24 h) 35

Figure-28: XRD Result Comparison, (a) Commercial 13-X Zeolite (b) Synthesized 13-X Zeolite 36
Figure-29: Adsorption Isotherm for Different Samples (at -196 ºC) 37
Figure-30: Adsorption Isotherm for Silica Gel (25 ºC) 38
Figure-31: Adsorption Kinetics for Silica Gel (25 ºC) 38
Figure-32: Adsorption Isotherm for Silica Gel (35 ºC) 39
Figure-33: Adsorption Kinetics for Silica Gel (35 ºC) 39
Figure-34: Adsorption Isotherm for Silica Gel (45 ºC) 40
Figure-35: Adsorption Kinetics for Silica Gel (45 ºC) 40
Figure-36: Adsorption Isotherm for Silica Gel (55 ºC) 41
Figure-37: Adsorption Kinetics for Silica Gel (55 ºC) 41
Figure-38: Adsorption Isotherm for Silica Gel (65 ºC) 42
Figure-39: Adsorption Kinetics for Silica Gel (65 ºC) 42
Figure-40: Adsorption Isotherm at Different Temperatures 43
Figure–41 : Adsorption Isotherm for Fly Ash (25 ºC) 43
Figure-42: Adsorption Isotherm for Fly Ash (65 ºC) 44
Figure-45: Adsorption Isotherm for Synthesized Na -A Zeolite (12 h) (35 ºC) 45
Figure-46: Adsorption Kinetics for Synthesized Na -A Zeolite (12 h) (35 ºC) 45
Figure-47: Adsorption Isotherm for Synthesized Na -A Zeolite (12 h) (45 ºC) 46
Figure-48: Adsorption Kinetics for Synthesized Na -A Zeolite (12 h) (45 ºC) 46
Figure-49: Adsorption Isotherm for Synthesized Na -A Zeolite (12 h) (55 ºC) 47
Figure-50: Adsorption Kinetics for Synthesized Na -A Zeolite (12 h) (55 ºC) 47
Figure-51: Adsorption Isotherm for Synthesized Na -A Zeolite (12 h) (65 ºC) 48
Figure-52: Adsorption Kinetics for Synthesized Na -A Zeolite (12 h) (65 ºC) 48
Figure-53: Adsorption Isotherm at Different Temperature (Synthesized Na-A Zeolite 12 h) 49
Figure-54: Adsorption Isotherm at 25 ºC (Commercial Na-A Zeolite) 49
Figure-55: Adsorption Isotherm for Synthesized Na -A Zeolite (24 h) (25 ºC) 51
Figure-56: Adsorption Kinetics for Synthesized Na -A Zeolite (24 h) (25 ºC) 51
Figure-57: Adsorption Isotherm for Synthesized Na -A Zeolite (24 h) (35 ºC) 52

Figure-58: Adsorption Kinetics for Synthesized Na -A Zeolite (24 h) (35 ºC)..... 52
Figure-59: Adsorption Isotherm for Synthesized Na -A Zeolite (24 h) (45 ºC)..... 53
Figure-60: Adsorption Kinetics for Synthesized Na -A Zeolite (24 h) (45 ºC)..... 53
Figure-61: Adsorption Isotherm for Synthesized Na -A Zeolite (24 h) (55 ºC)..... 54
Figure-62: Adsorption Kinetics for Synthesized Na -A Zeolite (24 h) (55 ºC)..... 54
Figure-63: Adsorption Isotherm for Synthesized Na -A Zeolite (24 h) (65 ºC)..... 55
Figure-64: Adsorption Kinetics for Synthesized Na -A Zeolite (24 h) (65 ºC)..... 55
Figure-65: Adsorption Isotherm at Different Temperature (Synthesized Na-A Zeolite 24 h) 56
Figure-66: Adsorption Isotherm for Synthesized 13-X Zeolite (25 ºC)..... 57
Figure-67: Adsorption Kinetics for Synthesized 13-X Zeolite (25 ºC)..... 58
Figure-68: Adsorption Isotherm for Synthesized 13-X Zeolite (35 ºC)..... 59
Figure-69: Adsorption Kinetics for Synthesized 13-X Zeolite (35 ºC)..... 59
Figure-70: Adsorption Isotherm for Synthesized 13-X Zeolite (45 ºC)..... 60
Figure-71: Adsorption Kinetics for Synthesized 13-X Zeolite (45 ºC)..... 60
Figure-72: Adsorption Isotherm for Synthesized 13-X Zeolite (55 ºC)..... 61
Figure-73: Adsorption kinetics for Synthesized 13-X Zeolite (55 ºC)..... 61
Figure-74: Adsorption Isotherm for Synthesized 13-X Zeolite (65 ºC)..... 62
Figure-75: Adsorption Kinetics for Synthesized 13-X Zeolite (65 ºC)..... 62
Figure-76: Adsorption Isotherm at Different Temperature (Synthesized 13-X Zeolite) 63
Figure-77: Adsorption Isotherm at 25 ºC Temperature (Commercial 13-X Zeolite)..... 63
Figure-78: Adsorption Isotherm for Synthesized 13-X Zeolite (25 ºC)..... 80
Figure-79: Adsorption Kinetics for Synthesized 13-X Zeolite (25 ºC)..... 80

List of abbreviation

CFA: Coal Fly Ash

CFC: Chlorofluorocarbon

COP: Coefficient of Performance

HCFC: Hydrochlorofluorocarbons

RH: Relative Humidity

SCP: Specific Cooling Power

1.0. Introduction

1.1. Topic Overview and Motivation of the Work

Modern civilization is driven by energy. The development and application of the latest technologies largely depend on energy. The main sources of this energy are fossil fuels such as Natural Gas, Oil and Coal. There are two main problems associated with the consumption of fossil fuels. The first one is the scarcity of these sources. They are running out fast. Secondly, the consumption of fossil fuels is the main reason for some of the greatest problems associated with the environment we have ever faced. Because burning of fossil fuels releases CO_2, NO_x, SO_2, N_2O etc. Moreover, the demand for energy is increasing day by day. That is why we are required to develop sustainable energy systems.

The demand for cold energy is also on the rise. The common refrigeration systems are usually driven by electricity. Large amount of this produced electricity is used for indoor cooling. Between 2003 and 2004, the electricity used for air conditioning in USA constituted 15.4% of total electricity consumption. In Shanghai city, China, the electricity used for air conditioning constituted 45 to 56% of total electricity consumption in summer 2010[1]. In the year of 2019, 8.5% of total generated electricity was used for indoor cooling. Energy demand for this purpose has increased more than three times from 1990 [2]. It just shows, how fast the demand for indoor cooling is growing. This demand for will grow in future. It has been projected that number of AC units will increase to 5600 million in 2050 from almost 1600 million in 2016, with significant increases in countries like China and India [3]. So, electricity consumption will also increase for the purpose of indoor cooling. This electricity mainly comes from fossil fuels. In the year 2018, coal, natural gas and oil constituted 39%, 26% and 3% of total electricity generation [4]. Also, electricity production has low efficiency, around 40-50% and the temperature of the waste heat ranges between 70-200 °C [1]. It ultimately affects the environment. Furthermore, CFC, which was used for refrigeration, caused significant damage to ozonosphere which stops dangerous ultraviolet rays coming from sun. HCFC is only a temporary alternative because it also has some greenhouse effect and causes damage to ozonosphere[1].

Another major problem the world is currently facing is the scarcity of drinking water. We have a large source of saline water, but they cannot be used for drinking and most of the other purposes. There are many ways to desalinate the saline water, such as multi-effect desalination, multi-stage flash desalination, membrane-based reverse osmosis [5]. These systems are very energy consuming and they also contribute to carbon emission. The reverse osmosis system requires 10-13-kilowatt hours (kwh) electricity per every thousand gallons [6]. Water desalination is a major energy consumer in many parts of the world. In 2016, 5% of Middle East's total energy consumption was for water desalination for supplying 3% of their water consumption [7]. From 2010 to 2016, world's total water desalination capacity has increased by 9% each year [8]. This process is also very costly. The cost is 0.647 USD/m^3 for multi-stage flash desalination, 0.520 USD/m^3 for multi-effect desalination, 0.366-0.403 USD/m^3 for reverse osmosis desalination and 0.067 USD/m^3 (the lowest) for adsorption desalination [5].

We have solar energy and geothermal energy in the environment and waste energy, coming from the industries with low to very low temperature ranges. Adsorption chiller can be used to utilize these small temperature range heats. There are existing sorption refrigeration and heat pump technologies which can be run with such low-grade heat, and they also use environment friendly refrigerants [1]. Adsorption refrigeration technologies can use different adsorbents which can be operated with low grade heat, such as zeolite-water pair works in the range of

70–250 °C, silica gel-water pair works in the range of 55–120 °C, activated carbon-methanol pair works up to 120 °C temperature and activated carbon-ammonia pair works usually up to 150 °C temperature (can be used even for 200 °C or more) [1,9]. The commonly used refrigerants are water, ammonia, methanol etc. They are called green refrigerants because of having no ODP (ozonosphere depletion potential) and GWP (greenhouse warming potential). Also, adsorption refrigeration system has some other advantages e.g. this equipment does not include solution pump and rectification equipment. Besides, solution crystallization is absent for such system. But there are some drawbacks as well. Adsorption refrigeration is not as efficient as absorption refrigeration and the volume of this system is also large [1].

Silica gel-water adsorption chiller has been marketed successfully. But there is still a lot of space for improvement in adsorption refrigeration system. Focus should be given on the facts that can improve the performance of the adsorption refrigeration technology such as adsorption working pairs and their working mechanism, structure and design of adsorption refrigeration device, improvement of heat and mass transfer of the adsorption/regeneration bed etc [1].

The performance of the adsorption chiller largely depends on the performance of the adsorption and desorption of the adsorbent, means the amount of adsorbed refrigerant, time required to reach equilibrium, the temperature of adsorption and desorption, heat of adsorption and desorption, heat and mass transfer of the adsorber bed etc [1]. The purposes of this thesis research include the systhesis of Na-A and 13X zeolite from fly ash and analyse the potential application of these adsorbents compared to the performance of silica gel with regard to adsorption chiller.

1.2. Objectives

a. Synthesis of zeolite from fly ash by a hydrothermal reaction process and modification with K_2CO_3.
b. Characterization of the source material, silica gel and the synthesised materials, such as specific area measurement and XRD analysis.
c. Determination of adsorption isotherm and adsorption kinetics of the samples in DVS Vacuum- Surface Measurement System.
d. Performance analysis of the synthesised materials in regard of adsorption chiller with comparison to silica gel.

2.0. Literature Review and State of Art

The surface of a solid material is usually characterized by the uneven distribution of energy. Therefore, if any adsorbate (gas, vapor or liquid) comes in close contact with the surface of any adsorbent (solid or liquid), it usually gets attracted and sticks to the surface of the adsorbent[10]. This phenomenon is called adsorption. In other words, **Adsorption** can be defined as the adhesion of molecules of gas, vapor or liquid on the external surface or internal surface of the solid or the surface of the liquid. The internal surface of the solid includes the walls of the capillaries or crevices[11]. Adsorption is an exothermic process, means, when any adsorbate molecule is adsorbed on the surface of the adsorbent, it releases heat [12]. The application of adsorption includes air pollution mask, water treatment, separation of noble gases, removal of moisture and humidity, adsorption chromatography, adsorption chiller etc[13]. The reverse process of adsorption is desorption, which is naturally an endothermic process. For this process, heat is required to be applied in the adsorber bed of an adsorption chiller [10,12]. There are two types of adsorptions, namely Physical Adsorption (Physisorption) and Chemical Adsorption (Chemisorption) [12].

2.1. Physical Adsorption

Physical adsorption occurs due to the van der walls bond between the adsorbent surface and the adsorbate. Physical adsorption largely depends on the inter-molecular force between the molecules of the adsorbent and the adsorbate, and between the molecules of the adsorbate. When the former is higher, adsorption takes place [12]. Physical adsorption first forms a monolayer and can form multi-layer later[12]. Physically adsorbed molecules are not bound to any specific location. Therefore, the adsorbed molecules can diffuse along the surface of the adsorbent. The van der walls bond is very weak, and the released energy does not exceed 80kj/mole. For this reason, physical adsorption is easily reversable [10]. This enables the use of low temperature heat in adsorption chiller. Both, physical adsorption and condensation of vapor are exothermic process. The heat released during the condensation of vapor is almost similar to the heat released during physical adsorption. Therefore, often physical adsorption is considered similar to condensation. During physisorption, no bonds are broken or formed. So, new type of molecules is not formed and during desorption, the adsorbed molecules do not get decomposed [1]. The performance of physical adsorption is significantly controlled by the mass transfer and heat transfer performance of the adsorbents. During the desorption process, if the pressure is very high, the rate of mass transfer will be also high because mass transfer is favoured by high pressure. When the mass transfer rate of the system is high, adsorption/desorption performance will be dictated by heat transfer performance of the system and, if the heat transfer is intensified, adsorbent's permeability becomes the main influencing factor. Usually, the adsorbents with small size grains possess better permeability [1]. The most commonly used refrigerants in adsorption refrigeration systems are some polar compounds such as ammonia, methanol and hydrocarbon, paired with adsorbents like activated carbon, silica gel and zeolite, working under the phenomenon of physisorption via the intermolecular adhesive force. For physisorption the cycle adsorption quantity is reasonably lower compared to chemisorption, usually varies between 10-20% [1].

2.2. Chemical Adsorption

In contrast to physical adsorption, the chemical adsorption occurs due to the formation of chemical bond between the adsorbate and adsorbent creating monolayer. The chemical bond can be both, covalent bond and ionic bond, suggesting that during chemisorption transfer or sharing of electron, or breakage of the adsorbate into atoms or radicals happen and such activities result into formation of new type of molecules. The formed bond in chemisorption is much stronger than the van der walls bond and the released heat is much higher than physisorption

[1,12]. Due to this reason, it requires much more energy to reverse the chemisorption [1, 10]. When heat is applied during the decomposition process, disassociation of the newly formed molecules (in the adsorption phase) occurs[1]. Chemisorption occurs only between specific adsorbent and adsorbates. For example, metals like W, Pt, and Ni can adsorb hydrogen (H_2), but some other metals like Cu, Ag, and Zn cannot do the same[1]. For any adsorbate to be chemically adsorbed, the adsorbate molecules have to be in direct contact with the surface of the adsorbent. This is the reason for which chemisorption is a mono-layer process. If the already adsorbed molecules are removed from the active surfaces, more adsorbate molecules adsorbed in case of chemical adsorption[10]. Along with the mass transfer and heat transfer performance, chemical adsorption is also influenced by the chemical reaction process and the reaction kinetic of the molecules [1]. Adsorption hysteresis also exists when chemical adsorption occurs. It happens because the activation energy for desorption is much higher than the activation energy of adsorption. Desorption activation energy includes the adsorption activation energy and the adsorption heat. It causes the adsorption and desorption to follow different path and results into significant hysteresis[1]. For chemisorption, the adsorption quantity per cycle is much higher than physisorption. For example, the cycle adsorption quantity for $CaCl_2$ is always larger than 0.4. This is one of the biggest advantages of chemical adsorption refrigeration system that significantly improves the specific cooling capacity per kilogram of adsorbent. But this system also brings some disadvantages, e.g. expansion and agglomeration occur in chemical adsorption, resulting into the requirement for much higher expansion space, almost the double of the size of the adsorbent [1]. Physical and chemical adsorption can occur at the same time. The chemisorbed layer can attract the adsorbate molecules due to inter molecular force, causing physisorption. Also, same surface can display physisorption and chemisorption e.g. liquid nitrogen is physically adsorbed on iron at 77 K but at 800 K, nitrogen forms iron nitride [10]. The effective distance of the van der Waals force (inversely proportional to distance at power of 7) is much longer than the effective distance for the chemical reaction. Therefore, physical adsorption takes place before chemical adsorption [1].

To improve the heat and mass transfer of the adsorber bed and increase the adsorption capacity, composite adsorbents are developed by combining physical and chemical adsorbents. Physical adsorbent has better heat and mass transfer characteristics and chemical adsorbent has much higher adsorption capacity. Therefore, the composite adsorbents have reasonable permeability and improved adsorption capacity[1].

Table-1: Difference between Physical Adsorption and Chemical Adsorption

Physical Adsorption	Chemical Adsorption
1. Physical adsorption occurs due to week van der walls force.	1. Chemical adsorption occurs due to ionic bond and covalent bond.
2. It can form in, both, monolayer and multilayer.	2. It only forms in monolayer.
3. It releases very low heat energy.	3. It releases very high heat energy.
4. It is easily reversible.	4. It is not easily reversible.
5. During physisorption, new molecules are not formed.	5. During chemisorption, new molecules are formed.
6. It is only affected by heat and mass transfer.	6. Along with heat and mass transfer, it is also affected by chemical reaction process and reaction kinetics.
7. Hysteresis mainly occurs due to capillary condensation.	7. Hysteresis occurs due to excessive release of heat during adsorption.

2.3. Adsorbent

2.3.1. Physical Adsorbents

Some of the common physical adsorbents are activated carbon, activated carbon fiber, silica gel, and zeolite [1].

2.3.1.1. Activated Carbon and Activated Carbon Fiber

Activated carbon is made by physically or chemically treating different carbon containing substances including wood, peat, coal, fossil oil, coconut shell etc. The structure includes six element carbo-atomic ring in microcrystals of 2.3 × 0.9 nm size. The specific surface area ranges from 500 to 1500 m^2/g [1].

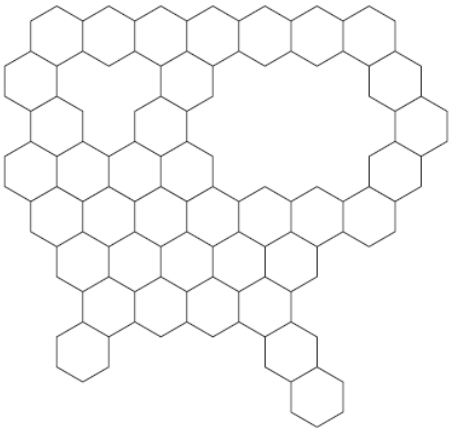

Figure-1: Structure of Activated Carbon [1]

The activated carbon obtained from petroleum residue or charred coal has small micro pores, large specific surface area and high density, while activated carbon is characterized by large micropores, small surface area and low density when produced from brown coal [1]. The functional group affects the adsorption performance of the activated carbon. There are many surface groups including Arene, Sulfonic, Hydroxyl, Carboxyl etc [1] [14]. The hydroxyl group can increase the water adsorption capacity by forming hydrogen bond with polar compounds. The arene group also increases the adsorption capacity, but the sulfonic group decreases it [1]. The arenes are basically aromatic hydrocarbons which can engage in the van der walls forces with water [15]. The acidic functional group will increase adsorption selectivity. Activated carbon contains oxide matrix and some inorganic materials on its surface. Therefore, it is non-polar or has a weak polarity, which causes a low desorption heat[1]. To improve the performance of the adsorbent and obtain desired composition and activity, activation is done by different methods, such as physical, chemical and electrochemical methods. For example, when carbon is oxidized in the gas phase, hydroxyl and carbonyl surface groups are increased, while oxidation is done in the liquid phase, carboxylic acids get increased [14, 16].

Activated carbon fiber (ACF) is a microporous material with fibrous structure. It can be manufactured from synthetic carbon fiber (CF) in commercial scale[17]. Compared to granular activated carbon, activated carbon fiber has better heat and mass transfer performance, larger specific surface area, more uniform pores. Moreover, it can adsorb 2-3 times more per cycle and obtain 10-20% more COP. But there are some problems associated with it, such as anisotropic thermal conductivity, larger contact thermal resistance and lower density [1].

2.3.1.2. Silica Gel

Silica gel is composed by hydrated SiO_4, forming a rigid structure [1]. Silica gel contains hydroxyl group. It improves the adsorption performance of silica gel because the hydroxyl group is polar in nature. Therefore, silica gel can engage in hydrogen bonds with polar oxides, such as water and alcohol and with increasing polarity, the adsorption ability also increases [1,19]. This structure with hydroxyl group is called silanol. Silica gel includes Vicinal Silanol, Geminal Silanol, Siloxane bridge etc [18, 19].

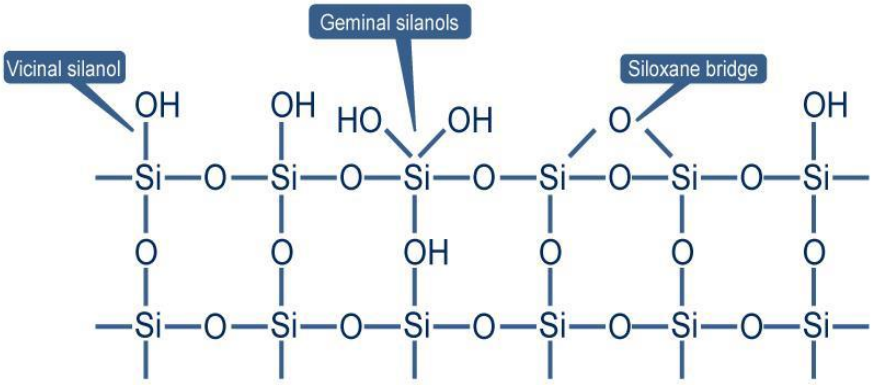

Figure-2: Silica Gel Structure [19]

When silicic acid goes under the process of condensation polymerisation, silica gel is formed. The silanol group is also formed during this process. There are two forms of the silanol group mainly, such as free silanol and hydrogen bonded silanol. These groups can be modified in numerous ways so that silica gel can be used in separation and other purposes [20]. Each type of silica gel contains one type of pore with various diameters, such 2 nm to 3 nm (A type), and 0.7 nm (B type). The specific surface area is about 100-1000 m^2 /g. Silica gel is used as desiccant as its water adsorption capacity is high due to the presence hydroxyl group. Type A silica gel could be used for all desiccation conditions, but for using B silica gel, more than 50% relative humidity (RH) is required [1].

2.3.1.3. Zeolite

Zeolite is a microporous material that contains aluminium, silicon, and oxygen in its main three-dimensional, crystalline structure and also carries cations and water [21]. The chemical formula of zeolite is as follows [1].

$M_{y/n}[(AlO_2)_y(SiO_2)_m]_zH_2O$

Here, y and m are all integers and m/y is equal to or larger than 1. n is the chemical valence of the positive ion, M and z is the number of water molecules inside a crystal cell unit [1]. The water contained in pores and cavities in the structural composition of zeolites is removed upon the application of heat [22]. The porosity ranges between 0.2 to 0.5. There are 40 types of natural zeolite and 150 types of artificially synthesized zeolite [1]. Most of the natural zeolites are obtained from volcanic eruption [22]. Synthesized zeolites are better than natural ones in various ways, such as they have higher specific weight and better heat transfer efficiency. But synthesized zeolites are costlier compared to natural zeolite[1].

In the tetrahedral structure, zeolite includes silicon cations (Si^{4+}) and aluminium cations (Al^{3+}). These ions are bonded with four oxygen anions (O^{2-}). Thus, oxygen ions connect the tetrahedrons. The ratio of Si:O is 1:2 [22].

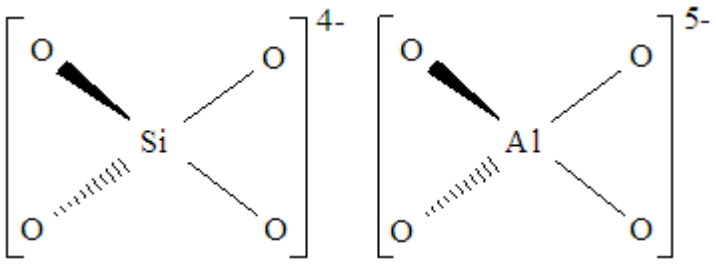

Figure-3: Tetrahedral arrangement of the SiO_4 and AlO_4 [22]

A negative charge is generated in the tetrahedron due to the fact that some Si^{4+} ions are substituted by Al^{3+} ions. Aluminium tetrahedron has the valency of -5 and silicon tetrahedron has a valency of -4, which causes the negative charge in the zeolite structure and to balance the negative charge, zeolite contains different cations, such as alkaline or alkaline earth metals, Na^+, K^+ or Ca^{2+} in most cases. Sometimes Li^+, Mg^{2+}, Sr^{2+} and Ba^{2+} are also found in some zeolites. These cations form weaker electrostatic bonds and connected to the surface of zeolite but do not attend in the main structure [22]. The water adsorption capacity increases with decreasing Si/Al ratio. The pore size of zeolite greatly influence which kind of molecules will be adsorbed (based on the size of the molecules). Zeolite has good thermal stability, but it can be destroyed at temperatures higher than 600–700 °C [1].

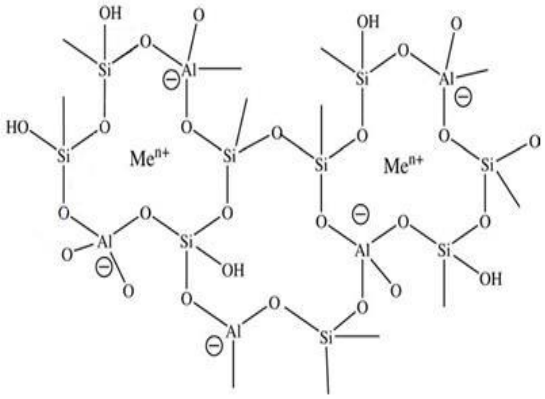

Figure-4: A two-dimensional representation of the framework structure of zeolites [22, 85]

Na-A zeolite is one of the aluminosilicate molecular sieves with a Si/Al ratio is 1, also known as Linde Type A. The chemical formula of this zeolite is $|(Na^{+}_{12}(H_2O)_{27}|8[Al_{12}Si_{12}O_{48}]_8$ [23]. The framework includes β-cages (SOD) and α-cages (supercages). Four-membered rings (D4R) link the β-cages with each other and form an inner cavity [24]. The diameter of the super cage is 11.4 Å and the aperture size is 4.1 Å. The Na^+ ion can be replaced with K^+, reducing the pore opening and replaced by Ca^{2+}, increasing the pore opening [23]. It can be used as desiccant, catalysis and also in detergents [23,25].

Na-X zeolite is also a type of aluminosilicate molecular sieve with Si/Al ratio that varies from 1 to 1.5. It has faujasite-type (FAU) structure that has chemical formula of $|(Ca, Mg, Na_2)_{29}(H_2O)_{240}|[Al_{58}Si_{134}O_{384}]$ [26]. The framework includes β-cages (SOD) and α-cages (supercages). Double six-membered rings (D6R) link the β-cages with each other and form an inner cavity [24]. The diameter of super cage is 13 Å and the aperture size is 8 Å [24, 26]. There are several uses of FAU type zeolites, such as ion exchangers, adsorbents or catalysts in chemical, oil

refining, natural gas purification from sulphur compounds, drying oils and gases, separation of hydrocarbon mixtures, sorption of radio nuclides etc [27].

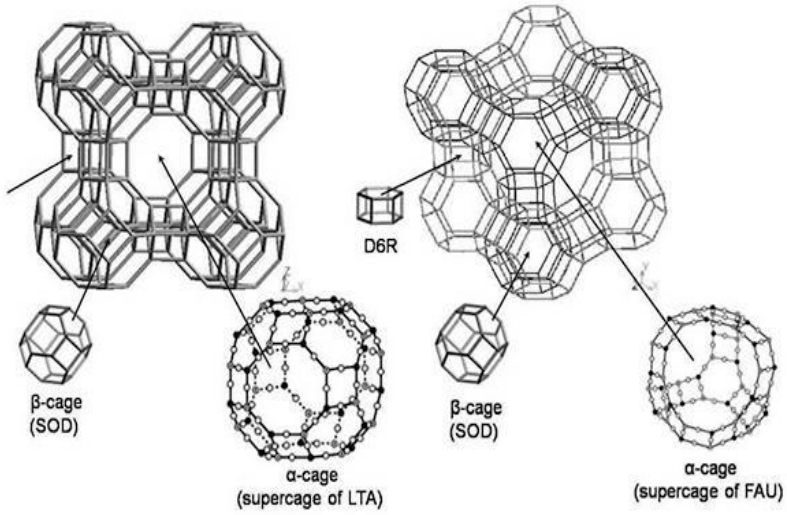

Figure-5: Framework of Na-A (LTA) and Na-X (FAU) Zeolite [24, 86, 87]

Both Na-A zeolite and Na-X zeolite can be synthesised from coal fly ash (CFA) which is obtained from coal fired power plant. CFA mainly includes SiO_2 and Al_2O_3 in its composition which are very stable. They can be used as precursor of Si and Al for zeolite synthesis [28]. For the synthesis of zeolite, they are treated with NaOH or KOH at high temperature. NaOH or KOH can be replaced with Na_2CO_3 as it is less expensive but requires higher temperature (800 °C). This causes the generation of sodium aluminium silicate ($NaAlSiO_4$) and sodium silicate (Na_2SiO_3) [28]. If we want to synthesise Na-X zeolite, we can follow the same procedure. But, in this case we might need to add some external source of silicon or reduce aluminium content to increase the Si/Al ratio [29].

2.3.1.4. Novel Porous Materials

Several novel porous materials such as aluminophosphates (AlPOs), silico-aluminophosphates (SAPOs), and metal organic frameworks (MOFs), can be used for adsorption refrigeration [1].

The AlPOs and SAPOs material sieves are often termed as “zeo-type materials” because they have similar framework, pore system and working mechanism. But they have narrower range of P/Al ratio compared to Si/Al ratio. They exhibit higher attraction to water than silica gel but less than zeolite. This affinity to water results from the difference in electronegativity between Aluminium and Phosphorus [1].

The chemical composition of AIPO is $xRA \cdot Al_2O_3 \cdot 1.0 \pm 0.2P_2O_5 \cdot yH_2O$ [1].

Here RA is an amine or quaternary ammonium ion. The average of the ionic radius of Al^{3+} (0.39Å) and P^{5+} (0.17Å) is 0.28Å, almost similar to the ionic radius of Si^{4+} (0.26Å). This causes the narrower range of chemical composition (P/Al ratio) in this material. The pore volume for AIPO ranges between 0.05 – 0.35 m^3/g with excellent thermal stability. Different metals can be substituted with P to obtain desired structure and adsorption properties of aluminosilicates. When the phosphorous is substituted silicon in the structure of AIPOs, SAPOs materials are formed (Si inserted instead of P) [1].

2.3.1.5. MOFs

MOFs (Metal Organic Framework) are not purely inorganic, but a hybrid of organic-inorganic crystalline porous structure [30]. It has a cage structure which contains a regular array of positively charged metal ions which are linked by organic linkers, resulting in large surface area (7800 square meters per gram)[30]. The organic ligands (linker) are at least bidentic ligands[1].

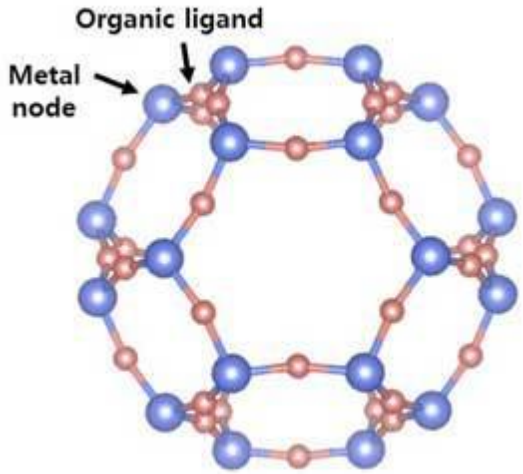

Figure-6: Structure of MOF [30]

It has large pore volume, and a huge geometric, chemical, and physicochemical diversity [1, 30]. The shape and chemical composition can be tailored according to the need and used for different purposes, such as H_2 and CH_4 storage and CO_2 capture [1,31]. But MOFs have stability issues in presence of water because it can displace the bound ligand, leading to the collapse of the MOF structure and also block the binding sites [31]. HKUST-1 (3D-{$[Cu_3(btc)_2(H_2O)_3]\cdot\sim 10H_2O$}s(btc=benzene-1, 3, 5-tricarboxylate)) is one of the first three 3D MOFs [1].

2.3.2. Chemical Adsorbent

Chemical adsorbents mainly include metal chlorides, metal hydrides, metal oxides and salt hydrates [1].

2.3.2.1. Metal Chlorides

Calcium chloride, strontium chloride, magnesium chloride, barium chloride etc are the most commonly used metal chloride for adsorption refrigeration. These metal chlorides form coordinated compound via complexation reaction. Different coordinated compound is formed if the elements are from different position the periodic system. In complexation reaction, the central atom provides the free hybrid orbit to incorporate lone pairs of electrons that causes the formation of bond between the central atom and the ligand. Such refrigeration system uses ammonia as refrigerant. Heat and mass tranfer performance are reduced by swelling and agglomeration that happen during the reaction [1].

2.3.2.2. Metal Hydrides

Reacting with IA and IIA subgroups, hydrogen can form compounds like LiH, CaH_2 etc. Metal hydrides have low electronegativity and high chemical activity. During the formation of metal hydride, hydrogen enters the crystal lattice of the parent metal and reacts with transitional metals. Both, salt and metal hydride are used for adsorption refrigeration [1].

2.3.2.3. Salt Hydrates

By interacting with water, inorganic salts can form hydrates. The salt hydrates can be in two different forms. Water molecules can be bound with the metal at the center of the salt or it can become integral part of the crystal at a certain ratio[1].

2.3.3. Composite Adsorbents

Both physical adsorbents and chemical adsorbents have respective problems. For physical adsorbents, the main problem is that the adsorption quantity is low. For chemical adsorbents, as mentioned earlier, they face the problem of swelling and agglomeration which ultimately affect the heat and mass transfer [1]. To address these issues, the composite adsorbents have been introduced.

Expanded graphite or activated carbon are combined with chemical adsorbents to form the composite adsorbent. The resultant adsorbents have better porous structure and thermal conductivity with higher adsorption capacity. Thus, it solves the problem for chemical adsorbents and physical adsorbent [1].

The methods for producing composite adsorbents are mainly as follows:

1. Simple Mixture [1]: The chemical adsorbents and the additives (physical adsorbents) are mixed at certain ratio by volume or mass.

2. Impregnation [1]: This method starts with dissolving the chemical adsorbent in water or any other suitable solvent. Then the additives are merged into the solution made in the previous step, followed by drying it up to remove the solvent. The chemical adsorbents and the additives used, largely affect the properties of the composite adsorbent. For example, if the carbon fiber is used as additive, the resultant adsorbent has good thermal conductivity in longitudinal direction, although the radial direction has low thermal conductivity. Also, such adsorbent has high contact resistance that affects the heat transfer.

3. Mixture or impregnation and consolidation [1]: For this kind of adsorbent, first composite adsorbent is produced by mixture or impregnation method and then, it is powdered. The powder is compressed for consolidation. Another way is that first the additive or physical adsorbent is compressed and then, impregnated with chemical adsorbent solution, followed by posterior drying to remove the solvent. Adsorbents prepared in such ways have high thermal conductivity in the direction perpendicular to compression.

2.4. Adsorption Working Pair

Adsorption working pair is the most important part of an adsorption refrigeration system. The thermal properties of the working pairs affect some of the most important factors of the adsorption refrigeration cycle such as the performance coefficient of the system, temperature increment velocity of the absorber and the initial investment. If the adsorption working pair is properly selected based on available heat source temperature and proper adsorption refrigeration cycle, adsorption refrigeration performs efficiently. To select a proper refrigerant, some important factors should be kept in mind, such as latent heat of vaporization, thermal stability, non-flammability, non-toxic nature, environmental feasibility and saturation pressure (at working temperatures of the refrigeration system)[1].

2.4.1. Physical Adsorption Refrigeration Working Pair

For physical adsorption refrigeration system, the most commonly used adsorption working pairs are activated carbon-methanol, activated carbon fibre-methanol, activated carbon-ammonia, zeolite-water, silica gel-water and for chemical adsorption refrigeration system, the most common adsorption working pairs are metal hydrides-hydrogen, calcium chloride-ammonia, and strontium chloride-ammonia and so on [1].

2.4.1.1. Activated Carbon-Methanol

Activated carbon can adsorb and desorb methanol at large amount. The regeneration temperature cannot exceed 120 ^{o}C because at higher temperature methanol gets decomposed [1,9]. The heat of adsorption varies between 1800 to 2000 kj/kg [1]. All these factors are advantageous for adsorption refrigeration system and results into good coefficient of performance (COP). For methanol, the latent heat of vaporization is 1102 kj/kg and the freezing temperature is less than 0 ^{o}C. [1,9]. Therefore, this working pair can be used for ice making adsorption refrigeration system. This working pair can also be used to harness the solar energy. The working pressure of such system is less than the atmospheric, that makes the design of this system more sensitive [1].

2.4.1.2. Activated Carbon-Ammonia

Compared to previous working pair, activated carbon-ammonia has some advantages, such as it can work in higher temperature because ammonia is less sensitive temperature change and the working pressure is also high, providing more flexibility to system design and better mass transfer with improved cycle time [1]. This working pair usually works within 150 °C [9]. This working pair can also be used at 200 °C or above [1]. The heat of adsorption is 2000 – 2700 kJ/kg. For ammonia, the latent heat of vaporization is 1368 kJ/kg [9]. But it has several disadvantages as well. The adsorption-desorption quantity for this working pair is low, the refrigerant is toxic, and it has a pungent odour [1].

For both of these working pairs (Activated Carbon-Methanol and Activated Carbon-Ammonia), the molecules of the refrigerants reach the micro pores via a network of large pores and get adsorbed there [1].

2.4.1.3. Silica Gel -Water

As previously mentioned, silica gel has hydroxyl (OH) group. It can form hydrogen bond with water as it is a polar compound, although the adsorption quantity is very low, 0.2kg/kg.. With increasing concentration of Si-OH, the hydrogen bond becomes the main adsorbing force and water adsorption increases as a result. The adsorbent, silica gel, gets decomposed at higher temperature and therefore, cannot be used at temperature higher than 120 ^{o}C. Previous experimental analysis established that the operating temperature can be as low as 55 °C, that makes this working pair suitable for solar energy [1]. For water, the latent heat of vaporization is 2258 kJ/kg, which is good for adsorption refrigeration [9]. Heat of adsorption is very high, around 2500 kj/kg [1].

2.4.1.4. Zeolite -Water

Zeolite is a suitable adsorbent for water, and it increases with decreasing Si/Al ratio. Zeolite-water working pair can be used for several cooling systems, such as dehumidification cooling system and adsorption refrigeration system [1]. Both zeolite and water have good thermal stability and it can work in high temperature, varying from 70 to 250 °C [1,9]. As the heat of vaporization for water is high, it is good for COP [9]. Other the other hand, the heat of adsorption for this working pair ranges between 3200–4200 kJ/kg which can cause lower COP. Another disadvantage of this system that it cannot be used for ice making because evaporation temperature is higher than 0 ^{o}C [1].

2.4.2. Chemical Adsorption Refrigeration Working Pair

Some of the most common chemical adsorption refrigeration working pairs are metal chloride-ammonia, metal hydride-hydrogen, metal oxide-water, metal oxide-carbon dioxide, salt hydrates etc. They are characterized with high adsorption capacity, high desorption temperature, high heat of adsorption and hysteresis [1].

2.4.2.1. Metal Chloride-Ammonia

Like other chemical adsorption refrigeration working pairs, metal chloride-ammonia working pair has high adsorption quantity per cycle. The calcium chloride-ammonia working pair can be used as an example to substantiate this claim. One mol of calcium chloride can adsorb 8 mol of ammonia [1]. It has several advantages, such as the working pressure is greater than the pressure of the surrounding environment, making the system simpler and the boiling temperature of the refrigerant is lower than -34 °C, therefore, it can be used for ice making. But it has issues like agglomeration and expansion [1]. The reaction between $CaCl_2$ and ammonia can be written as follows:

$$CaCl_2 \cdot n_1NH_3 + n_2\Delta Hr \leftrightarrow CaCl_2 \cdot (n_1 - n_2)NH_3 + n_2NH_3$$

Here ΔHr is the reaction enthalpy, (J/mol), the numbers of n_1 and n_2 could be 2, 4, and 8 [1].

2.4.2.2. Metal Hydrides–Hydrogen

Usually adsorbent-refrigerant working pairs take the approach of adsorption-desorption, but metal hydrides–hydrogen working pair functions unusually, taking the path of resorption-desorption. Several metals can form hydrides, such as Ni, Fe, La, and Al. As a usual pattern of chemical adsorption, heat of adsorption is very high and per cycle adsorption quantity is also higher [1]. The reaction process is as follows:

$$M(s) + n/2H_2(g) \rightarrow MHn(s)$$

This working pair has several advantages, such as it works in a wide range of temperature, varies from -100 to 500 °C and the volume of this system is very low. The disadvantages include high cost of metal and explosive nature of hydrogen [1].

Metals can also adsorb-desorb oxygen in molecular or atomic form and produce cold energy. Application of heat during desorption can lead to formation of stable oxygen [1].

2.4.2.3. Metal Oxides-Water and Metal Oxides-Carbon Dioxide

Hydration and carbonation processes occur in metal oxide-water and metal oxide-carbon dioxide working pairs respectively to store high amount of energy in thermochemical system. For example, the energy storage capacity for calcium oxide in the hydration and carbonation process varies between 800–900 kJ/kg. Such working pairs are used to develop highly efficient heat pumps[1].

2.4.2.4. Salt Hydrates and Water

Different salt hydrates are used for thermochemical energy storage by hydration reaction, such as magnesium chloride ($MgCl_2$), sodium sulfide (Na_2S), strontium bromide ($SrBr_2$) amd magnesium sulfate ($MgSO_4$) and the used working fluid is water. During this process, when the relative humidity (RH) is very high, the hydration of salt leads to the formation of saturated salt solution, instead of forming hydrates. This phenomenon is called deliquescence and the relative humidity, at which deliquescence happens, is called the deliquescence relative humidity (DRH). The DRH is affected by different factors, such as salt properties and temperature. Deliquescence causes several problems, e.g. corroding metals and hindrance to hydration. Therefore, use of salt hydrate-water system should be avoided if DRH is low. For example, at 30 °C, the DRH for LiBr, $MgCl_2$ and $MgSO_4$ are 6.2, 32.4 and 90% respectively. At this condition $MgSO_4$ should be used and other two should be avoided if possible [1]

Table-2: Different Properties of Working Pair (Physical) [1,9]

Working Pair	Heat of Adsorption [kJ/kg]	Heat of Vaporization[kJ/kg]	Operating Temperature[°C]
Silica Gel-Water	2500	2258	Below 90
Zeolite-Water	3200–4200	2258	70–250
Activated Carbon-Methanol	1800–2000	1102	Below 120
Activated Carbon-Ammonia	2000 – 2700	1368	Usually up to 150, Can be 200 or above

2.5. Adsorption Theories

Adsorption phenomenon is the most important part of the adsorption refrigeration system. Different adsorption theories help us to understand the factors that affect the adsorption process and to what extent, these factors affect the amount of adsorption and adsorption kinetics. This part includes adsorption equilibrium models and adsorption rate models, which give information on what factors affect equilibrium adsorption quantity and how quickly the adsorption occurs.

2.5.1. Equilibrium Adsorption Models

At certain temperature and pressure, an adsorbent can adsorb certain amount of adsorbate and when the time is infinite, the maximum possible adsorption occurs. This is called equilibrium adsorption quantity. The equilibrium adsorption models for are different for physical and chemical adsorption. In case of physical adsorption, both pressure and temperature are considered as independent property whereas in chemical adsorption either one of them is considered as independent property[1].

2.5.1.1. Equilibrium Models for Physical Adsorption

As already mentioned earlier, the equilibrium model for physical adsorption includes both, temperature and pressure [1]. The equation for the equilibrium model for physical adsorption is as follows:

$$x_\infty = f(p, T) \quad \text{.....(1)}$$

Models with different fundamental processes are as follows:

$$x_\infty = f(p)_T \text{ (Isothermal) } \text{.....(2)}$$

$$x_\infty = f(T)_p \text{ (Isobaric) } \text{.....(3)}$$

$$p = f(T)_x \text{ (Isosteric) } \text{.....(4)}$$

As we know that adsorption is an exothermic process and adsorption causes release of heat. Therefore, during the development of adsorption isotherm, a little mass of adsorbent is used or else, the released heat might affect temperature, thus, corrupting the experiment. For isobaric models, the quantity of the refrigerant desorbed and adsorbed during a cycle can be easily calculated, therefore used for designing. Isosteric model is used to calculate the adsorption heat and select the working pair [1].

Adsorption refrigeration cycle suggests that the adsorption and desorption process in the adsorption refrigeration system are isobaric processes. It will be explained in the later part. After getting condensed, the refrigerant gets evaporated, that gives the cooling effect. Refrigeration is created during this evaporation-adsorption step only. Therefore, multiple adsorber beds are required when we need continuous refrigeration [1].

2.5.1.2. Equilibrium Models for Chemical Adsorption

As mentioned already, equilibrium model for adsorption has only one independent property. At a certain temperature, when the system reaches the equilibrium, increasing pressure does not result in increased adsorption. A stepwise trend is observed during chemical adsorption process, means sharp rise in adsorption followed by no change at all with changing pressure at certain temperature [1]. The equilibrium adsorption model for chemical adsorption is as follows [1]:

$$p = f(T)_{adsorbent\ x\infty = xn} \text{.....(5)}$$

Here, n is the mole number of refrigerants adsorbed by the adsorbent [1].

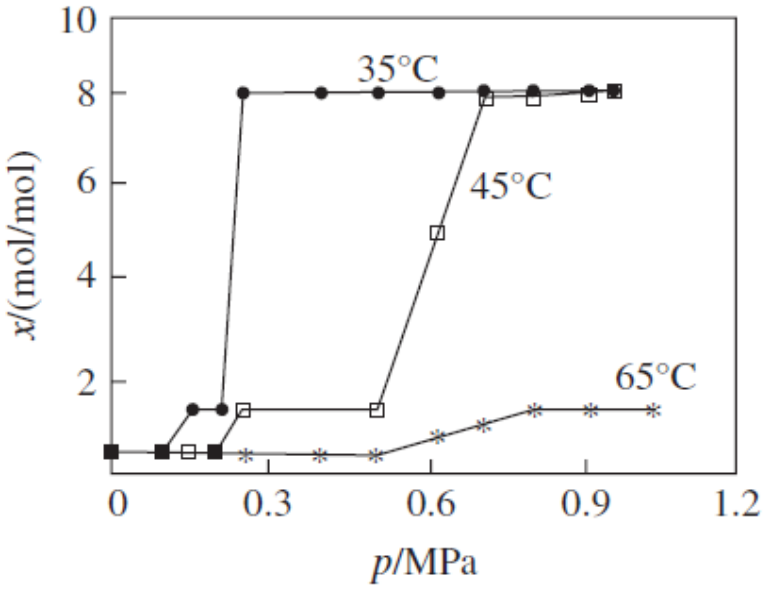

Figure-7: Adsorption curves of strontium chloride–ammonia [1]

Large amount of heat released during chemisorption and therefore, the activation energy for adsorption is different form desorption, higher for the later and they follow different path. Let us consider chloride for an example. For chloride, adsorption process is the complexation reaction and desorption process is decomposition of the newly formed molecules. Activation energy for both of these processes is different [1]. The chemical reaction between chloride and ammonia can be written as [1]

$$M_yCl_z \cdot n1NH_3 + n_2\Delta H_r \leftrightarrow M_yCl_z \cdot (n_1 - n_2)NH_3 + n_2NH_3$$

Here, .H_r where is chemical reaction enthalpy (J/mol); n_1 and n_2 are values of 2, 4, 8 (or 6), respectively. M_yCl_z is the metal chloride [1].

2.5.1.3. Adsorption Rate Models

For physical adsorption, Sokoda established a model for quantifying the adsorption rate suitable for silica gel-water working pair. This model can be applied to other working pairs, with suitable coefficient for respective working pairs. This model considers the dynamic adsorption process and the mass transfer process inside the adsorber [1]. The equations are as follows.

$$\frac{dx}{dt} = K_s a_p (x^* - x) \text{.....6}$$

$$K_s a_p = \frac{15 D_{so}}{R_p^2} \exp\left(-\frac{E_a}{RT}\right) \text{.....7}$$

Here, x* is the equilibrium adsorption quantity, $K_s a_p$ is the coefficient for the velocity of surface diffusion, D_{so} is the surface diffusion coefficient, E_a is activated energy for the surface diffusion and Rp is the average diameter of the adsorbent granules.

The adsorption rate models for **chemical adsorption** are much more complex compared to models for physical adsorption [1]. Several models have been developed over the time. Based on the research and findings of Spinner and Rheault, Mazet et al. and Lebrun developed an equation [1].

$$\frac{dx}{dt} = K_i(1-x)\exp\left(-\frac{A_0}{T}\right)\ln\left(\frac{P_c}{P_{eq}(T)}\right) \quad \text{.....8}$$

where x is adsorption quantity, dx/dt is adsorption rate, K_i is dynamic coefficient, subscript i=s for adsorption process, and i=d for desorption process. P_c, P_{eq} and T represent constrained pressure of the condenser and evaporator, equilibrium pressure, and adsorption temperature respectively[1].

In the experiment, the influence of A_0 is insignificant. Therefore, Mazet has made a logarithm transformation in equation 8 to address this issue. Based on that Goetz developed a model [1].

$$\frac{dN_g}{dt} = 4\pi r_c^2 K_i\left(\frac{P_c - P_{eq}(T)}{P_{eq}(T)}\right)^{Ma} \quad \text{.....9}$$

where Ng is the molar adsorption quantity, r_c is the diameter of reaction surface, and Ma is the reaction dynamic coefficient. This model considers the mass transfer process inside the grains [1].

The reaction rate model which considered the Darcy equation for reaction surface and grain surface is the following.

$$\frac{dx}{dt} = f(x, r_g)\left(\frac{P_c - P_i}{T_c}\right)K_n(m, c) \quad \text{.....10}$$

Here, Kn is Knudsen diffusion rate which is related to the diameter of the pore and porosity, f(x,rg) is a function which is related to adsorption quantity x and the radius of grain r_g, and p_i is the pressure inside the pore [1].

Same models can be used for adsorption and desorption. But a study of chemical and composite adsorption under non-equilibrium heating and cooling process by SJTU established that adsorption and desorption followed different paths, resulting into hysteresis. It needs to be considering during the application of the models [1].

As previously mentioned, composite adsorbents are composed of physical and chemical adsorbents. The main adsorption occurs in the chemical adsorbent part and therefore, the models for chemical adsorbent can be applied for composite adsorbent as well but for equilibrium adsorption only. For non-equilibrium adsorption, the process is more complex, and heat and mass transfer process are needed to be considered. As the adsorption progresses, several properties of the systems are affected, such as volume of chemical adsorbent and density of the porous part. These factors are also required to be considered [1].

2.6. Adsorption Isotherm

Adsorption isotherm is a graph that represents the amount of adsorbed adsorbate on the surface of the adsorbent at changing pressure (as a percentage of saturation pressure at respective temperature, P/Po) at constant temperature [32]. There are different models for adsorption isotherm such as the Langmuir model, the Freundlich model, the Brunauer, Emmett, and Teller (BET) model, etc. The BET model has been used to determine the surface area of the samples from nitrogen adsorption isotherms (at -196 °C).

2.6.1. The Langmuir Model

Langmuir isotherm model is used for monolayer adsorption in low pressure condition [33]. Langmuir model established a relationship between equilibrium site occupancy, θ, (in fraction) and the pressure, P, at which θ is obtained. It has been developed on three assumptions [34]. Those are as follows:

a. At constant temperature, the rate of incidence of the adsorbate molecules is proportional to the pressure, according to the kinetic theory of gases [34].
b. Along with the rate of incidence, the adsorption rate is also affected by probability of adsorption and the probability of incidence at a vacant adsorption [34].
c. The rate of desorption at any particular fraction of surface coverage is obtained by multiplying the maximum rate of adsorption at maximum surface coverage with the fraction of surface coverage [34].

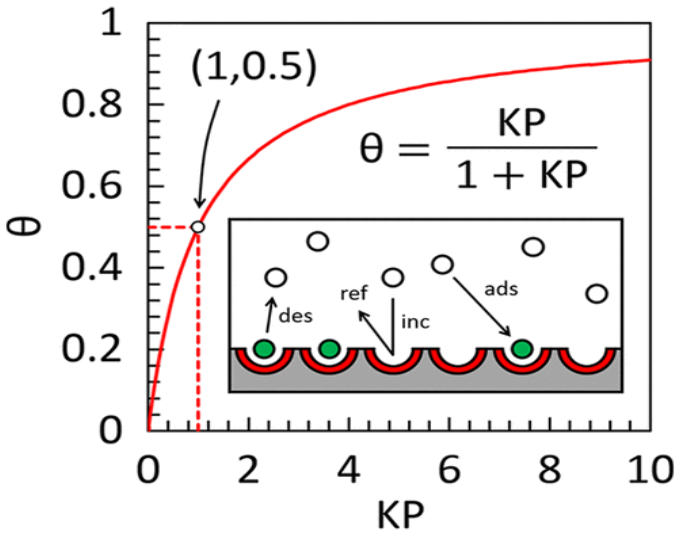

Figure-8: Langmuir's kinetic model of adsorption [34]

At equilibrium, rate of adsorption is equal to rate of desorption [33]. From Langmuir model, we get the following equation [34]

$$\boldsymbol{\theta = \frac{KP}{1+KP}} \text{.....11}$$

Here, K is a constant that is independent on pressure and only depends on temperature.

Now if we consider "a" is the concentration of the occupied active sites on the surface and "a_m" is the surface concentration at the monolayer coverage of the adsorbate then, $\theta = a/a_m$

So, we can write [33]

$$\boldsymbol{a = \frac{a_m KP}{1+KP}} \text{.....12}$$

This equation can be written in a linear form [33].

$$\boldsymbol{\frac{P}{a} = \frac{1}{a_m} P + \frac{1}{a_m K}} \text{.....13}$$

Plotting this equation, we can find the value for K and a_m

2.6.2. The Freundlich Model

The Freundlich model is also applied to monolayer adsorption [35].

Now, if we consider "a" is the amount of the adsorbed adsorbate on the adsorbent and C is the concentration of adsorbate at equilibrium, the equation proposed by Freundlich Model is as follows [35].

$$a = KC^{\frac{1}{n}} \text{.....(14)}$$

Here, K is the Freundlich constant and 1/n is adsorption intensity

This equation can be written in another form.

$$\log (a) = \log (K) + \frac{1}{n}\log (C) \text{ .....(15)}$$

Plotting graph between log (a) and log(C), we get a straight line with the slope value equal to 1/n and log k as y-axis intercept [35, 36].

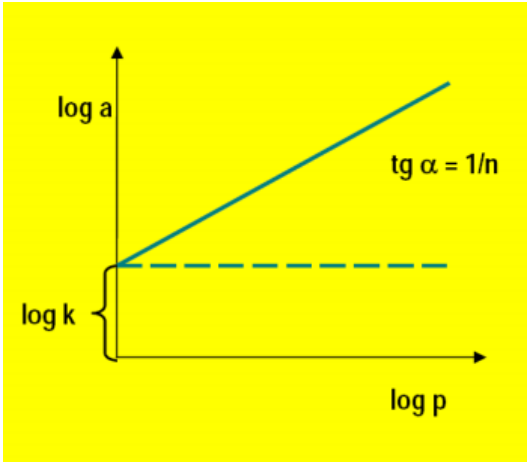

Figure-9: Determination of the constant from the logarithmic form of Freundlich isotherm [36].

2.6.3. BET Model

The BET model is the extension of Langmuir adsorption model and is applicable to multi-layer adsorption [38].

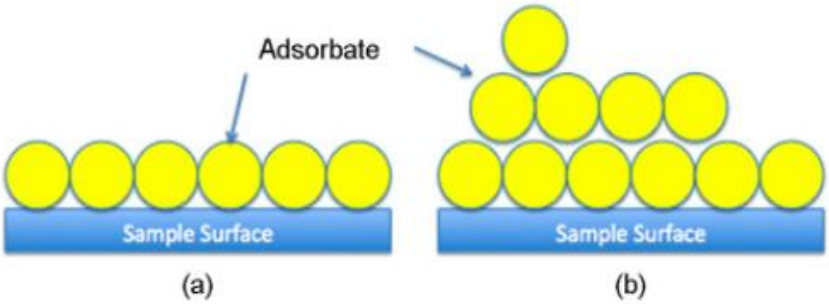

Figure-10: Schematic of the adsorption of gas molecules onto the surface of a sample showing (a) the monolayer adsorption model assumed by the Langmuir theory and (b) s the multilayer adsorption model assumed by the BET theory [38].

According to the BET theory, the equation for surface coverage is as follows [39],

$$a = \frac{a_m C \frac{P}{P_O}}{\left(1-\frac{P}{P_O}\right)\left[1+(C-1)\frac{P}{P_O}\right]} \text{.....16}$$

Here, "a" is the total amount of adsorbed vapour, "a_m" is the monolayer capacity, C is the BET constant, P is the pressure and P_0 is the saturation pressure [39]. C is exponentially adsorbed to the energy of monolayer adsorption [39]. C can be defined as following [40].

$$C = EXP\left(\frac{H_l - H_1}{RT}\right) \text{.....16}$$

Here, $H_1$and H_l are, respectively, the adsorption enthalpies of the first layer and its subsequent ones. T is absolute temperature and R is the universal gas constant [40].

Plotting $(p/p_o)/(a(1–p/p_o))$ vs P/P_o, we get the following graph and from this graph we can get the values for the constants of this equation such as C and a_m [39].

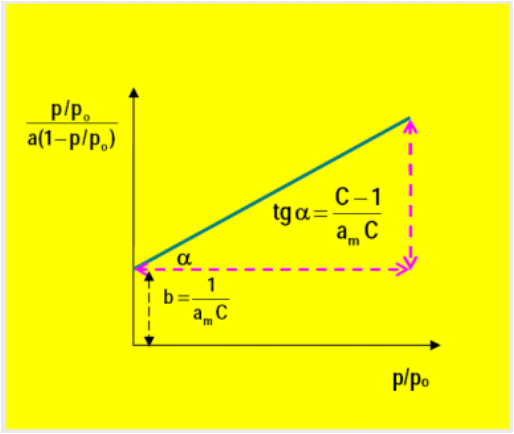

Figure-11: Determination of the constants of the BET adsorption isotherm [36].

When the value of a_m is known, we can calculate the specific surface area of the studied adsorbent can be calculated from the following equation [39].

$$S=a_m.L.\ \sigma_m/m \text{……..17}$$

Here, S is specific surface area, L is avogadro constant, σ_m is molecular cross-sectional area and m is the mass of adsorbent [39].

2.6.4. Adsorption Isotherm Types

There are mainly 5 types of adsorption isotherm, namely Type I, Type II, Type III, Type IV and Type V. Among them Type I, Type II and Type III are for reversible adsorption types, whereas Type IV and Type V are for irreversible adsorption types [38, 41, 42, 43]. These isotherms have significant use in this research work. The determined water isotherms are compared with these standard isotherm types to find out similar shapes and that can give us some important hints on the material's adsorption process, porosity type, etc.

2.6.4.1. When strong attraction between adsorbate–adsorbent forms a monolayer adsorption in microporous materials, type I adsorption isotherm is obtained [38,44]. With respect to the pressure axis, this isotherm shape is concave [44]. For type I adsorption isotherm, P/Po < 1 and c > 1 in BET equation [38]. The adsorption of NH_3 in charcoal creates such kind of isotherm [36]. Figure-12 suggests, there is no hysteresis [42].

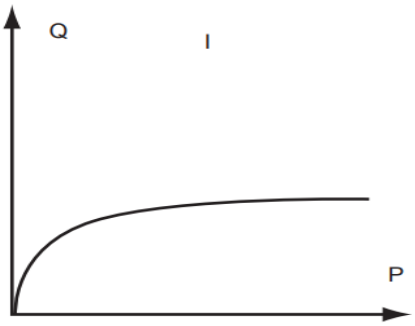

Figure-12: Type I Adsorption Isotherm [42]

2.6.4.2. Type II adsorption isotherm is one of the most common adsorption isotherms, obtained for monolayer-multilayer adsorption that occurs in non-porous or macro-porous [38,44]. For type II adsorption isotherm, C > 1

in BET equation [38]. The flatter region is the indication of monolayer formation, while the increased adsorption at higher pressure is for multilayer adsorption [38]. Figure-13 suggests, there is no hysteresis [42].

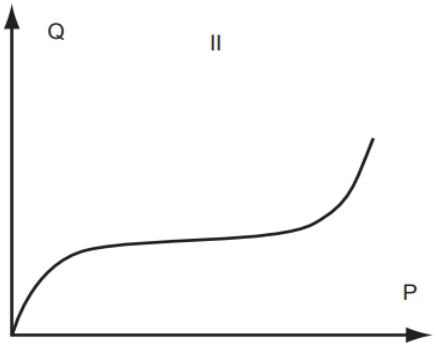

Figure-13: Type II Adsorption Isotherm [42]

2.6.4.3. When the attraction force between the molecules of adsorbates is higher than the attraction force between adsorbate-adsorbent molecules, a very unusual adsorption isotherm is formed that has a convex shape with respect to pressure axis[44]. For type III adsorption isotherm, $C < 1$ in BET equation. There is no flat region in the curve, so no monolayer is formed. BET model cannot be applied for this one [38]. Adsorption of bromine in silica is one of the examples for Type III adsorption isotherm [36]. Figure-14 suggests, there is no hysteresis [42].

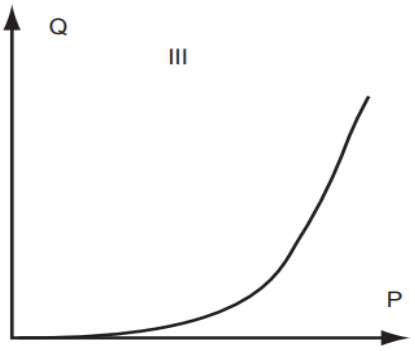

Figure-14: Type III Adsorption Isotherm [42]

2.6.4.4. Type IV adsorption isotherm is obtained when adsorption in mesoporous materials is accompanied by capillary condensation and results in hysteresis. Therefore, it is an irreversible adsorption system [38,44]. Similar to type II isotherm, the flatter region is the indication of monolayer formation, while the increased adsorption at higher pressure is for multilayer adsorption for this isotherm as well [38]. Figure-14 suggests, there is hysteresis [42]. Adsorption of benzene in silica is one of the examples for Type IV adsorption isotherm [36].

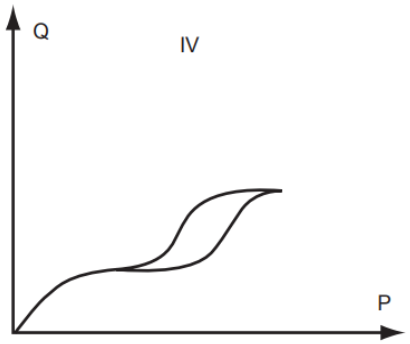

Figure-15: Type IV Adsorption Isotherm [42]

2.6.4.5. Another rare adsorption isotherm is Type V, which is irreversible. For this case, the adsorption mechanism like Type III, means that attraction between the adsorbate molecules is higher than the adsorbate-adsorbent molecules. It also characterised by hysteresis for the same reason as Type IV adsorption isotherm, the capillary condensation [44]. Adsorption of H_2O in charcoal is one of the examples for Type IV adsorption isotherm [36].

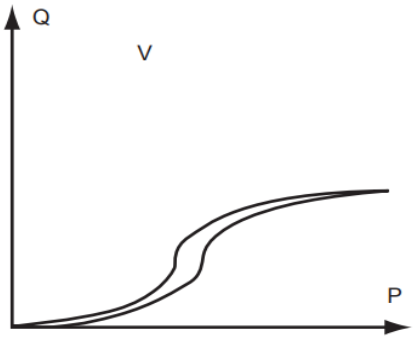

Figure-16: Type V Adsorption Isotherm [42]

2.6.4.6. Type VI adsorption isotherm is also very uncommon. It depicts stepwise adsorption [44,46]. It appears when the surface of a uniform non-porous solid material contains different adsorption sites, and they have different energy characteristics [42, 46]. Some of the examples of such isotherm are well crystallized zeolites like X (one step fills cavities) or silicate (two steps of adsorption for channel filling and adsorbent–adsorbate transition respectively) [46].

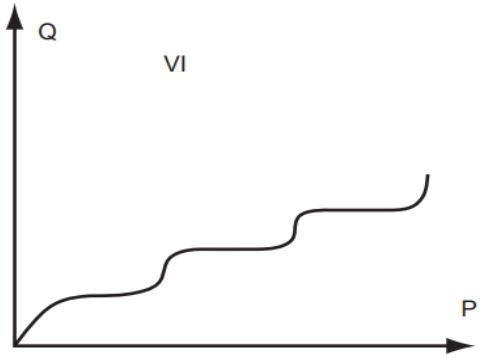

Figure-17: Type VI Adsorption Isotherm [42]

2.7. Hysteresis

Adsorption hysteresis is a phenomenon that occurs due to fact that the adsorption branch and desorption branch follow different path, creating a loop [47]. For physisorption, hysteresis is observed mainly in mesoporous

materials, resulting from capillary condensation and for chemisorption, it occurs due to different activation energy for adsorption and desorption[1, 47]. Foster (1932) mentioned, desorption branch, that is characterized by capillary condensation equilibrium, can be explained from Kelvin equation, while adsorption branch is characterized by multilayer adsorption [37]. According to IUPAC, there are five types of hysteresis loops such as H_1, H_2, H_3, H_4 and H_5 [43]

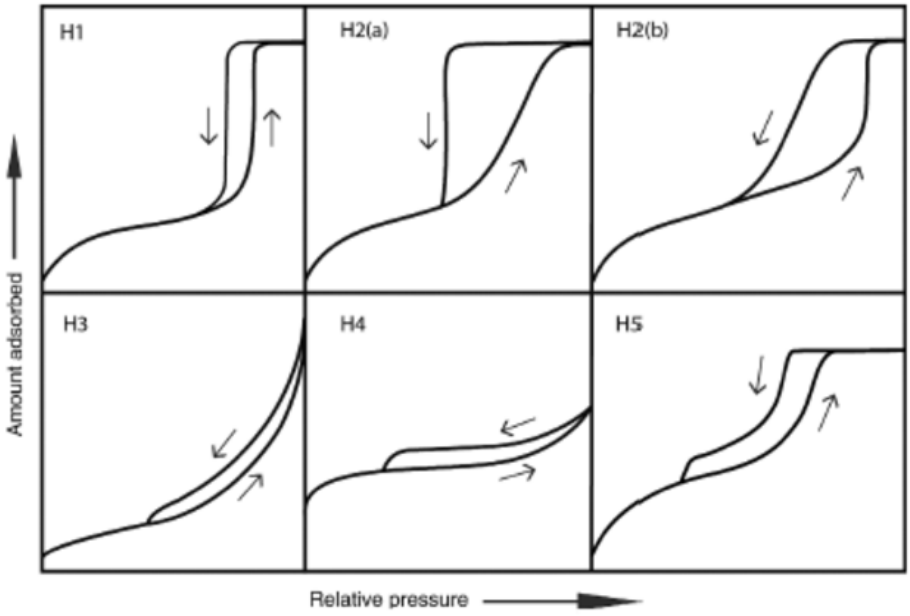

Figure-18: IUPAC Classification of Hysteresis Loops [43]

When the capillary condensation occurs in cylindrical pores (open from both ends), H_1 hysteresis loop is obtained [48]. H2(a) hysteresis loop is characterized by sharp decrease is hysteresis and occurs in inkbottle shaped uneven pore structures. The pores are also characterised by poor connectivity[43, 48]. If the relative pressure reduces to a certain level, the bottle neck gets unblocked and only after that the condensate inside the pore is released [37]. H2(b) hysteresis is observed for the pores with thicker neck than pores of H2 (a) [49]. H3 hysteresis loop occurs in wedge-shaped pores that is formed when plate shaped grains accumulate in parallel manner [48, 49]. H4 hysteresis loop occurs in slit-shaped pores. Parallel pore structure results into such type of pores [48]. The most unusual hysteresis loop, H5 is the characteristics of adsorption in materials with open and partially open mesopores [49].

2.8. Adsorption Refrigeration Process

The adsorption refrigeration system occurs in four steps which can be divided into of two sperate processes, such as heating-desorbing process and cooling adsorbing process. The traditional adsorption refrigeration cycle does not provide refrigeration continuously. If we need continuous refrigeration, we will need to design a refrigeration system with two or more adsorber beds, working in a proper sequence. Also, it will require continuous supply of heat. It is a suitable for utilization of solar heat to produce cold energy [1].

2.8.1. The basic adsorption refrigeration cycle

The basic adsorption refrigeration cycle includes the following steps.

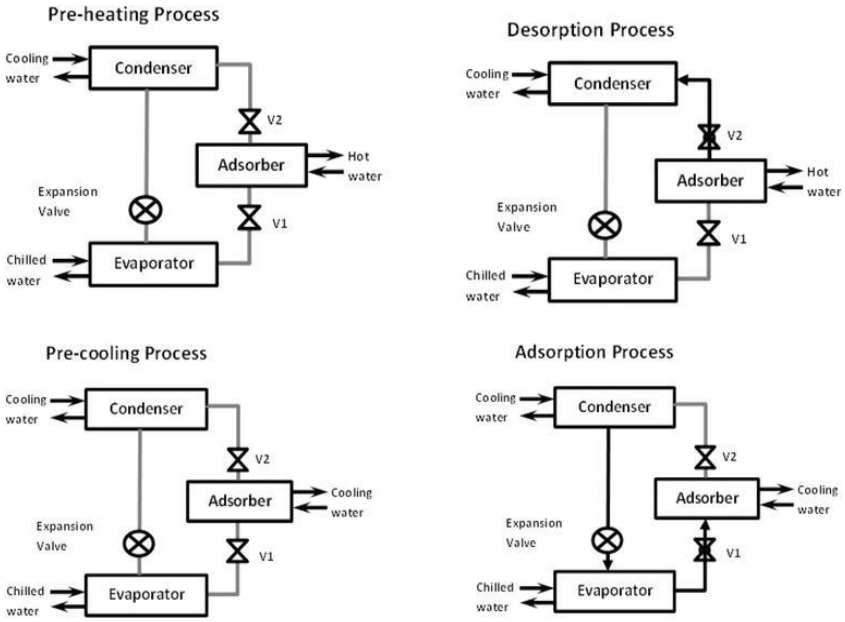

Figure-19: Basic adsorption cooling system under one complete cycle[50].

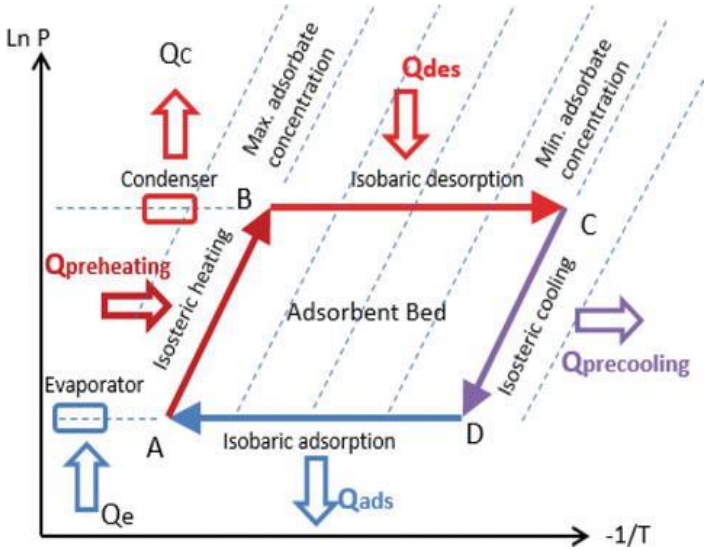

Figure-20: Clapeyron diagram of an ideal adsorption refrigeration cycle [50].

Pre-heating process (A−B) [50]: This section represents isosteric heating in a closed system, resulting in increase of pressure and temperature. The closed system is created by closing the vales of both sides of the adsorber bed. This takes place after the adsorber bed has adsorbed the refrigerant. This isosteric heating continues until the pressure reaches the desired condensation pressure which is represented by point B [50].

Desorption process (B−C)[50]: This section represents the isobaric desorption process. In this section temperature keeps increasing while the pressure remains constant. It causes the adsorbed refrigerant to desorb. This process starts when the valve, that connects the adsorber and the condenser, is opened. The desorbed refrigerant leaves the adsorber bed surface and reaches the condenser to get condensed. Then desorbed vapor condenses in the condenser by giving up heat [50].

Pre-cooling process (C−D) [50]: The desorption process is followed by the isosteric cooling, It results in the decrease in temperature and pressure in the bed. Again, for this process, the valves are closed. The temperature is decreased to such a level that pressure reduces to the level of the pressure of evaporator [50].

Adsorption process (D−A) [50]: The adsorption process comes after the isosteric cooling. In this process, the evaporation and adsorption occur simultaneously. This is the only period the effective cooling takes place. This cooling results from the fact that the refrigerant tales the heat of vaporization from the cooling space, thus the cooling is created [50].

2.8.2. Adsorption Refrigeration Using Solar Energy

As previously mentioned, adsorption refrigeration system can be driven with low temperature heat energy when physical adsorbent-refrigerant working pair is used. As solar energy is low temperature heat, this energy can be utilized with such refrigeration system. For utilizing this low-grade heat energy, different adsorbent-adsorbate working pair can be used, such as activated carbon-methanol, silica gel-water etc. The COP of the adsorption refrigeration system, driven by solar energy is lower than 0.2. In some of the research works, this system has been coupled with solar collector to increase the performance of the system. The basic steps for solar energy driven adsorption refrigeration are almost similar to conventional adsorption refrigeration system, but adsorption cycle time different [1].

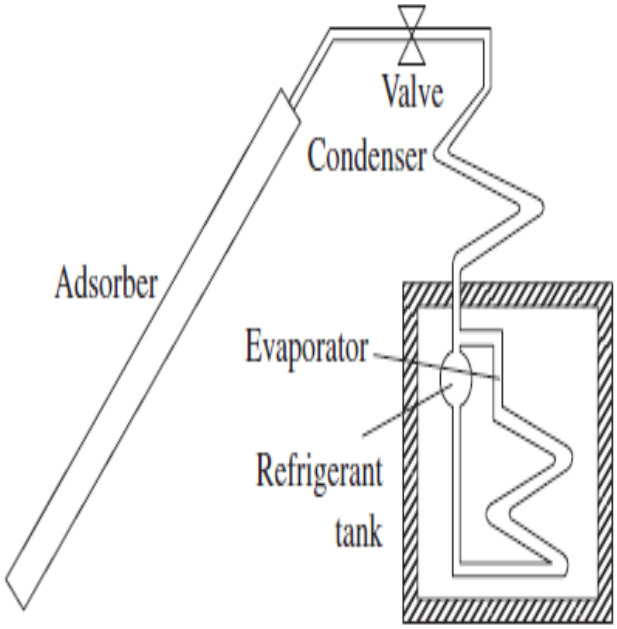

Figure-22: The solar powered adsorption refrigeration system [1]

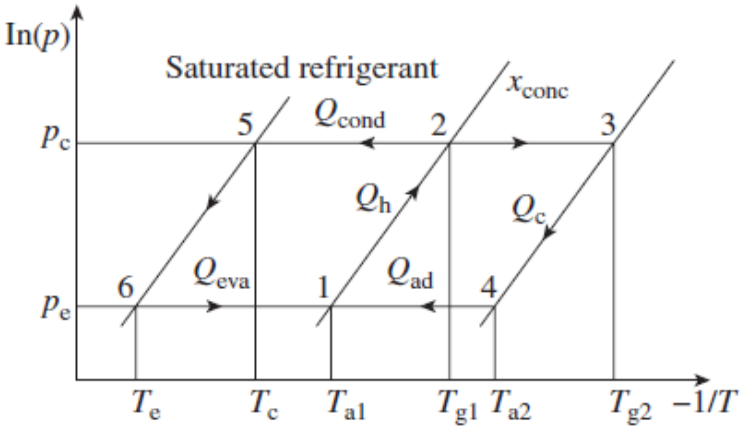

Figure-23: The p-T diagram of adsorption refrigeration cycle [1]

Step 1 [1]: The process starts in the morning by closing the valves that creates a closed system. As the system keeps receiving the solar heat, causing the pressure and the temperature of the systems to increase. At the end of this process, the obtained pressure in the system equalizes the saturation pressure corresponding to the condensing temperature. The temperature of the adsorber at this point is $T_{g1.}$

Step 2 [1]: In the second step, the valve, that connects the condenser and the adsorber bed, is opened. This causes the desorbed refrigerant to flow from adsorber to the condenser, where the refrigerant condenses to liquid by giving up the heat. The heat leaving process is the natural convection. The condensed liquid then flows to evaporator.

Step 3 [1]: In the evening, the adsorber section is again turned into a closed system by closing the valves. As there is no or very little solar energy available, the adsorber does not receive any heat, causing the pressure and temperature of the adsorber to decrease. The obtained pressure equalizes to the saturation pressure, corresponding to the evaporating temperature.

Step 4 [1]: In this step, the connecting valve between the evaporator and the adsorber is opened. The pressure difference between adsorber and evaporator causes the liquid refrigerant in the evaporator to evaporate and the refrigerant vapor flows the adsorber to be adsorbed by the adsorbent. This evaporation gives the cooling effect. This phase continues until the liquid refrigerant is left in the evaporator, usually till the next morning.

2.8.3. Adsorption Desalinisation

World's first large desalination plant was installed in 1960. Since then, 20000 plants have been installed till 2020. Out of those 2000 plants, almost 16000 plants are currently operational which produce 95 million m^3/day of freshwater. 48% of the desalinated water is produced in Middle East and North Africa region. This amount of water is served to more than 300 million people [51,52].

The working cycle for adsorption desalination is almost similar to any other adsorption refrigeration system. This system includes three major components such as condenser, adsorber bed and evaporator. The mentioned adsorption desalination system, here in figure-24, has two silicas gel bed as adsorbers. The working fluid is saline water [5].

The cycle starts with the loading of the saline water in the evaporator, followed by a vacuum created in the system. It causes the saline water to evaporate, creating vapor of drinkable water, leaving behind the salt. Then valve 1 (connecting the evaporator and silica-gel bed) is opened and evaporated water travels to Bed-1. There the vapor

gets adsorbed. Valve 1 is closed when the adsorber bed gets saturated with adsorbed vapor. Then, the heat is applied to the adsorber bed by flowing hot fluid. The application of heat causes the adsorbed vapor to be desorbed and also, the pressure increases to the condensation pressure. Valve 2 (connecting the adsorber and condenser) is opened and the desorbed water vapor flows to the condenser and gets condensed, which is pure water. When the regeneration process comes to an end, valve 2 is closed to create the closed system again. Then temperature and pressure of the adsorber bed are reduced by circulating cold water. Two adsorber beds are used for better efficiency and they have the same working procedure [5].

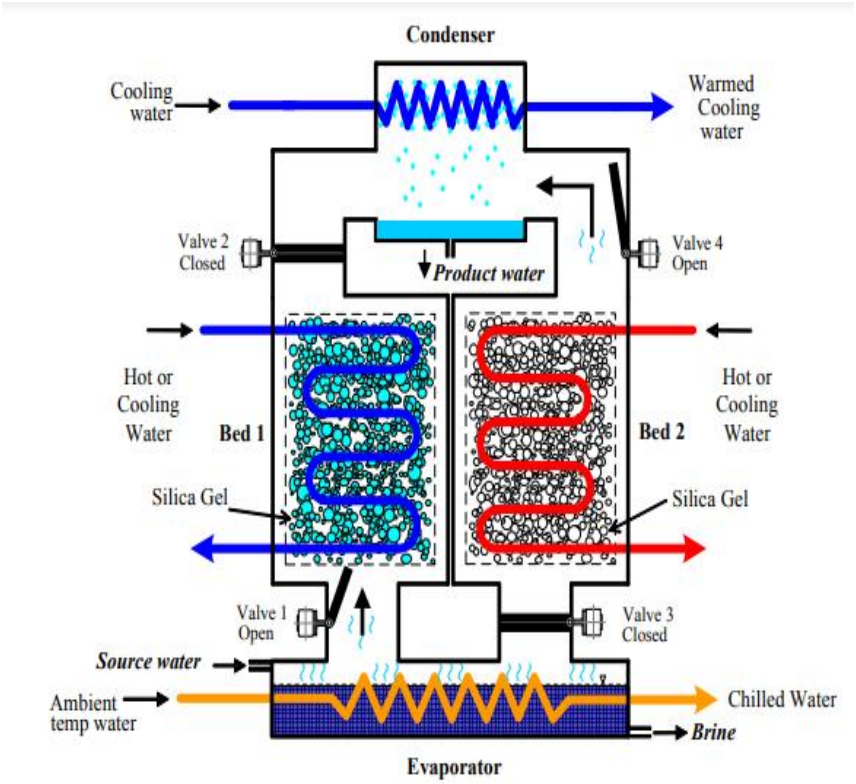

Figure-24: Two Bed Desalination System [5]

2.9. Coefficient of Performance (COP)

COP is a good parameter to analyse the performance of the adsorption refrigeration system. During the evaporation process, the refrigerant in the evaporator receives heat (Q_e) from the cooling space as heat of vaporization. On the other hand, heat (Q_h) is delivered to the adsorber for heating up the adsorber and for desorption of the adsorbed refrigerant [53]. The ratio of Q_e to Q_h is termed as COP. The equation for COP is as follows [53].

$$\text{COP} = \frac{Q_e}{Q_{12}+Q_{23}} \quad \text{.....19}$$

where Q_e is evaporator cooling heat (kJ), Q_{12} is isosteric heat of adsorption bed (kJ), Q_{23} is isobaric desorption heat of adsorption bed (kJ) [53].

Now [53],

$$Q_e = m_{R,C} \times (h_{g,e} - h_{l,c}) \quad \text{.....20}$$

$$Q_{12} = m_{AC} \times (C_{p,AC} + C_{max} \times C_{p.R})(T_2 - T_1) \quad \text{.....21}$$

$$Q_{23} = m_{AC} \times (C_{p,AC} + C_{ave} \times C_{p.R})(T_3 - T_2) + m_{R,C} \times H_{ads} \quad \text{.....22}$$

Here, $m_{R,C}$ is mass of refrigerant in a cycle (kg), m_{AC} is mass of adsorbent in the adsorption bed (kg), $h_{g,e}$ is enthalpy of saturated vapor of refrigerant in evaporator (kJ/kg), hl,c is enthalpy of saturated liquid of refrigerant in evaporator (kJ/kg), $c_{p,AC}$ is specific heat of adsorbent (kJ/kg·K), $c_{p,R}$ is specific heat of refrigerant (kJ/kg·K), C_{max} is maximum adsorption capacity of adsorbent in adsorption bed (kg refrigerant/kg of adsorbent), C_{ave} is average adsorbent capacity of adsorbent in adsorption bed (kg refrigerant/kg adsorbent), T_1 is the final adsorption temperature (K), T_2 is desorption initial temperature (K) and T_3 is the final desorption temperature (K) [53].

2.10. Specific Cooling Power

Specific cooling power (SCP) represents how quickly an adsorption refrigeration system can produce cold energy. SCP can be defined by the following equation [1].

$$\mathbf{SCP} = \frac{L\Delta x}{t_c} \text{.....(23)}$$

Here, where L is the latent heat of vaporization of the refrigerant, t_c is cycle time, and Δx is cycle adsorption quantity. This equation clearly shows that SCP increases with decreasing t_c.

The cycle time of such system can be reduced by heat transfer intensification. Equation 23 suggests that reduced cycle time will result in improved SCP [1]. Several approach can be taken to intensify the heat transfer, such as, development of new adsorbent with improved heat transfer characteristics and development of better heat exchanger for the adsorber. Along with the heat transfer intensification, improving the mass transfer performance of the adsorber bed can also reduce cycle time [1].

Table-3: COP-SCP for Different Adsorption Chiller [54, 55, 56, 57, 58]

Working Pair	Temperature °C (Heat Source)	Temperature °C (Cooling)	COP	SCP (W/kg)
Silica Gel-Water (Two Bed)	80	30	0.45	176
Silica Gel-Water (Two Bed-Solar Powered)	80	30	0.37	72
Silica Gel-Water (Three Bed)	95 (regenerator)	30 (adsorber)	0.63	SCE=337.5 (kj/kg)
Zeolite 13X-Water (Two Bed-Waste heat)	450	40	0.27	200
Activated Carbon-Methanol (Solar Powered)	100 (regenerator)	30 (adsorber)	0.0827-0.1271	18.39-18.83

2.11. Previous Research Works

Zeolite Synthesis: Tu W. W. et. al. have worked on the synthesis of 13-X zeolite from coal fly ash using the alkali fusion-hydrothermal method to dissolve Si and Al sources from fly ash, and with the addition of Si source. The obtained XRD peaks correspond to the pattern of X-type zeolite. Also, from IR spectra, it has been found that the morphology of zeolite 13X is accordance with the standard zeolite 13X. Besides, it has been found that The adsorption and ion exchange capacity are far better than the commercial zeolite 13X [59]. Panitchakarn P. et. al. have synthesized highly pure zeolite from coal fly ash. They achieved the high purity by pre-treatment of the coal fly ash (CFA) with various acids to find which acid is more effective for obtaining high purity. Zeolite was

produced from treated CFA by the fusion reaction under various Si/Al molar ratios, ranging between 0.54–1.84. In case of Si/Al<1, Zeolite type A was formed and in case of Si/Al>1 molar ratio, sodium aluminium silicate hydrate was formed. When, HCl (20%wt) and acid/CFA ratio of 20 mLHCl/g fly ash were used, zeolite with highest purity achieved (up to 97%) [60].

Adsorption Refrigeration System: Previous research work on adsorption provide us with some significant knowledge on adsorption chiller. They suggest that during adsorption, the pressure of the adsorbent bed is always lower, usually above 15% of the saturation pressure and sometimes can be as high as 45% [61, 62, 64, 65, 69-78]. The temperature usually ranges between 25-40 ^{o}C mostly [61, 62, 64, 65, 69-78]. Same papers suggest, during desorption of the refrigerant the temperature varies significantly (usually more than 65 ^{o}C and can get as high as 120 ^{o}C for solar energy), whereas the pressure is usually less than 5% of the saturation pressure of the respective temperature and sometimes it can be more than 10% as well [61, 62, 64, 65, 69-78]. COP and SCP get affected by many parameters. With increasing cycle time, COP keeps increasing, while SCP reaches a maximum value, followed by a decrease. With the increasing heat source temperature, COP initially increases and later decreases, while SCP increases. On the other hand, both of them decreases with increasing cooling fluid temperature. Both, COP and SCP, are increased by increasing adsorption amount, increasing outlet temperature of the chilled water and increasing chilled water inlet temperature. Design of the adsorption refrigeration system also affects its COP. With increasing number of adsorber bed, COP increases. Heat recovery system also increases COP [61-78]. Below, we can see the summary of some works done by previous researchers.

A work has been done by Ambarita H. et. al. to test the performance of different mixture of activated alumina (AA) and activated carbon (AC) as adsorbent in adsorption chiller and the used refrigerant is methanol. It has been found that for Indonesian condition and flat-plate type solar collector the pair of activated carbon and methanol is the better than activated alumina. Also, they have found that, using such collector can achieve temperature in the adsorbent as high as 100 °C during desorption and the pressure can be around 150-160 mbar (4.3%). During adsorption, the obtained lowest temperature and pressure are around 25 °C and 45-50 mbar (27%) respectively (around 6 in the morning). The lowest temperature can be reached in evaporator is 10 to 11 °C [61].

Wang, X. et. al. have worked on performance analysis of an adsorption chiller with silica gel-water working pair. The temperature of the adsorber bed increases up to 83 °C during desorption and decreases to as low as 33 °C during adsorption, whereas the pressure has been 3.8 kPa (7%) and 0.8 kPa (16%) respectively. The temperature of the chilled water is around 7 °C. This work suggests that COP and adsorption capacity increases with cycle time [62].

Sayfikar M. et. al. have worked on performance analysis of an adsorption chiller with silica gel- water working pair which uses solar energy. The temperature of the adsorber bed increases up to 85 °C during desorption and decreases to as low as 35 °C during adsorption, at those conditions the pressures are 2.8 (4.85%) and 1.2 (21.4%) kPa. The temperature at the evaporator gets as low as 9 °C [64].

Brites G. et. al. have worked on performance analysis of an adsorption chiller with silica gel- water working pair which uses solar energy. The temperature of the adsorber bed increases up to 100 °C during desorption and decreases to as low as 25 °C during adsorption, at those conditions the pressures are 8.5 (7.9%) and around 0.7 (22%) kPa [65].

Omisanya N. O. et. al. have worked on performance analysis of an adsorption chiller with zeolite 4A-water working pair which uses solar energy. The temperature of the adsorber bed increases up to 110 °C during desorption and decreases to as low as 25 °C during adsorption. The temperature at the evaporator gets as low as 11 °C [66].

Uyun, A. S. et. al. have worked on performance analysis of a three-stage adsorption chiller with silica gel-water working pair. This improves the performance compared to a single- stage chiller. They also considered heat recovery system which leads to better COP. The temperature of the adsorber bed increases up to 70 °C during desorption and decreases to as low as 30 °C during adsorption, whereas the pressure has been 4.35 kPa (13.6%) and 1.23 kPa (29%) respectively [69].

Saha, B. B. et. al. have worked on performance evaluation of a low-temperature waste heat driven multi-bed adsorption chiller. Here also, the working pair is silica gel-water. The obtained result shows, highest temperature is 80 °C during desorption and decreases to as low as 30 °C during adsorption, whereas the pressure has been 3.5 kPa (7.4%) and 0.8 kPa (18.9%) respectively. The calculated value of COP for this simulation is 0.38. The delivered chilled water temperature is about 6 °C when the inlet temperature is 14°C [70].

Sharafian, A. et. al. have worked on effects of different adsorber bed designs on in-situ water uptake rate measurements of AQSOA FAM-Z02 for vehicle air-conditioning applications. Here the working refrigerant is water. The obtained result shows, highest temperature is 90 °C during desorption and decreases to as low as 30 °C during adsorption, whereas the pressure has been 3 kPa (4.3%) and 0.7 kPa (16.5%) respectively. When AQSOA FAM-Z02 as adsorbent and a well-designed adsorber bed are used, a SCP of 112.9 W/kg and a COP of 0.34 are achieved at cycle time of 10 min [71].

Khanam M. et. al. have worked on performance analysis of an adsorption chiller with activated carbon-ethanol working pair which uses solar thermal energy. The temperature of the adsorber bed increases up to 74 °C during desorption and decreases to as low as 27 °C during adsorption, whereas the pressure has been 10.4 kPa (14%) and 3.8 kPa (43%) respectively. It says such system obtains a COP of 0.616 and corresponds to ice production of 27 kg per cycle at from water at a source temperature of 25°C [72].

Sitorus T. B. et. al. have worked on performance analysis of an adsorption chiller with activated carbon-methanol working pair which uses solar energy. The temperature of the adsorber bed increases up to 100 °C during desorption and decreases to as low as 30 °C during adsorption, at those conditions the pressure is 0.3 bar (8.8%) and 0.075 (44%) bar respectively. The temperature at the evaporator gets as low as 11 °C [73].

Sharafian, A. et. al. have worked on performance analysis of a novel expansion valve and control valves designed for a waste heat-driven two adsorber bed adsorption cooling system. Here the working pair is silica gel/$CaCl_2$-water. The obtained result shows, highest temperature is 90 °C during desorption and decreases to as low as 30 °C during adsorption, whereas the pressure has been 6 kPa (8.5%) and 0.9 kPa (21.3%) respectively. The study is this work suggest that SCP increases with cycle time, heating fluid temperature and chilled water inlet temperature and decreases with coolant fluid inlet temperature and cooling fluid inlet temperature [74].

Myat, A. et. al. have worked on experimental investigation on the optimal performance of zeolite–water adsorption chiller. The obtained result shows, highest temperature for adsorbent is 80 °C during desorption and decreases to

as low as 25 °C during adsorption, whereas the pressure has been 5.3 kPa (11.2%) and 0.67 kPa (21.6%) respectively. This system obtained chilled water outlet temperature as low as 7 °C while the inlet temperature is set to be about 12 C. In such system COP could be as high as 0.48 [75].

Tchernev D. has worked on a waste heat driven automotive air-conditioning system. The used working pair is zeolite-methanol. The obtained result shows, highest temperature for adsorbent is 100 °C during desorption and decreases to as low as 35 °C during adsorption, whereas the pressure has been 35 kPa (11.2%) and 7.5 kPa (26%) respectively [76, 84].

Schawe, D. has worked on theoretical and experimental investigations of an adsorption heat pump with heat transfer between two adsorbers. For the Na-Y zeolite adsorber, two refrigerants were used, pure water and glycol-water mixture. For pure water, the obtained result shows, highest temperature for adsorber bed is 130 °C during desorption and decreases to as low as 35 °C during adsorption, whereas the pressure has been 0.88 kPa (2.16%) and 5.8 kPa (17.6%) respectively [77].

For achieving PhD degree, Trindade M. V. worked on modelling and optimization of an adsorption cooling system for automotive applications. The working pair is sorbsil A and water. The operation modes were with and without heat recovery. The obtained result shows, highest temperature for adsorbent is 92 °C during desorption and decreases to as low as 35 °C during adsorption, whereas the pressure has been 5.2 kPa (6.8%) and 1 kPa (18%) respectively. From the experiment, it has been found that a mean cooling capacity of 1893 W and a COP of 0.29 for without heat recover system and a mean cooling capacity of 1912 W and a COP of 0.44 for the with heat recover system second configuration mode [78].

2.12.Commercialized Adsorption Chillers

Nishiyodo Kuchouki Co., Ltd invented a silica gel–water adsorption chiller system. Heating and cooling were provided by flowing hot and cold water respectively. The temperature of the heat used for regeneration ranged between 50–90 °C, producing chilled water of 3 °C [1].

The very first CCHP (cogeneration system for cooling, heat, and power) system were set up by the Malteser Hospital in Kammenz of Germany. It was integrated with an adsorption chiller to produce the cold energy by using solar energy and waste heat from fuel cells. The achieved cooling power was 105kW [1].

Macom, a Japanese company, is manufacturing silica gel–water adsorption refrigeration system since 2003. The temperature of the heat used for regeneration is 75°C, producing chilled water of 14 °C. The obtained COP is 0.6 [1].

In April 2003, a Japanese company, Tokai Optical Co. Ltd. set up an adsorption CCHP system. The system was powered by waste heat coming from a 185kW diesel engine is used. The waste heat can be used for both, heating and cooling. This system has the potential to reduce the annual energy consumption and CO_2 by 10% and by 12% respectively[1].

SJTU has developed small scale silica gel–water adsorption refrigerators with power ranging between 10–200kW. The temperature of the heat used for regeneration is 65 °C [1].

3.0. Experimental Methods

3.1. Sample Preparation Method

Three different zeolites were prepared from fly ash via a hydrothermal treatment in an alkaline solution. The prepared samples are Na-A zeolite (12 h), Na-A zeolite (24 h) and 13X zeolite. The Na-A zeolites were also modified with K_2CO_3 for increasing the water adsorption capacity. The fly ash was collected from a power plant in Poland. The composition of the fly ash is SiO_2=45.50%, Al_2O_3=23.10%, Fe_2O_3=7.38%, CaO=6.30%, MgO=4.22%, Active CaO+MgO=0.55%, S=0.54%, SO_4^{2-}=1.62%, TiO_2=0.72%, P_2O_5=0.29%, Mn_3O_4=0.17, Na_2O=1.55%, K_2O=2.96 and Combustion Loss = 6.42%.

3.1.1. Na-A Zeolite (12 h) Preparation

Synthesis:

1. 10 g fly ash was mixed with 12 g NaOH.
2. The mixture was exposed to 550 °C temperature for 1 h.
3. It was cooled downed to room temperature and grinded for 1 h.
4. Then distilled water was added at 4: 1 ratio.
5. This slurry was stirred at room temperature for 12 hours.
6. Later it was exposed to 100 °C for 12 h.
7. Then the sample was washed several times with distilled water filtered.
8. The obtained sample was dried in 100 °C for 12 h.

Modification with K_2CO_3:

1. 5 g of zeolite was added with 2.5 g of K_2CO_3 and 25 ml of distilled water.
2. It was stirred at room temperature for 24 h.
3. Then it was dried at 60 °C.
4. The last step was the calcination at 300 °C for 4 h.

3.1.2. Na-A Zeolite (24 h) Preparation

Synthesis:

1. 10 g fly ash was mixed with 12 g NaOH.
2. The mixture was exposed to 550 °C temperature for 1 h.
3. It was cooled downed to room temperature and grinded for 1 h.
4. Then distilled water was added at 4: 1 ratio.
5. This slurry was stirred in room temperature for 12 hours.
6. Later it was exposed to 100 °C for 24 h.
7. Then the sample was washed several times with distilled water filtered.
8. The obtained sample was dried in 100 °C for 12 h.

Modification with K_2CO_3:

1. 5 g of zeolite was added with 2.5 g of K_2CO_3 and 25 ml of distilled water.
2. It was stirred at room temperature for 10 h.
3. Then it was dried at 105 °C.
4. The last step was the calcination at 300 °C for 2 h.

3.1.3. 13X Zeolite Preparation

Synthesis:

1. Fly ash was calcined at 800 °C to remove remaining carbon and volatile materials.
2. The calcined sample was treated with HCl to dealuminate the fly ash and removed iron oxide to a certain extent.
3. Then NaOH was added to fly ash at ratio of 1.5:1 (weight).
4. This mixture was exposed to 550 °C for 1 h and later cooled down to room temperature.
5. Later the sample was grinded and distilled water was added at the ratio of 10 g fly ash/100 mL water.
6. The obtained mixture was stirred for hours.
7. Then, it was allowed to settle at 90 °C for 6 h.
8. After that, distilled water was used wash the sample and filtered to get rid of the remaining sodium hydroxide, and later dried.

3.2. XRD Analysis

XRD analysis was done to the powdered samples to determine the presence of synthesized zeolite and other crystalline phases. The test was done at room temperature, using CuKα radiation. The used instrument was Panalytical Empyrean diffractometer equipped with PIXel3D detector. The powdered samples were loaded in the holder, along the axis of the goniometer and exposed to radiation at different values of 2θ. The applied 2θ range was 10-110 degree. The percentage of crystalline phases were determined by semi-quantitative method, and it was implemented in the HighScore software. It is based on the relative intensity of the reflections of the phases, as compared with references included in the ICDD database.

3.3. Surface Area Analysis

The surface area of the samples was determined using the BET model. The required adsorption-desorption isotherms were developed using nitrogen as adsorbent at -196 °C. The used instrument was Gemini V 2.00 (model 2380). All the samples were dehydrated overnight at 250 °C temperature before the start of the nitrogen adsorption process.

3.4. Isotherm Determination

3.4.1. DVS Vacuum- Surface Measurement System

The DVS vacuum -surface measurement system is used for determination of the dynamic isotherm [79]. The amount of adsorbed water/adsorbent is measured with a gravimetric method [79]. It gives real-time data of adsorption and desorption [79]. It can perform multi-component experiments using vapor and/or gas sorbate molecules with the in-situ sample degassing up to 400°C and high vacuum [79]. This device is used to analyse the performance of Zeolites, porous polymers, composites, Aluminophosphates (AlPOs) and Silica aluminophosphates (SAPOs), silica gels, activated carbons and Metal Organic Frameworks (MOFs) [79].

3.4.1.1. Components of DVS Vacuum- System Measurement System

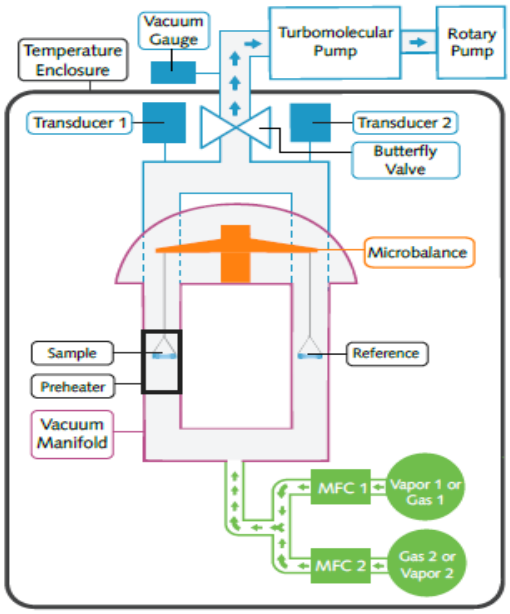

Figure-25: DVS Vacuum Schematic [79]

1. High temperature preheater for in-situ degassing/activation [79]

The maximum obtainable temperature is 400ºC with a heating rate up to 10ºC/min. The used sensor is Pt-100 thermocouple.

2. Gas /vapor injection system (upstream control) [79]:

Injection system consists of mass flow controllers (upstream) which can deliver vapor and gases of desired flow rates. There are two controllers, and the highest capacity is 200 sccm.

3.Butterfly valve (downstream control) [79]:

The butterfly valve regulates the amount of vapour or gas in the system by opening and closing based on pressure inside the chamber [79].

4. Water vapor and organic vapours [79]:

Water vapor is generated up to 90% P/Po in the temperature range between 20 to 70ºC. Water vapor can be generated in a limited P/Po range above 70ºC up to 150ºC. Organic vapor generation is limited to solvents' boiling point temperatures.

5. Vacuum System [79]:

There is one rotary vane pump with ultimate vacuum of 1x10-3 Torr and one high vacuum Turbomolecular pump with ultimate vacuum of 4x10-8 Torr.

6. Vacuum Stand [79]:

It is made of manifolded 316 stainless steel. Diaphragm valves are orbital welded The used seals are Viton, Kalrez (MFCs) and Cu gaskets. The tubing is 1/4 inch stainless steel.

3.4.1.2. Working Procedure of DVS Vacuum- System Measurement System

1. Measuring the sample that will be set in the container. In my case, the sample is zeolite. The amount should be between 25 to 30 mg.
2. Pouring water in vapour reservoir if necessary.

3. If the system is in vacuum pressure, it has to be increased to atmospheric pressure by opening the valve. Up to 10 Torr, the rate of pressure increase should be 0.1 torr/s. After 10 torr, the pressure increase rate should be 1 torr/s.

4. Then the sample container should be opened, sample should be set, and the container should be closed again.

5. The next step is to close the atmospheric valve. We have to make sure that the atmospheric valve and the sample container system are closed properly.

6. Then vacuum should be created again by switching on the vacuum pump (rotary pump) and opening the valve. The pressure reduction rate should be 0.1 torr/s up to 500 torr and the after that, the pressure reduction rate should be 0.8 torr/s.

7. The final step is setting the software. It includes editing, loading and running the method. We set parameters like system temperature (25,35,45,55 and 65 ^{o}C), relative pressure step (P/Po), time duration for each step, setting the activation temperature (170 ^{o}C) for 90 minutes, incubator temperature (same as system temperature) and vapor flow rate. In the meantime, initial mass is set, after system pressure reaches vacuum. The method is run after this. It is a system where pressure increase, and decrease (for adsorption and desorption) happen automatically. The system temperature can be changed remotely.

The data for dynamic sorption is created and recorded automatically in the software which is used for determining the isotherm.

4.0. Results and Discussion

4.1. Sample Characterization

4.1.1. XRD Analysis

4.1.1.1 Na - A Zeolite (12 h)

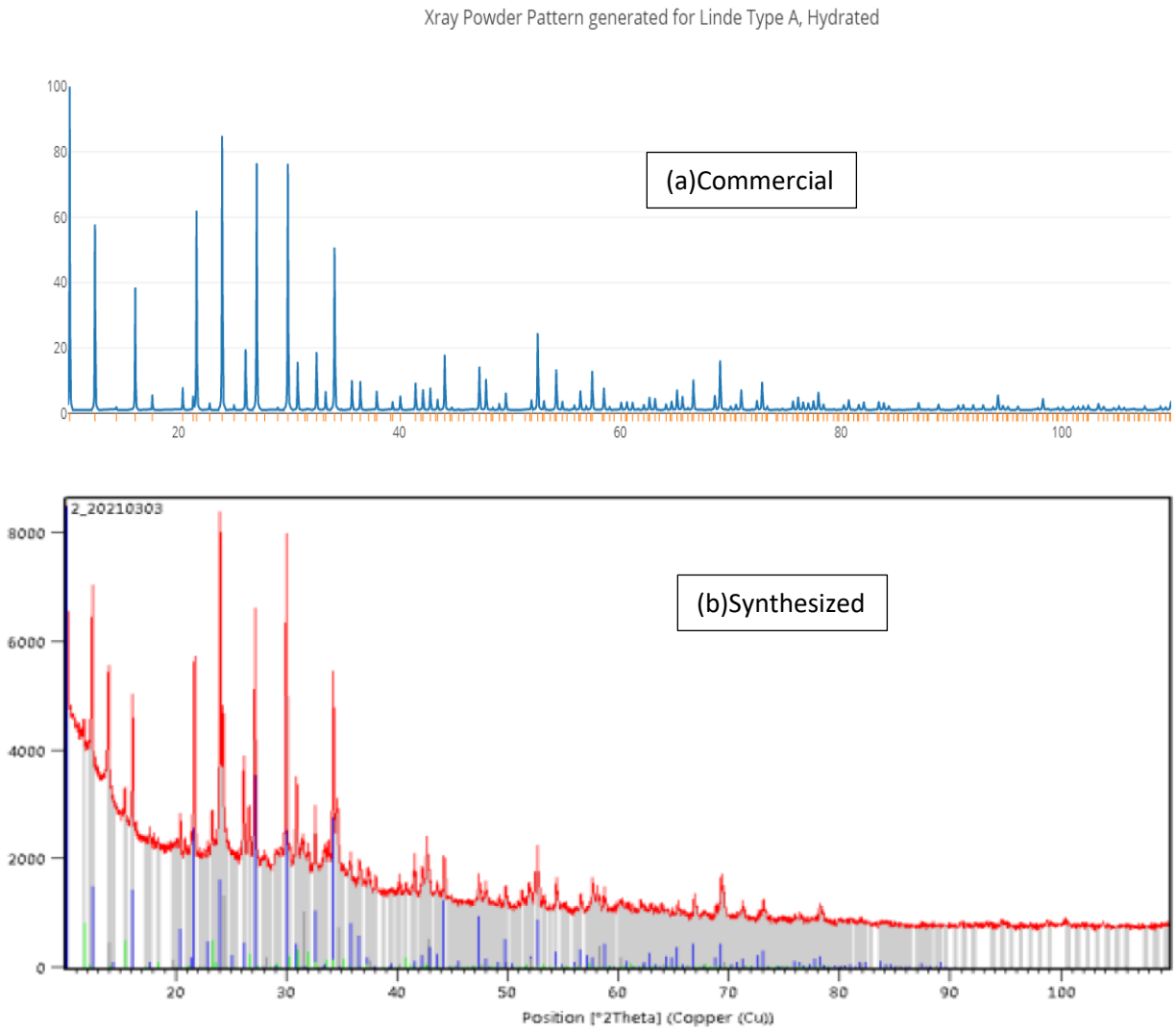

Figure-26: XRD Result Comparison, (a) Commercial Na-A Zeolite [80] (b) Synthesized Na-A Zeolite (12 h)

Discussion: Figure-26 represents XRD pattern for commercial zeolite (top) and synthesized zeolite (bottom). For commercial Na-A zeolite, we see peaks at 10.08, 12.4, 16.04, 21.64, 23.96, 26.08, 27.06, 29.92, 30.08, 32.58, 34.18, 35.78, 36.48, 41.46, 44.14, 47.24, 47.86, 52.58, 54.26, 57.46, 66.62 and 69.12. For synthesized Na-A zeolite (12 h), we see reflections at 10, 12.5, 16.1, 21.6, 24,26,30, 32.8, 34.3, 35.8, 36.5, 41.5, 44.15, 47.25, 47.9, 52.6, 57.5, 66.7 and 69.12, which almost superimposes on the reflection peaks of commercial zeolite. We see other peaks as well, which indicate the presence of other crystalline phases. Other detected phases are Potassium Aluminium Silicon Oxide and Sodium Calcium Aluminium Silicate Hydrate. Zeolite constitutes 66% of the total crystalline phase and the rest of the crystalline phases constitute 34%.

4.1.1.2 Na - A Zeolite (24 h)

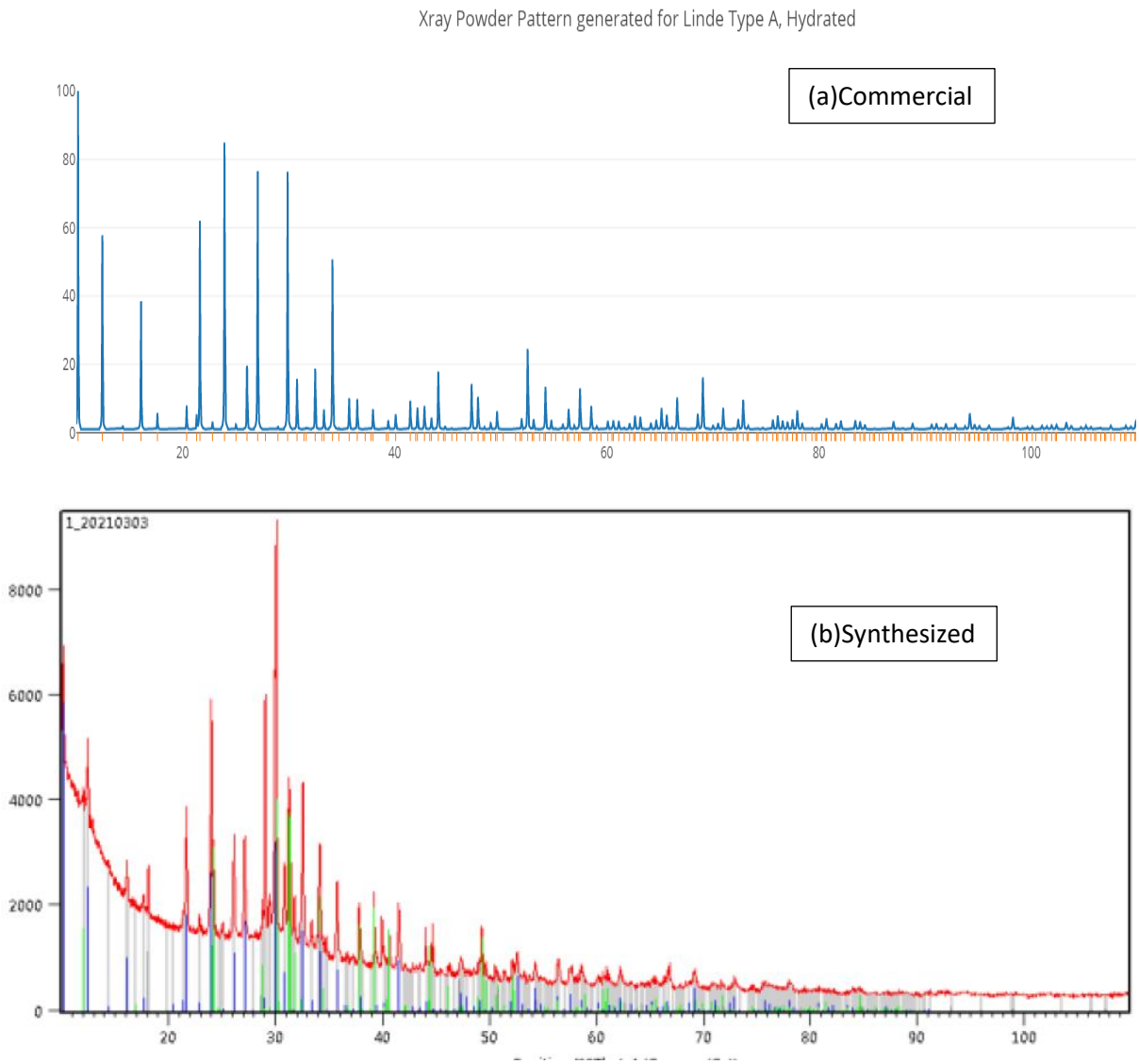

Figure-27: XRD Result Comparison, (a) Commercial Na-A Zeolite [80] (b) Synthesized Na-A Zeolite (24 h)

Discussion: Figure-27 represents XRD pattern for commercial zeolite (top) and synthesized zeolite (bottom). For commercial zeolite, we see peaks at 10.08, 12.4, 16.04, 21.64, 23.96, 26.08, 27.06, 29.92, 30.08, 32.58, 34.18, 35.78, 36.48, 41.46, 44.14, 47.24, 47.86, 52.58, 54.26, 57.46, 66.62 and 69.12. For our sample, we see reflections at 10.08, 12.5, 16.04, 21.6, 24, 26,08, 27.1, 30, 32.6, 34.2, 35.8, 36.5, 41.5, 44.14, 47.25, 52.6, 54.3, 66.7 and 69.1, which almost superimposes on the reflection peaks of commercial zeolite. We see other peaks as well, which indicate the presence of other crystalline phases as well. Other detected phases are Calcium Hydroxide and Potassium Hydrogen Carbonate. Zeolite constitutes 47% of the total crystalline phase and the rest of the crystalline phases constitute 53%.

4.1.1.3. 13X Zeolite

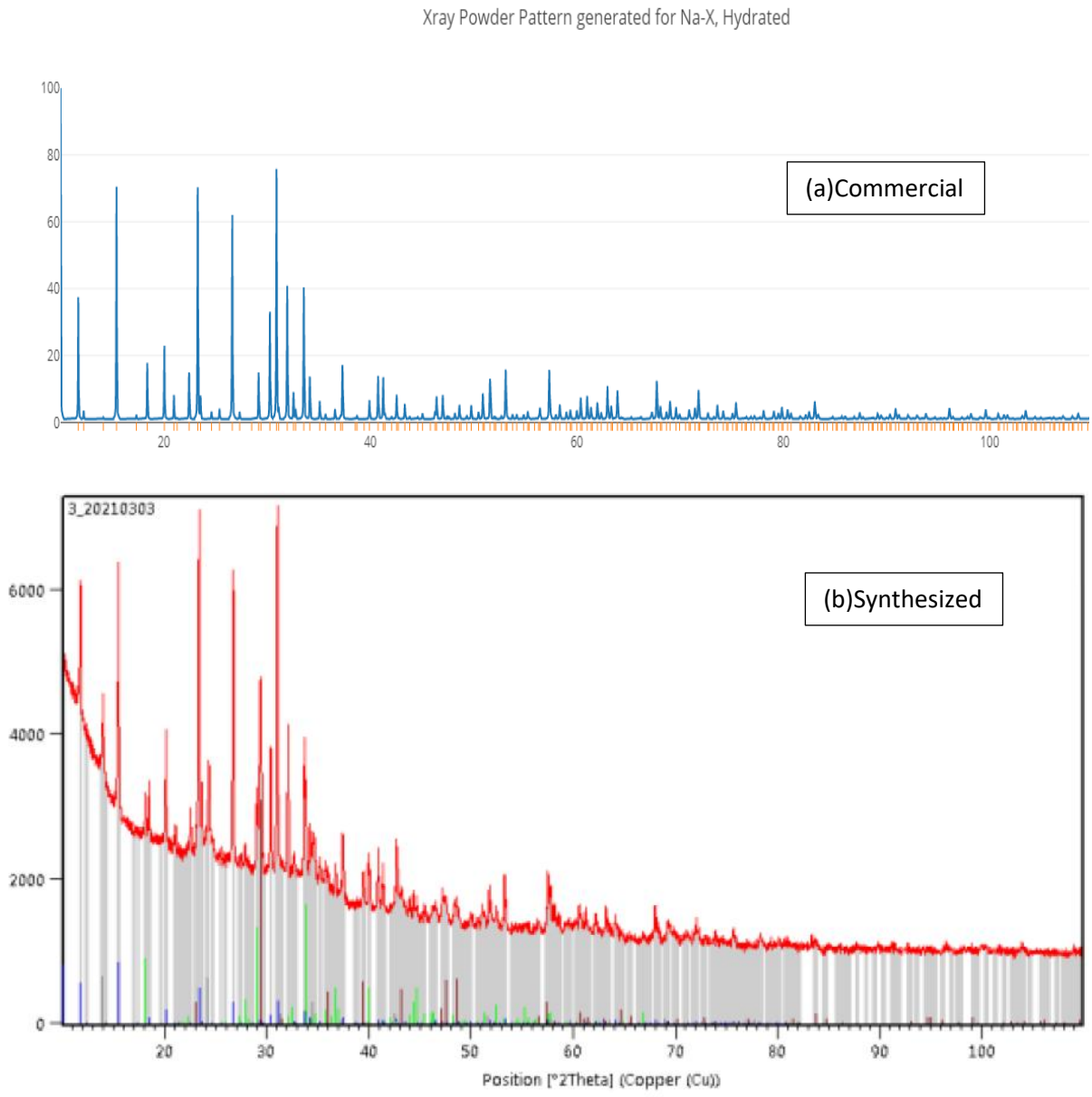

Figure-28: XRD Result Comparison, (a) Commercial 13-X Zeolite [81] (b) Synthesized 13-X Zeolite

Discussion: Figure-28 represents XRD pattern for commercial zeolite (top) and synthesized zeolite (bottom). For commercial zeolite, we see peaks at 9.9, 11.68, 15.42, 18.36, 20.04, 22.44, 23.34, 26.62, 29.2, 30.26, 30.88, 31.96, 32.58, 33.56, 34.08, 37.28, 40.76, 41.2, 51.6, 53.12, 57.38, 63, 64, 67.8 and 71.78. For our sample, we see reflections at 11.7, 15.45, 18.4, 20.04, 22.45, 23.4, 26.6, 29.2, 30.3, 30.8, 32,05, 32.6, 33.8, 34.1, 37.3, 40.7, 41.2, 51.6, 53.13, 57.4, 63.1, 68 and 72, which almost superimposes on the reflection peaks of commercial zeolite. We see other peaks as well, which indicate the presence of other crystalline phases as well. Other detected phases are Sodium Hydrogen Carbonate, $CaCO_3$, Sodium Aluminium Silicon Carbonate Oxide. Zeolite constitutes 60% of the total crystalline phase and the rest of the crystalline phases constitute 40%.

4.1.2. Surface Area Analysis

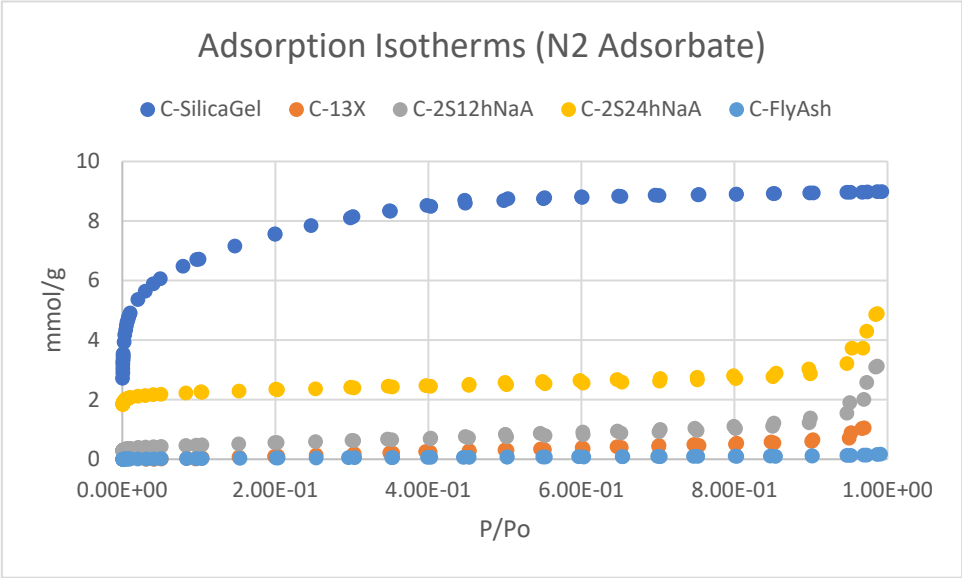

Figure-29: Adsorption Isotherm for Different Samples (at -196 ºC)

In the figure-29, we can see adsorption isotherm for Silica gel, Synthesized 13X Zeolite, Synthesized Na-A zeolite (12 h), Synthesized Na-A zeolite (24 h) and Fly Ash. The used adsorbate is nitrogen.

Using this data, the BET analysis has been done to determine the specific surface area of these samples. It has been found that the specific surface area for Silica Gel is 613 m^2/g. The surface area of silica gel ranges between 10 to 1000 m^2/g [1]. Also, during this analysis it has been found that at P/Po = 9.92474e-01, the volume of adsorbed nitrogen is 0.255g/g of the silica gel.

For synthesized Na-A Zeolite (12 h), the obtained specific surface area is 45 m^2/g. Usual specific surface area for commercial A type Zeolite is around 850 m^2/g [82], suggesting that the synthesized sample has only 5.3% zeolite. So, conversion of fly ash to zeolite was very low. From XRD analysis it has also been found that the desired zeolite was formed, along with some no-porous crystalline phases. These phases can block void spaces. Also, there are possible presences of some amorphous phases present which are apparently nonporous. This resulted into lower specific area. Also, during this analysis it has been found that at P/Po = 9.86300e-01, the volume of adsorbed nitrogen is 0.089 g/g of the Na-A Zeolite (12 h).

For synthesized Na-A zeolite (24 h), the obtained specific surface area is 185 m^2/g, which is 78% lower compared to commercial A zeolite, suggesting that the synthesized sample has only 22% zeolite. Just like the previous case, XRD analysis suggests that the desired zeolite was formed, along with some nonporous crystalline phases. Also, there are possible presence of some amorphous phases which are apparently nonporous. This resulted into lower specific area. Also, during this analysis it has been found that at P/Po = 9.86606e-01, the volume of adsorbed nitrogen is 0.14 g/g of the Na-A Zeolite (24 h).

For both, synthesized 13X Zeolite and Fly Ash, the obtained specific surface area is almost negligible. It suggests that these are almost nonporous materials. But XRD suggests that desired zeolite was formed. So, from XRD and surface area analysis we can deduce that only a very little portion was converted to zeolite and the sample contains significant amount of non-porous amorphous mass.

4.2. Adsorption Isotherm and Potential Use in Adsorption Chiller

4.2.1. Silica Gel

Temp: 25 °C

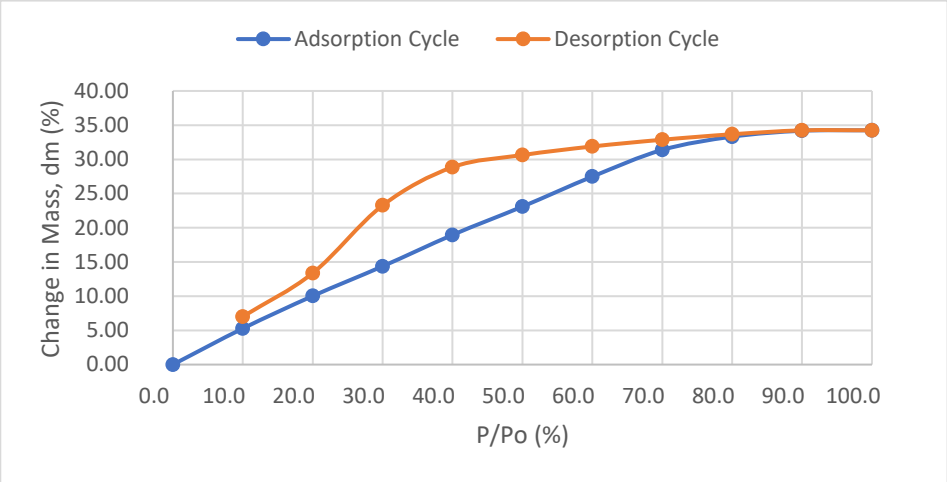

Figure-30: Adsorption Isotherm for Silica Gel (25 °C)

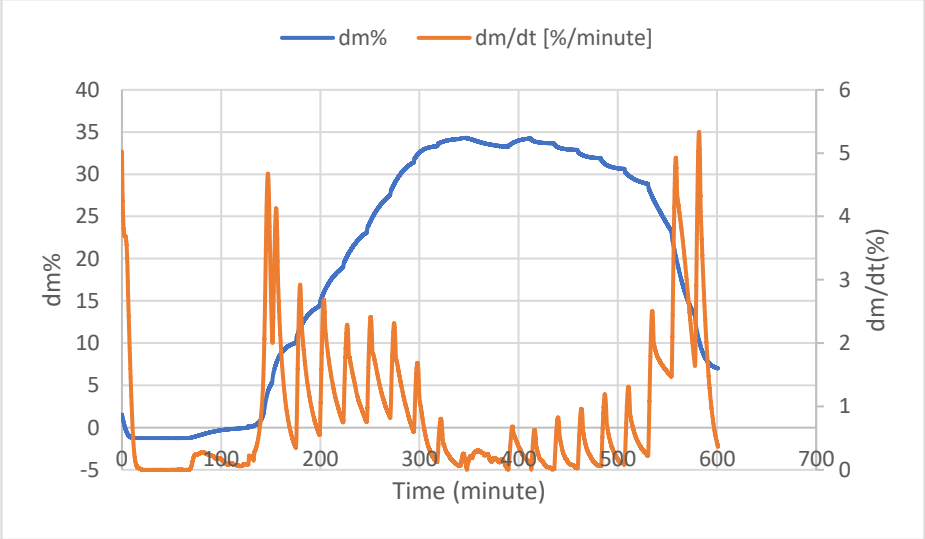

Figure-31: Adsorption Kinetics for Silica Gel (25 °C)

Discussion:

Table-4 (Appendix) represents the data for adsorption capacity of Silica Gel at 25 °C. For P/P_o=10%, the adsorption capacity is 5.28%. It increases up to 33.25% for P/P_o=100%. This amount of adsorption was achieved in 25 minutes. Within this time, silica gel almost reached its highest adsorption capacity. But adsorption kinetics suggests that it could have adsorbed and desorbed (for lower P/Po) more if time for each step was increased. It would result in less hysteresis.

1. From the shape of the isotherm in figure-30, it can be said that it is a type IV isotherm [41, 42, 43]. It has multilayer adsorption.
2. It also has hysteresis issue. From the shape it looks like a H2(b) type hysteresis which usually happens from pore neck blocking [43].

Temp: 35 °C

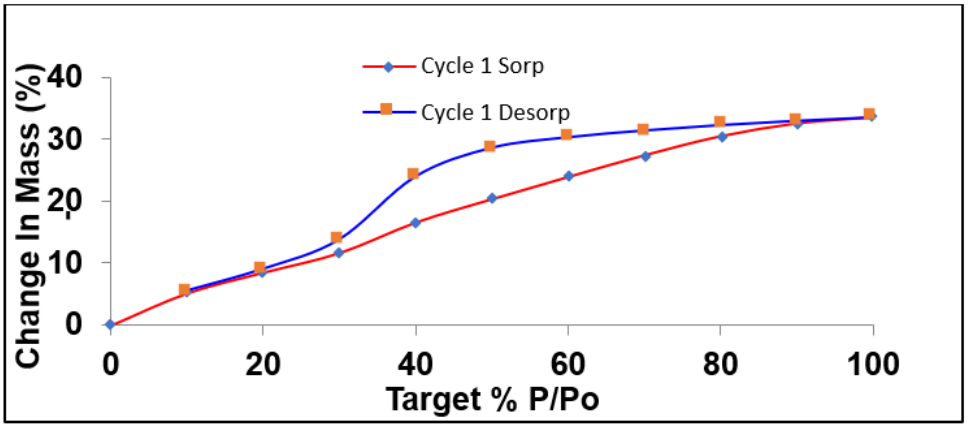

Figure-32: Adsorption Isotherm for Silica Gel (35 °C)

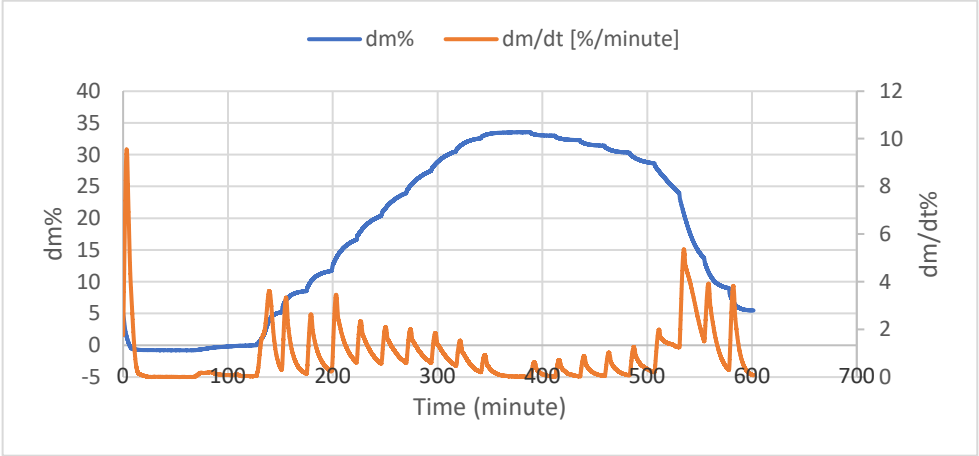

Figure-33: Adsorption Kinetics for Silica Gel (35 °C)

Discussion:

Table-5 (Appendix) represents the data for adsorption capacity of Silica Gel at 35 °C. For P/P_o=10%, the adsorption capacity is 5.19%. It increases up to 33.53% for P/P_o=100%. This amount of adsorption was achieved in 25 minutes. Within this time, silica gel almost reached its highest adsorption capacity. But adsorption kinetics suggests that it could have adsorbed and desorbed (for lower P/Po) more if time for each step was increased. It would result in less hysteresis.

1. From the shape of the isotherm in figure-32, it can be said that it is a type IV isotherm [41, 42, 43]. It has multilayer adsorption.
2. It also has significant hysteresis issue. From the shape it looks like a H2(b) type hysteresis which usually happens from pore neck blocking [43]. It closes at P/P_o=20%.

Temp: 45 °C

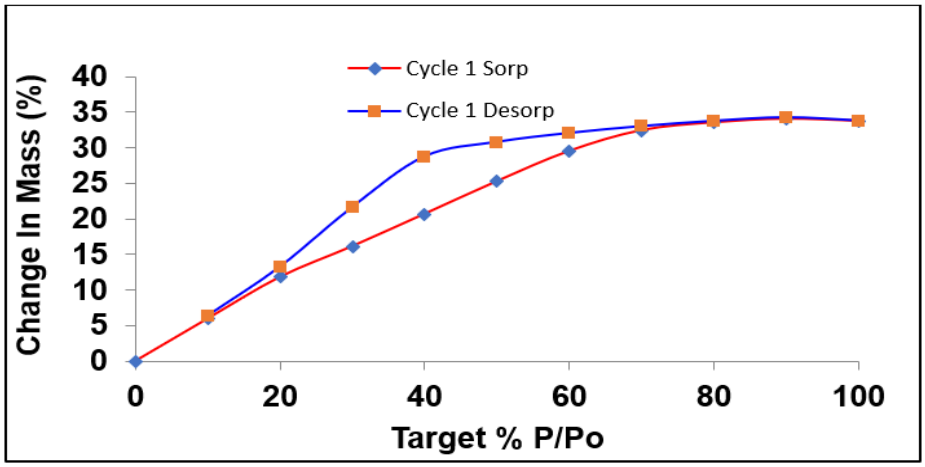

Figure-34: Adsorption Isotherm for Silica Gel (45 °C)

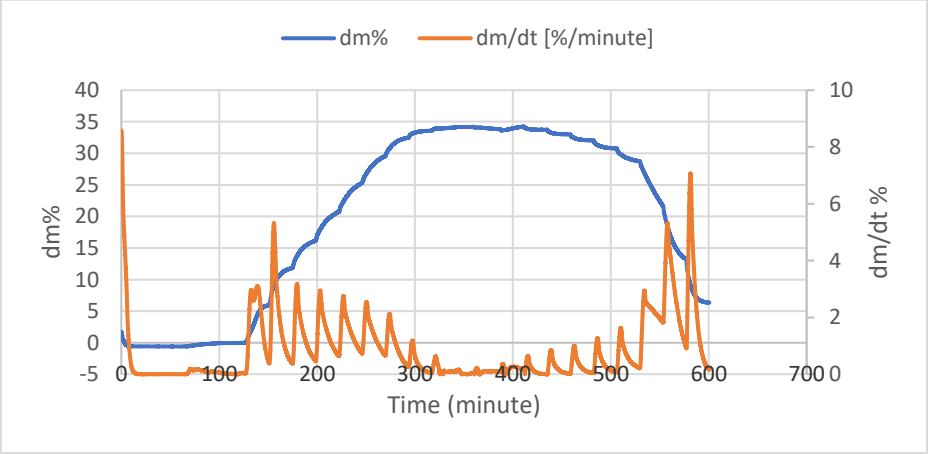

Figure-35: Adsorption Kinetics for Silica Gel (45 °C)

Discussion:

Table-6(Appendix) represents the data for adsorption capacity of Silica Gel at 45 °C. For P/P_o=10%, the adsorption capacity is 5.96%. It increases up to 33.78% for P/P_o=100%. This amount of adsorption was achieved in 25 minutes. Within this time, silica gel almost reached its highest adsorption capacity. But adsorption kinetics suggests that it could have adsorbed and desorbed (for lower P/Po) more if time for each step was increased. It would result in less hysteresis.

1. From the shape of the isotherm in figure-34, it can be said that it is a type IV isotherm [41, 42, 43]. It has multilayer adsorption.
2. It also has significant hysteresis issue. From the shape it looks like a H2(b) type hysteresis which usually happens from pore neck blocking [43].

Temp: 55 °C

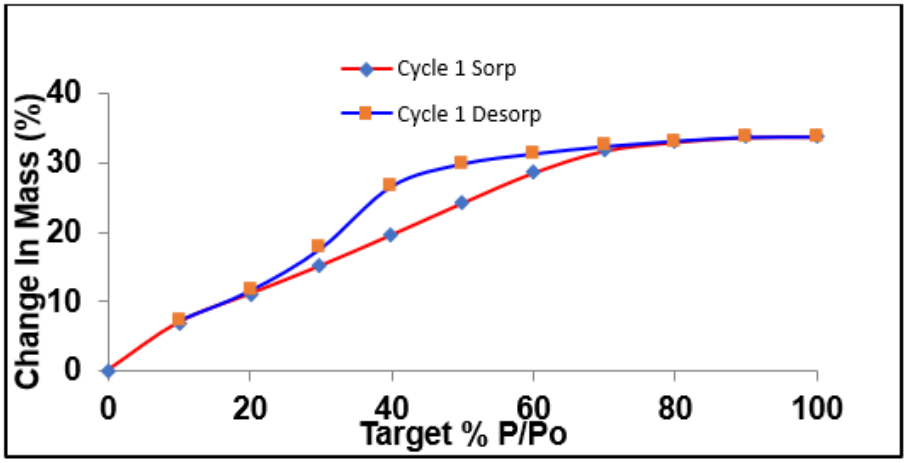

Figure-36: Adsorption Isotherm for Silica Gel (55 °C)

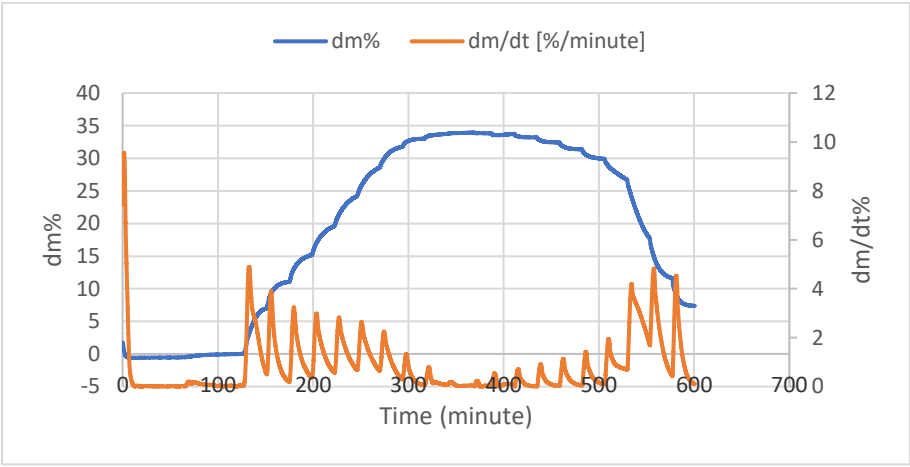

Figure-37: Adsorption Kinetics for Silica Gel (55 °C)

Table-7 (Appendix) represent the data for adsorption capacity of Silica Gel at 55 °C. For P/P_o=10%, the adsorption capacity is 6.98%. It increases up to 33.82% for P/P_o=100%. This amount of adsorption was achieved in 25 minutes. Within this time, silica gel almost reached its highest adsorption capacity. But adsorption kinetics suggests, it could have adsorbed and desorbed (for lower P/Po) more if time for each step was increased. It would result in less hysteresis.

1. From the shape of the isotherm in figure-36, it can be said that it is a type IV isotherm [41, 42, 43]. It has multilayer adsorption.
2. It also has significant hysteresis issue. From the shape it looks like a H2(b) type hysteresis which usually happens from pore neck blocking [43]. But closes at P/P_o=20%.

Temp 65 °C

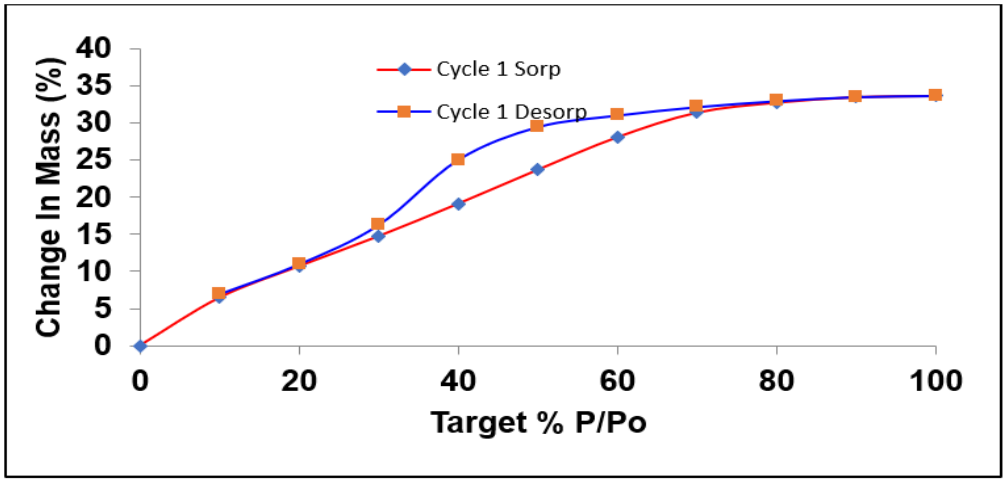

Figure-38: Adsorption Isotherm for Silica Gel (65 °C)

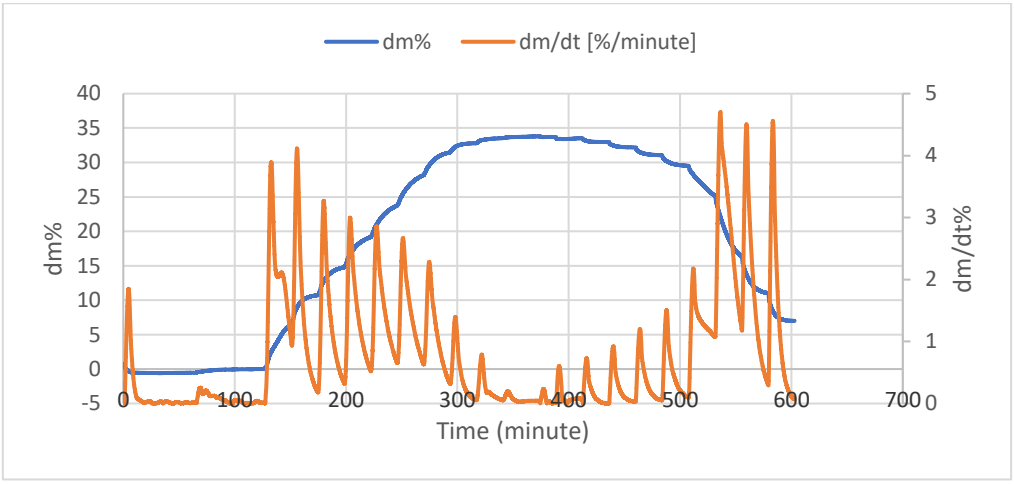

Figure-39: Adsorption Kinetics for Silica Gel (65 °C)

Discussion:

Table-8 (Appendix) represents the data for adsorption capacity of Silica Gel at 65 °C. For P/P_o=10%, the adsorption capacity is 6.47%. It increases up to 33.69% for P/P_o=100%. This amount of adsorption was achieved in 25 minutes. Within this time, silica gel almost reached its highest adsorption capacity. But adsorption kinetics suggests that it could have adsorbed and desorbed (for lower P/Po) more if time for each step was increased. It would result in less hysteresis.

1. From the shape of the isotherm in figure-38, it can be said that it is a type IV isotherm [41, 42, 43]. It has multilayer adsorption.
2. It also has significant hysteresis issue. From the shape, it looks like a H2(b) type hysteresis which usually happens from pore neck blocking [43]. The hysteresis loop is smaller due to increased temperature. It closes at P/P_o=20%.

Overall Discussion:

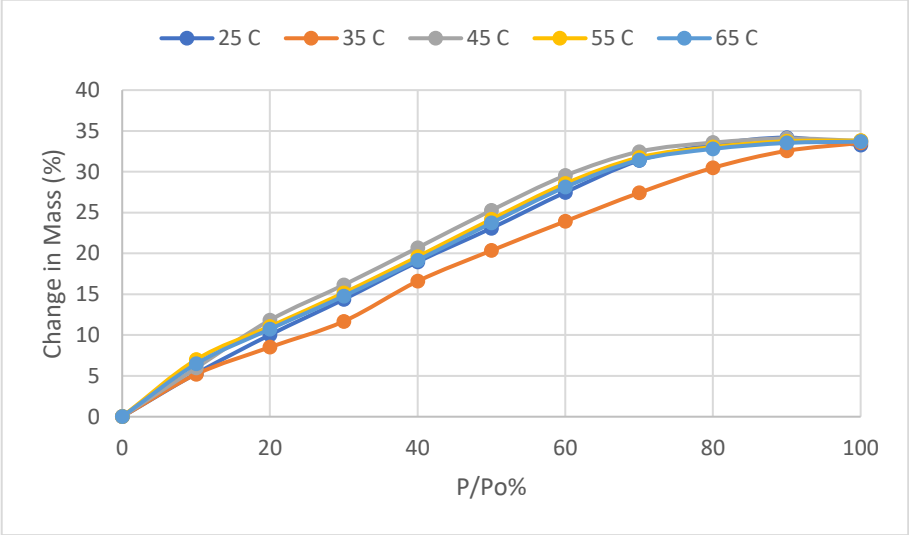

Figure-40: Adsorption Isotherm at Different Temperatures

Figure-40 shows the isotherm at different temperature (for respective saturation pressure). It seems, the shape of the isotherms is almost similar and does not represent a particular trend regarding the amount of adsorption in case of isosteric change in pressure and temperature.

4.2.2. Fly Ash

Temp: 25 °C

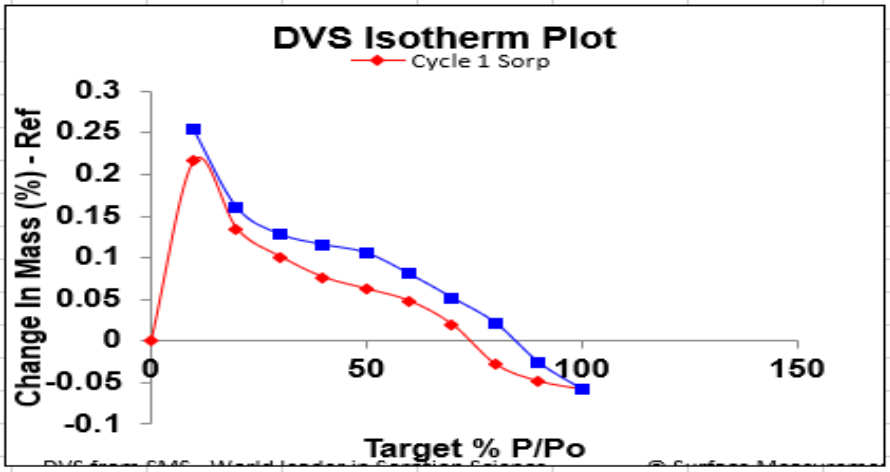

Figure–41 : Adsorption Isotherm for Fly Ash (25 °C)

Temp: 65 °C

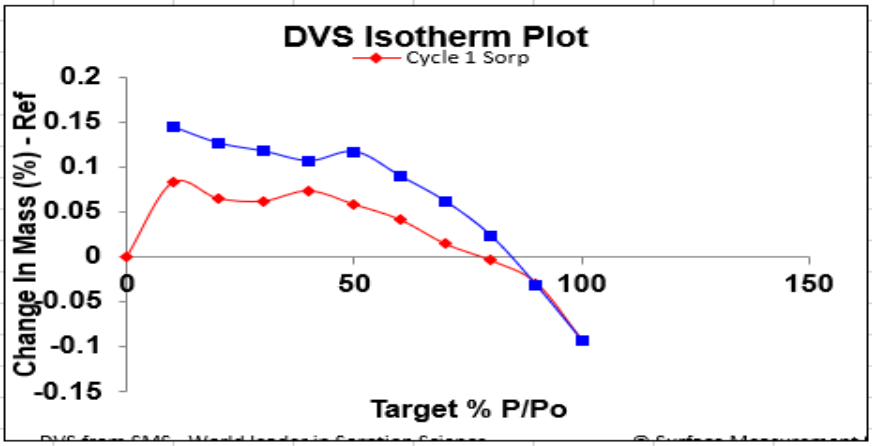

Figure-42: Adsorption Isotherm for Fly Ash (65 °C)

Discussion

The adsorption isotherms for fly ash look very strange and are definitely erroneous. It happens because the adsorption capacity is very small, and it is within the range of error of the device.

4.2.3 Synthesized Na – A Zeolite (12 h)

Temp: 25 °C

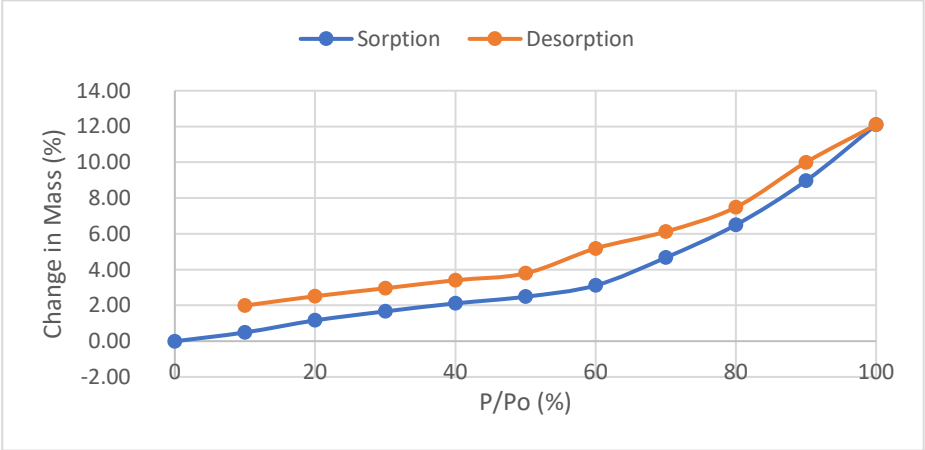

Figure-43: Adsorption Isotherm for Synthesized Na -A Zeolite (12 h) (25 °C)

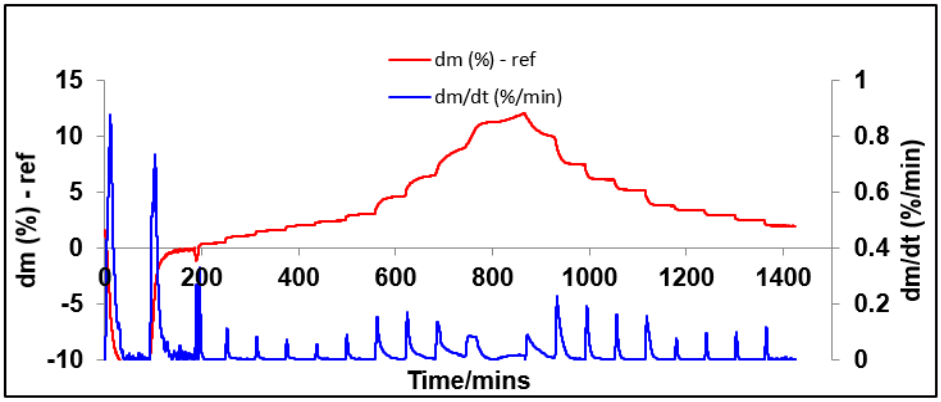

Figure-44: Adsorption Kinetics for Synthesized Na -A Zeolite (12 h) (25 °C)

Discussion:

Table-11(Appendix) represents the data for adsorption capacity of Na-A Zeolite (12 h) at 25 °C. For P/P_o=10%, the adsorption capacity is 0.49%. It increases up to 12.09% for P/P_o=100%. This amount of adsorption was achieved in 60 minutes. The adsorption kinetics (figure-44) suggests that for higher pressure if we increased the duration of adsorption, this sample would have been able to adsorb a little more water vapor. But for lower P/Po (which is actually the working condition for adsorption chiller[61, 62, 64, 65, 69-78]), equilibrium was almost reached in less than 20 minutes.

1. From the shape of the isotherm in figure-43, it can be said that it is a type IV isotherm[41, 42, 43]. The flat region indicates monolayer adsorption, followed by a rise (after P/P_o=50%) which indicates multilayer adsorption. It is a trait of mesoporous materials [41, 42, 43], but it does not seem to be the case here. The adsorption in lower pressure region occurred due to presence of zeolite. The increase in adsorption higher pressure region occurred due to capillary condensation in intergranular voids. Also, hydration probably played a part.
2. It also has significant hysteresis issue. The hysteresis loop does not close even at lower pressure. It reaches the highest value, 2.07, at P/P_o=60%. It remains almost similar for rest of the pressure regions, although increases a little at lower pressure region.

Temp: 35 °C

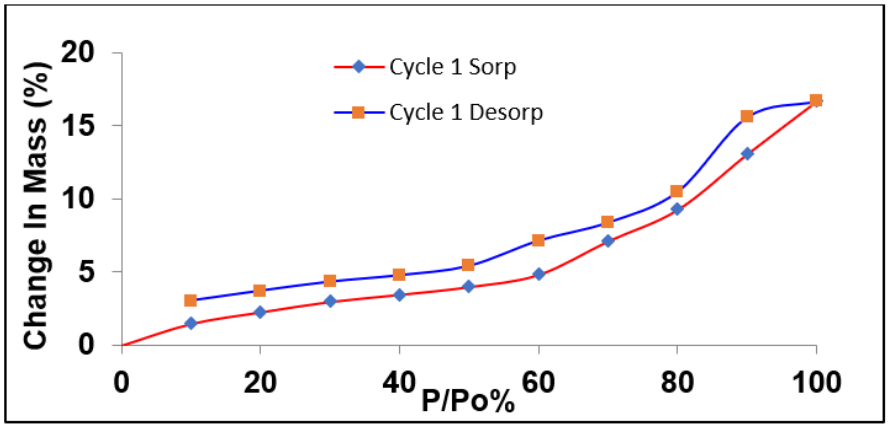

Figure-45: Adsorption Isotherm for Synthesized Na -A Zeolite (12 h) (35 °C)

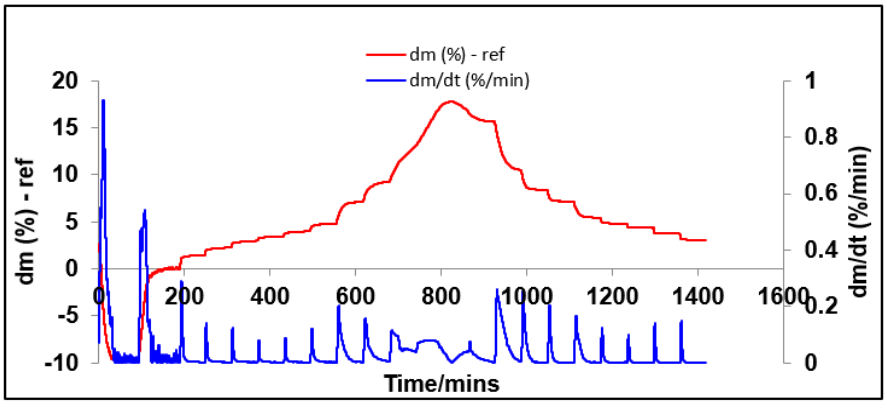

Figure-46: Adsorption Kinetics for Synthesized Na -A Zeolite (12 h) (35 °C)

Discussion:

Table-12 (Appendix) represents the data for adsorption capacity of Na-A Zeolite (12 h) at 35 °C. For P/P_o=10%, the adsorption capacity is 1.48%. It increases up to 16.70% for P/P_o=100%. This amount of adsorption was achieved in 60 minutes. The adsorption kinetics (figure-46) suggests that for higher pressure if we increased the duration of adsorption, this sample would have been able to adsorb a little more water vapor. But for lower P/Po (which is actually the working condition for adsorption chiller[61, 62, 64, 65, 69-78]), equilibrium was almost reached in less than 20 minutes.

1. From the shape of the isotherm in figure-45, it can be said that it is a type IV isotherm. The flat region indicates monolayer adsorption, followed by a rise (after P/P_o=50%.) which indicates multilayer adsorption [41, 42, 43]. The adsorption in lower pressure region occurred due to presence of zeolite. The increase in adsorption higher pressure region occurred due to capillary condensation in intergranular voids. Also, hydration played a part probably.
2. It also has significant hysteresis issue. The hysteresis loop does not close even at lower pressure. It reaches the highest value, 2.32, at P/P_o=60%. It remains almost similar for rest of the pressure regions.

Temp: 45 °C

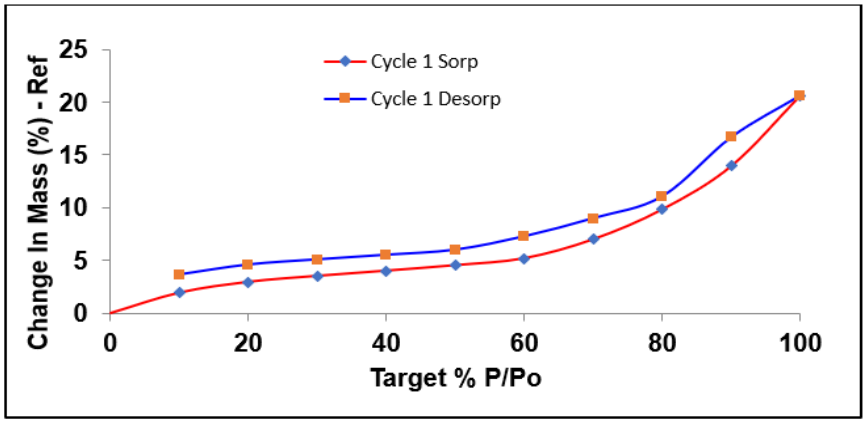

Figure-47: Adsorption Isotherm for Synthesized Na -A Zeolite (12 h) (45 °C)

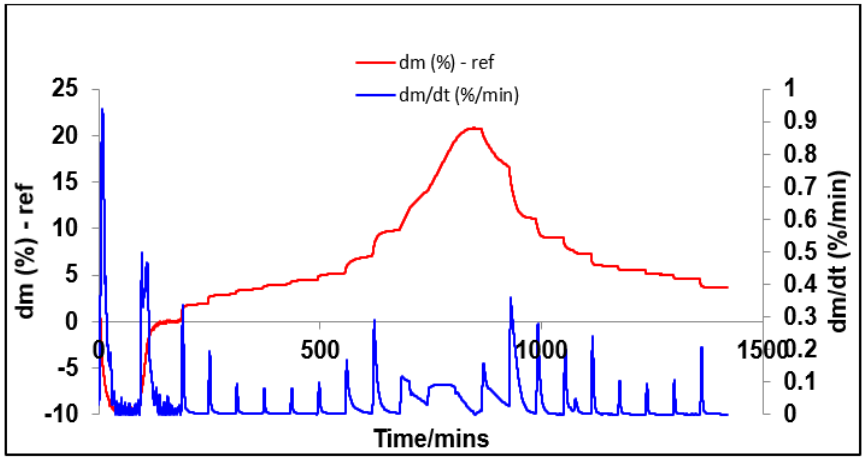

Figure-48: Adsorption Kinetics for Synthesized Na -A Zeolite (12 h) (45 °C)

Discussion:

Table-13(Appendix) represents the data for adsorption capacity of Na-A Zeolite (12) at 45 °C. For P/P_o=10%, the adsorption capacity is 1.94%. It increases up to 20.65% for P/P_o=100%. This amount of adsorption was achieved in 60 minutes. The adsorption kinetics (figure-48) suggests that for higher pressure if we increased the duration of adsorption, this sample would have been able to adsorb a little more water vapor. But for lower P/Po (which is actually the working condition for adsorption chiller[61, 62, 64, 65, 69-78]), equilibrium was almost reached in less than 20 minutes.

1. From the shape of the isotherm in figure-47, it can be said that it is a type IV isotherm. The flat region indicates monolayer adsorption, followed by a rise (after P/P_o=60%,) which indicates multilayer adsorption. The adsorption in lower pressure region occurred due to presence of zeolite. The increase in adsorption higher pressure region occurred due to capillary condensation in intergranular voids. Also, hydration played a part probably.
2. The hysteresis loop does not close even at lower pressure. It reaches the highest value, 2.06, at P/P_o=60%. It remains almost similar for rest of the pressure regions.

Temp: 55 °C

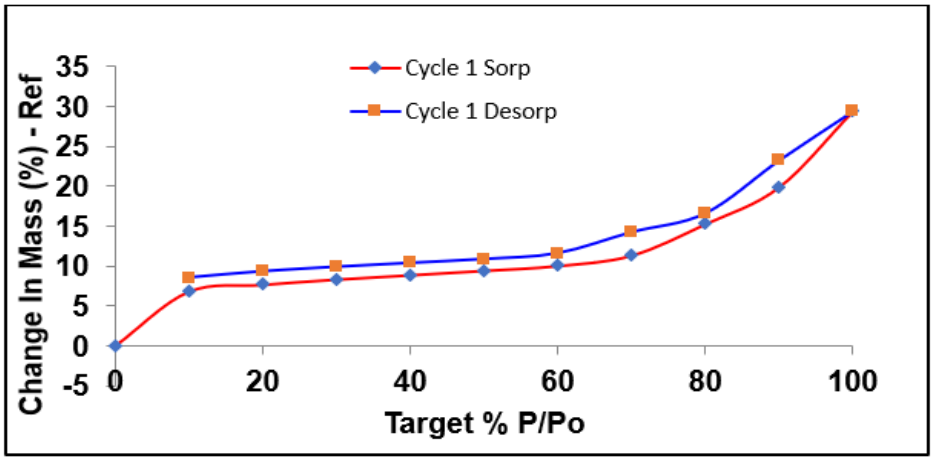

Figure-49: Adsorption Isotherm for Synthesized Na -A Zeolite (12 h) (55 °C)

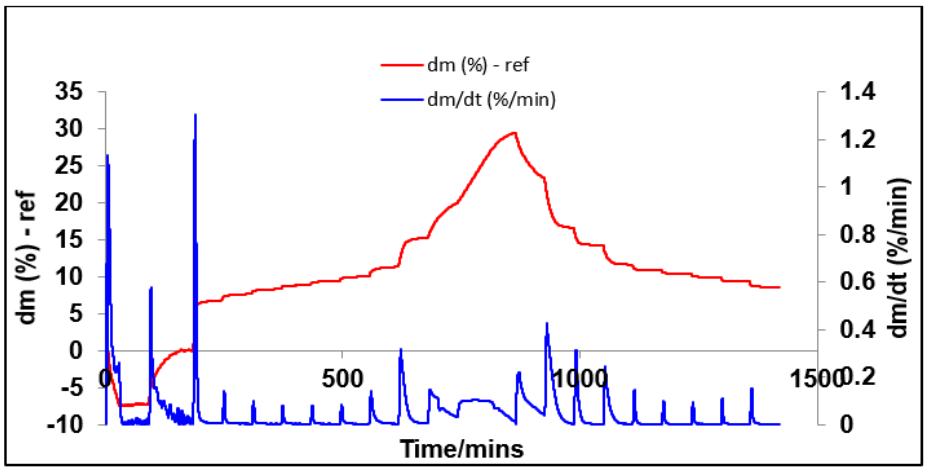

Figure-50: Adsorption Kinetics for Synthesized Na -A Zeolite (12 h) (55 °C)

Discussion:

Table-14 (Appendix) represents the data for adsorption capacity of Na-A Zeolite (12 h) at 55 °C. For P/P_o=10%, the adsorption capacity is 6.83%. It increases up to 29.45% for P/P_o=100%. This amount of adsorption was achieved in 60 minutes. The adsorption kinetics (figure-50) suggests that for higher pressure if we increased the duration of adsorption, this sample would have been able to adsorb a little more water vapor. But for lower P/Po (which is actually the working condition for adsorption chiller[61, 62, 64, 65, 69-78]), equilibrium was almost reached in less than 20 minutes.

1. From the shape of the isotherm in figure-49, it can be said that it is a type IV isotherm. The flat region indicates monolayer adsorption, followed by a rise (after P/P_o=70%,) which indicates multilayer adsorption [41, 42, 43]. The adsorption in lower pressure region occurred due to presence of zeolite. The increase in adsorption higher pressure region occurred due to capillary condensation in intergranular voids. Also, hydration played a part probably.
2. It also has significant hysteresis issue. The hysteresis loop does not close even at lower pressure. It reaches the highest value, 2.91, at P/P_o=70%. It remains almost similar for rest of the pressure regions.

Temp: 65 ° C

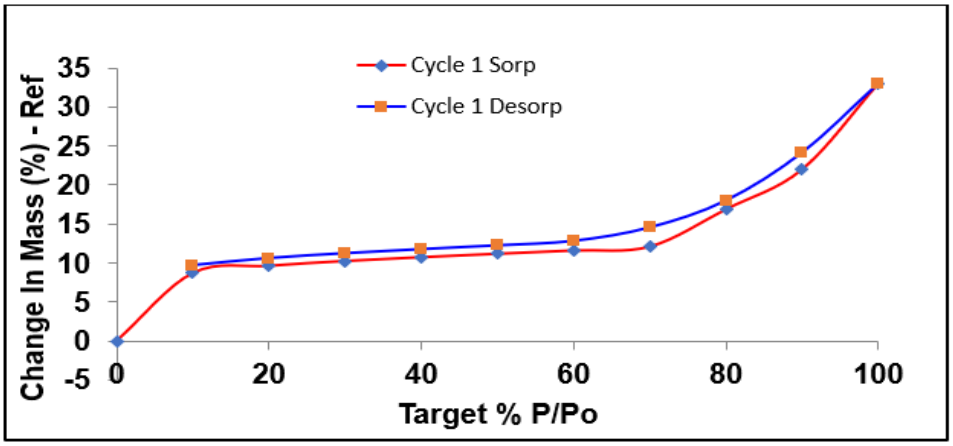

Figure-51: Adsorption Isotherm for Synthesized Na -A Zeolite (12 h) (65 °C)

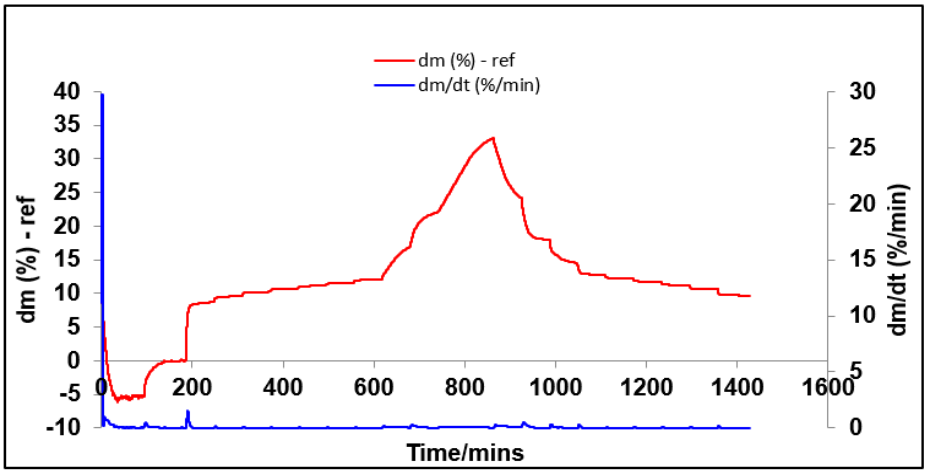

Figure-52: Adsorption Kinetics for Synthesized Na -A Zeolite (12 h) (65 °C)

Discussion:

Table-15 (Appendix) represents the data for adsorption capacity of Na-A Zeolite (12) at 65 ºC. For P/P_o=10%, the adsorption capacity is 8.71%. It increases up to 33.07% for P/P_o=100%. This amount of adsorption was achieved in 60 minutes. If we look at the adsorption kinetics (figure-46), it can be observed that if we increased the duration of adsorption, this sample would have been able to adsorb a little more water vapor for higher pressure. But for lower P/Po (which is actually the working condition for adsorption chiller[61, 62, 64, 65, 69-78]), equilibrium was almost reached in less than 15 minutes.

1. From the shape of the isotherm in figure-51, it can be said that it is a type IV isotherm. The flat region indicates monolayer adsorption, followed by a rise (after P/P_o=70%) which indicates multilayer adsorption. The adsorption in lower pressure region occurred due to presence of zeolite. The increase in adsorption higher pressure region occurred due to capillary condensation in intergranular voids. Also, hydration played a part probably.
2. It also has significant hysteresis issue. The hysteresis almost closes at P/P_o=10%. It reaches the highest value, 2.43, at P/P_o=70%. Then it keeps decreasing.

Overall Discussion:

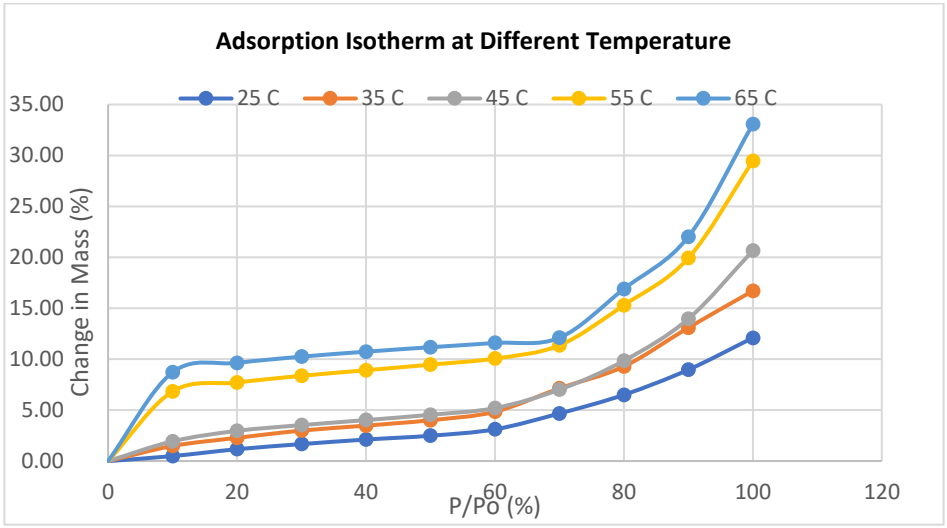

Figure-53: Adsorption Isotherm at Different Temperature (Synthesized Na-A Zeolite 12 h)

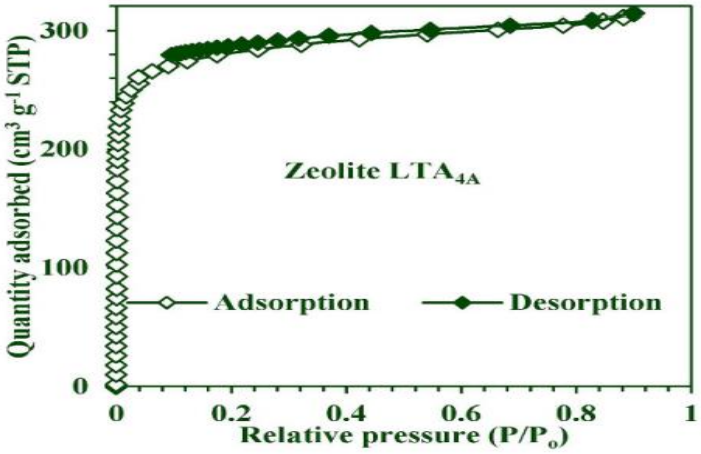

Figure-54: Adsorption Isotherm at 25 ºC (Commercial Na-A Zeolite) [83]

Figure-53 shows that the isotherm at different temperature (for respective saturation pressure). It seems, the shape of the isotherms is similar and represent a particular trend regarding the amount of adsorption in case of isosteric change in pressure and temperature. It increases with increasing temperature and pressure. As already mentioned, the shape looks like type IV, although the usual shape for commercial Na-A zeolite is Type I(figure-54) and the adsorption capacity is also very high at lower P/P_o compared to synthesized Na-A Zeolite (12 h). For commercial Na-A zeolite and synthesized Na-A zeolite (12 h), the adsorption capacity at 25 ^oC and P/Po=20% is 28% and 1.66% respectively. XRD and surface area analysis suggest that there are presences of other non-porous crystalline phases and amorphous phases, which explain the reason for having a different type of isotherm and lower adsorption capacity.

If we look at the adsorption kinetics (figure-44), we can observe that the sample mass actually increased at P/P_o=0% (almost 10 %) at 25 ^oC. It reduced with increasing temperature. But there was no vapor flow according to the method. It happened due to the fact that temperature was only applied in the sample carrier only and that affected the mass. Also, it indicates that even after the degasification period, there was vapor in the system which was re-adsorbed.

Potential Use in Adsorption Chiller: The performance of adsorption refrigeration system is determined by COP and SCP. These two parameters largely depend on how the adsorbent-adsorbate working pair performs, such as how quickly the adsorbent can adsorb and desorb the refrigerant and at what amount under the working condition (pressure and temperature) [1,53].

For this sample, the adsorption occurred for 60 minutes. But, if we look at adsorption kinetics for our sample in figure-44, 46, 48, 50 and 52, it actually took less than 20 minutes to reach equilibrium (almost) at lower P/P_o, whereas for silica gel it was around 25 minutes. It implies that this sample will have better adsorption refrigeration cycle time compared to silica gel.

To analyse the potentiality of our sample, we are considering the operating condition and performance of adsorption chillers from previously published papers [61, 62, 64, 65, 69-78]. For those chillers, during adsorption, the pressure of the adsorbent bed is always lower, usually above 15% of the saturation pressure and sometimes can be as high as 45% [61, 62, 64, 65, 69-78]. The temperature usually ranges between 25-40 ^oC mostly [61, 62, 64, 65, 69-78]. Same papers suggest, during desorption of the refrigerant the temperature varies significantly (usually more than 65 ^oC and can get as high as 120 ^oC for solar energy), whereas the pressure is usually less than 5% of the saturation pressure of the respective temperature and sometimes it can be more than 10% as well [61, 62, 64, 65, 69-78]. Based on these research works, two different working conditions have been considered.

First, for adsorption, if we consider 25 ^oC temperature and 30% of saturation pressure (for water at 25 ^oC), we can observe that silica gel (14.37 %) adsorbed much more water vapor than this sample (1.66%) at this temperature and pressure. For desorption, if we consider the temperature is 65 ^oC and pressure is 10% of the saturation pressure, the adsorption amount at this condition is 9.68% and 6.99% for our sample and silica gel, respectively. So, at this condition, the amount of water refrigerant available for vaporization at the evaporator in case of our sample and silica gel should be 0% and 7.38% respectively. So, our sample cannot produce any cold energy and replace silica gel as adsorbent for adsorption chiller.

Second, for adsorption, if we consider 25 ^oC temperature and 20% of saturation pressure (for water at 25 ^oC), we can observe that silica gel (10.02 %) adsorbed much more water vapor than this sample (1.16%) at this temperature and pressure. For desorption, if we consider the temperature is 65 ^oC and pressure is 10% of the saturation pressure,

the adsorption amount at this condition is 9.68% and 6.99%. So, at this condition, the amount of water refrigerant available for vaporization at the evaporator in case of our sample and silica gel should be 0% and 3.03% respectively. So, again, our sample cannot produce any cold energy and replace silica gel as adsorbent for adsorption chiller.

4.2.4 Synthesized Na-A (24 h) Zeolite

Temp: 25 °C

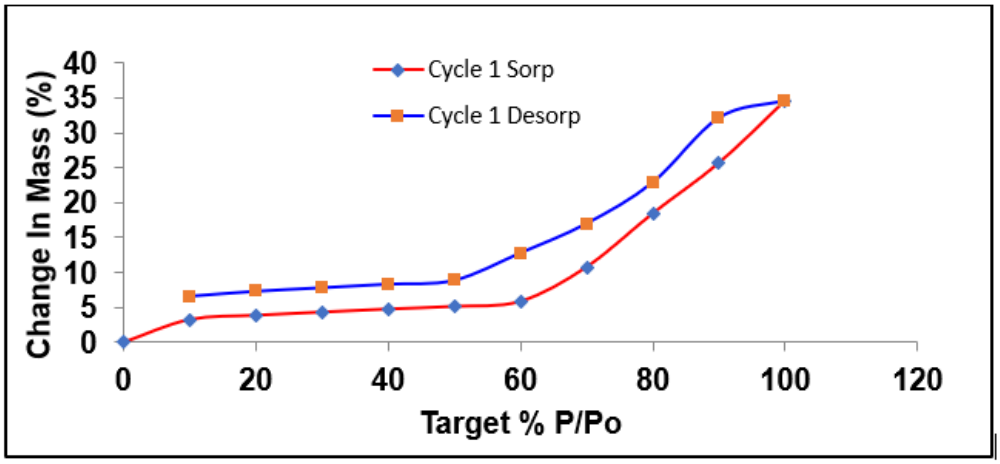

Figure-55: Adsorption Isotherm for Synthesized Na -A Zeolite (24 h) (25 °C)

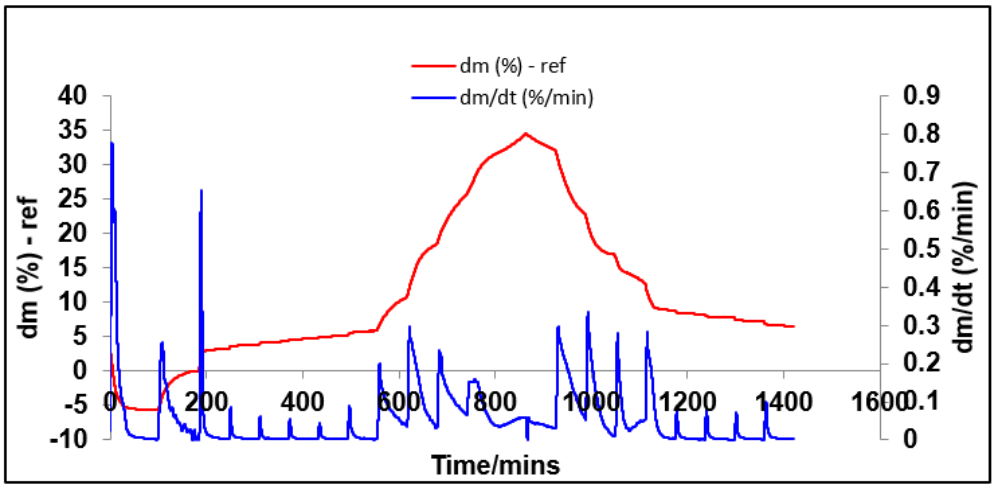

Figure-56: Adsorption Kinetics for Synthesized Na -A Zeolite (24 h) (25 °C)

Discussion:

Table-16(Appendix) represents the data for adsorption capacity of Na-A Zeolite (24 h) at 25 °C. For P/P_o=10%, the adsorption capacity is 3.28%. It increases up to 34.57% for P/P_o=100%. This amount of adsorption was achieved in 60 minutes. The adsorption kinetics (figure-56) suggests that for higher pressure if we increased the duration of adsorption, this sample would have been able to adsorb a little more water vapor. But for lower P/Po (which is actually the working condition for adsorption chiller[61, 62, 64, 65, 69-78]), equilibrium was almost reached in less than 20 minutes.

1. From the shape of the isotherm in figure-55, it can be said that it is a type IV isotherm. The flat region indicates monolayer adsorption, followed by a rise (after P/P_o=60%,) which indicates multilayer adsorption that starts after P/P_o=60% [41, 42, 43]. It is a trait of mesoporous materials [41, 42, 43], but it

does not seem to be the case here. The adsorption in lower pressure region occurred due to presence of zeolite. The increase in adsorption higher pressure region occurred due to capillary condensation in intergranular voids. It seems $KHCO_3$ also contributed, while hydration played a part probably.

2. It also has significant hysteresis issue. The hysteresis does not close even at lower pressure. It reaches the highest value, 6.88, at P/P_o=60%. Then it decreases and remains almost similar.

Temp: 35 °C

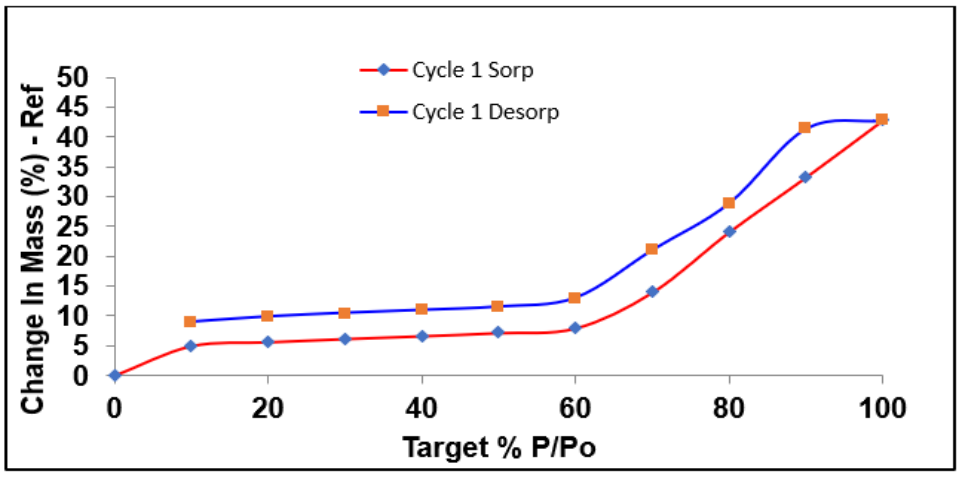

Figure-57: Adsorption Isotherm for Synthesized Na -A Zeolite (24 h) (35 °C)

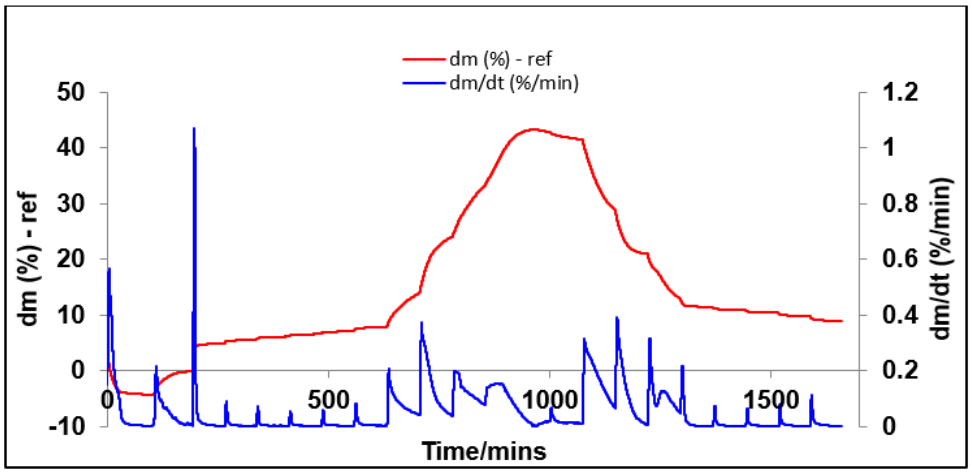

Figure-58: Adsorption Kinetics for Synthesized Na -A Zeolite (24 h) (35 °C)

Discussion:

Table-17 (Appendix) represents the data for adsorption data of synthesized Na-A Zeolite (24) at 35 °C. For P/P_o=10%, the adsorption capacity is 4.97%. It increases up to 42.81% for P/P_o=100%. This amount of adsorption was achieved in 60 minutes. The adsorption kinetics (figure-58) suggests that for higher pressure if we increased the duration of adsorption, this sample would have been able to adsorb a little more water vapor. But for lower P/Po (which is actually the working condition for adsorption chiller[61, 62, 64, 65, 69-78]), equilibrium was almost reached in less than 20 minutes.

1. Isotherm in figure-57 suggests that it is a type IV isotherm. The flat region indicates monolayer adsorption, followed by a rise which indicates multilayer adsorption that starts after P/P_o=60% [41, 42, 43]. The adsorption in lower pressure region occurred due to presence of zeolite. The increase in

adsorption in higher pressure region occurred due to capillary condensation in intergranular voids. It seems $KHCO_3$ also contributed, while hydration played a part probably.

2. It also has significant hysteresis issue. The hysteresis does not close even at lower pressure. It reaches 8.20 at P/P_o=90% and 7.08 at P/P_o=70%. Then it decreases and remains almost similar.

Temp: 45 °C

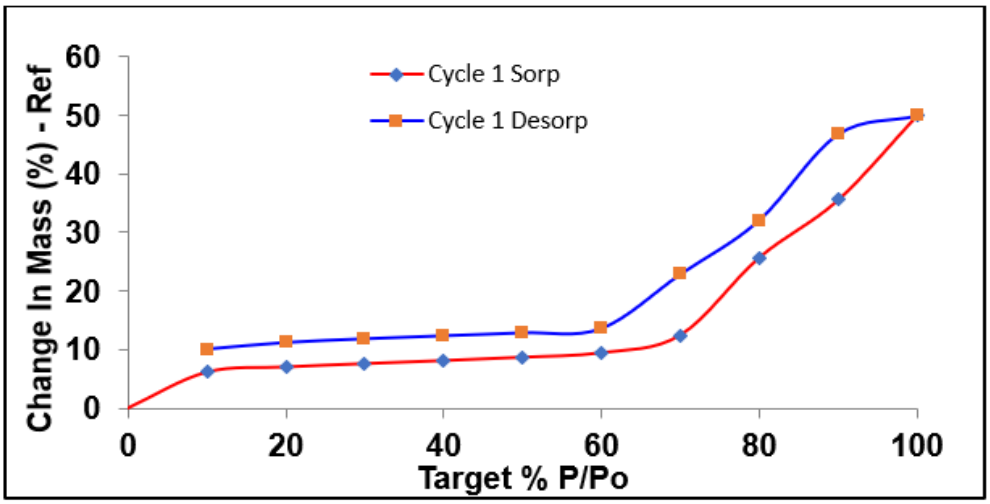

Figure-59: Adsorption Isotherm for Synthesized Na -A Zeolite (24 h) (45 °C)

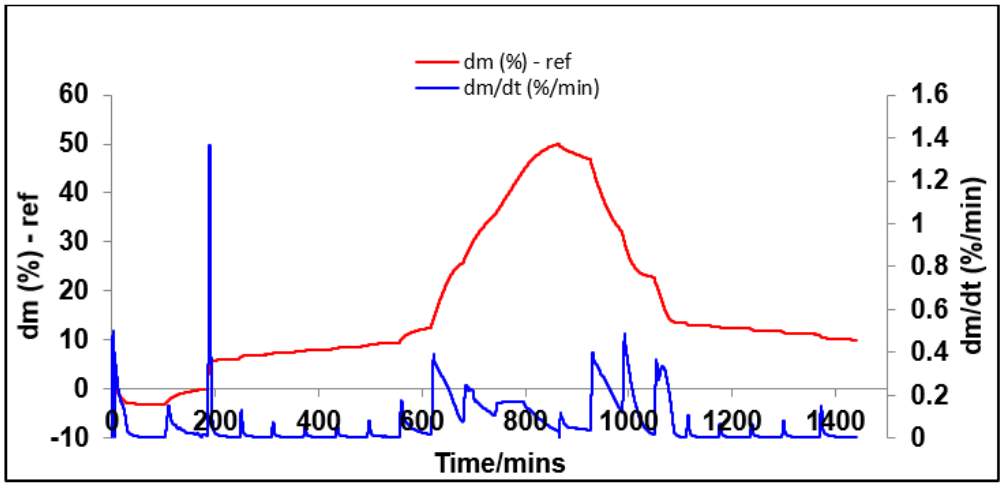

Figure-60: Adsorption Kinetics for Synthesized Na -A Zeolite (24 h) (45 °C)

Discussion:

Table-18 (Appendix) represents the data for adsorption capacity of Na-A Zeolite (24h) at 45 °C. For P/P_o=10%, the adsorption capacity is 6.16%. It increases up to 50.02% for P/P_o=100%. This amount of adsorption was achieved in 60 minutes. The adsorption kinetics suggests (figure-60) that for higher pressure if we increased the duration of adsorption, this sample would have been able to adsorb a little more water vapor. But for lower P/Po (which is actually the working condition for adsorption chiller[61, 62, 64, 65, 69-78]), equilibrium was almost reached in less than 20 minutes.

1. From the shape of the isotherm in figure-59, it can be said that it is a type IV isotherm. The flat region indicates monolayer adsorption, followed by a rise which indicates multilayer adsorption that starts after P/P_o=70% [41, 42, 43]. The adsorption in lower pressure region occurred due to presence of zeolite. The

increase in adsorption in higher pressure region occurred due to capillary condensation in intergranular voids. It seems $KHCO_3$ also contributed, while hydration played a part probably.

2. It also has significant hysteresis issue. The hysteresis does not close even at lower pressure. It reaches 11.25 at P/P_o=90% and 10.35 at P/P_o=70%. Then it decreases and remains almost similar.

Temp: 55 °C

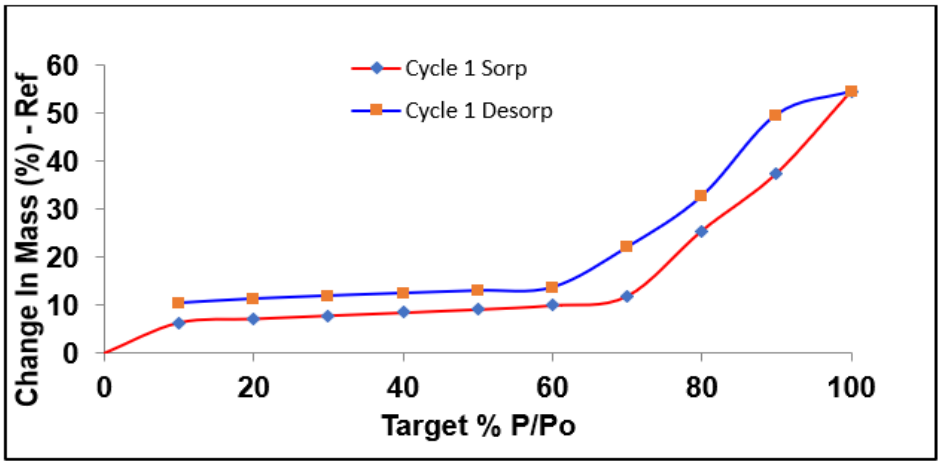

Figure-61: Adsorption Isotherm for Synthesized Na -A Zeolite (24 h) (55 °C)

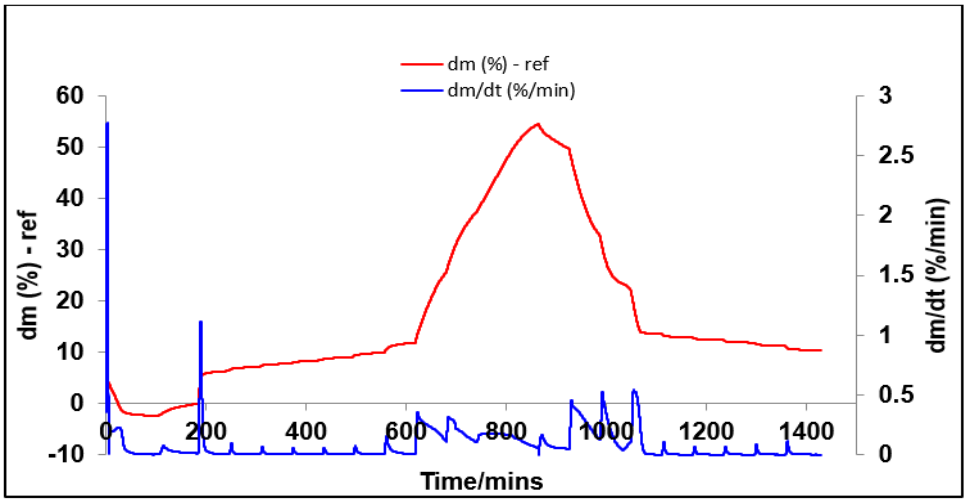

Figure-62: Adsorption Kinetics for Synthesized Na -A Zeolite (24 h) (55 °C)

Discussion:

Table-19 (Appendix) represents the data for adsorption capacity of Na-A Zeolite (24) at 55 °C. For P/P_o=10%, the adsorption capacity is 6.37%. It increases up to 54.51% for P/P_o=100%. This amount of adsorption was achieved in 60 minutes. The adsorption kinetics (figure-62) suggests that for higher pressure if we increased the duration of adsorption, this sample would have been able to adsorb a little more water vapor. But for lower P/Po (which is actually the working condition for adsorption chiller[61, 62, 64, 65, 69-78]), equilibrium was almost reached in less than 15 minutes.

1. From the shape of the isotherm figure-61, it can be said that it is a type IV isotherm. The flat region indicates monolayer adsorption, followed by a rise which indicates multilayer adsorption that starts after P/P_o=70% [41, 42, 43]. The adsorption in lower pressure region occurred due to presence of zeolite. The

increase in adsorption in higher pressure region occurred due to capillary condensation in intergranular voids. It seems $KHCO_3$ also contributed, while hydration played a part probably.

2. It also has significant hysteresis issue. The hysteresis does not close even at lower pressure. It reaches 12.25 at P/P_o=90% and 10.14 at P/P_o=70%. Then it decreases and remains almost similar.

Temp: 65 °C

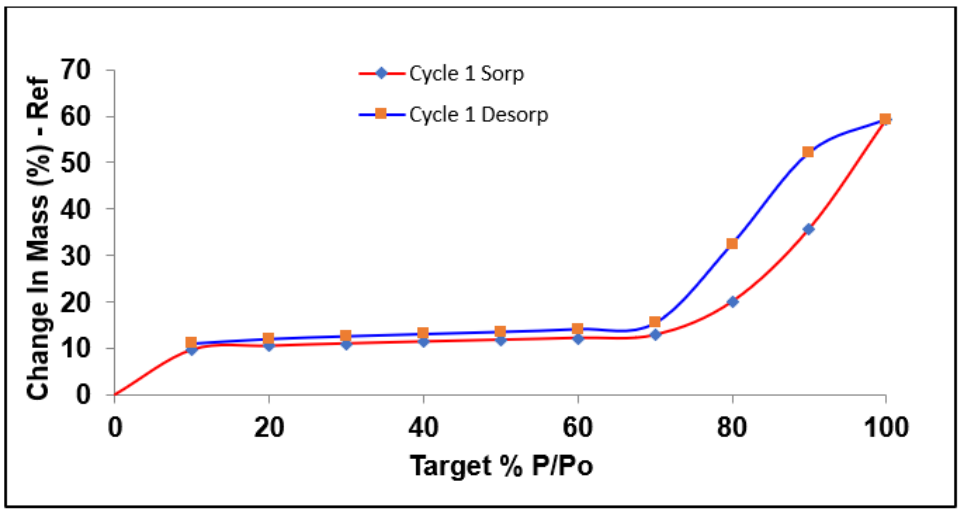

Figure-63: Adsorption Isotherm for Synthesized Na -A Zeolite (24 h) (65 °C)

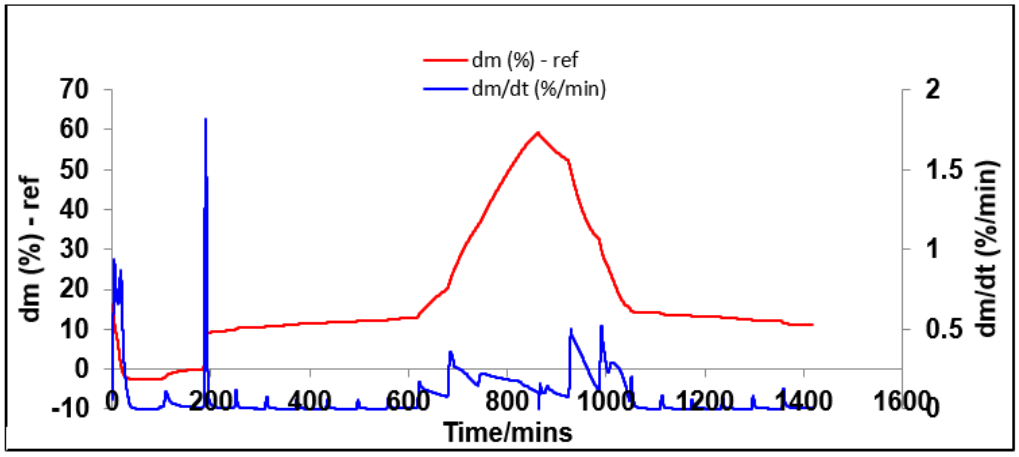

Figure-64: Adsorption Kinetics for Synthesized Na -A Zeolite (24 h) (65 °C)

Discussion:

Table-20 (Appendix) represents the data for adsorption capacity of Na-A Zeolite (24) at 65 °C. For P/P_o=10%, the adsorption capacity is 9.66%. It increases up to 59.33% for P/P_o=100%. This amount of adsorption was achieved in 60 minutes. The adsorption kinetics (figure-64) suggests that for higher pressure if we increased the duration of adsorption, this sample would have been able to adsorb a little more water vapor. But for lower P/Po (which is actually the working condition for adsorption chiller[61, 62, 64, 65, 69-78]), equilibrium was almost reached in less than 15 minutes.

1. This isotherm in figure-63 suggests that it is a type IV isotherm. The flat region indicates monolayer adsorption, followed by a rise which indicates multilayer adsorption that starts after P/P_o=70% [41, 42, 43]. The adsorption in lower pressure region occurred due to presence of zeolite. The increase in

adsorption in higher pressure region occurred due to capillary condensation in intergranular voids. It seems $KHCO_3$ also contributed, while hydration played a part probably.

2. It also has significant hysteresis issue. It reaches 16.41 at P/P_o=90% and 12.49 at P/P_o=80%. Then it decreases and almost decreases to zero at P/P_o=10%.

Overall Discussion:

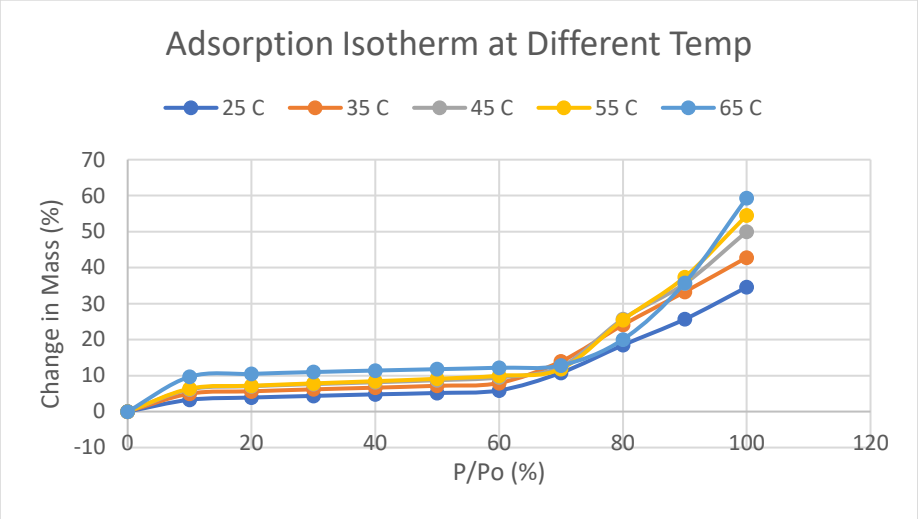

Figure-65: Adsorption Isotherm at Different Temperature (Synthesized Na-A Zeolite 24 h)

The above figure-65 shows that the isotherm at different temperature (for respective saturation pressure). It seems, the shape of the isotherms is similar and represent a particular trend regarding the amount of adsorption in case of isosteric change in pressure and temperature. It increases with increasing temperature and pressure. As already mentioned, the shape looks like type IV, although the usual shape for commercial Na-A zeolite is Type I(figure-54) and the adsorption capacity is also very high at lower P/P_o compared to synthesized Na-A Zeolite (24 h). For commercial Na-A zeolite and synthesized Na-A Zeolite (24 h), the adsorption capacity at 25 ^oC and P/Po=20% is 28% and 3.90% respectively. XRD and surface analysis suggest that there are presences of other non-porous crystalline phases and amorphous phases, which explain the reason for having a different type of isotherm and lower adsorption capacity.

If we look at the adsorption kinetics (figure-56), we can observe that the sample mass actually increased at P/P_o=0% (almost 5 %) at 25 ^oC. It reduced with increasing temperature. But there was no vapor flow according to the method. It happened due to the fact that temperature was only applied in the sample carrier only and that affected the mass. Also, it indicates that even after the degasification period, there was vapor in the system which was re-adsorbed.

Potential Use in Adsorption Chiller: The performance of adsorption refrigeration system is determined by COP and SCP. These two parameters largely depend on how the adsorbent-adsorbate working pair performs, such as how quickly the adsorbent can adsorb and desorb the refrigerant and at what amount under the working condition (pressure and temperature) [1,53].

For this sample, the adsorption occurred for 60 minutes. But, if we look at adsorption kinetics for our sample in figure-56, 58, 60, 62 and 64, it actually took less than 20 minutes to reach equilibrium at lower P/P_o, whereas for silica gel it was around 25 minutes. It implies that this sample will have better adsorption refrigeration cycle time compared to silica gel.

As I previously explained, based on the previous research works, the author is considering two different working conditions for this sample as well.

First, for adsorption, if we consider 25 °C temperature and 30% of saturation pressure (for water at 25 °C), we can observe that silica gel (14.37 %) adsorbed much more water vapor than this sample (4.35%) at this temperature and pressure. For desorption, if we consider the temperature is 65 °C and pressure is 10% of the saturation pressure, the adsorption amount at this condition is 11.03% and 6.99% for our sample and silica gel respectively. So, at these conditions, the amount of water refrigerant available for vaporization at the evaporator in case of our sample and silica gel should be 0% and 7.38% respectively. So, our sample cannot produce any cold energy and replace silica gel as adsorbent for adsorption chiller.

Second, for adsorption, if we consider 25 °C temperature and 20% of saturation pressure (for water at 25 °C), we can observe that silica gel (10.02 %) adsorbed much more water vapor than this sample (3.90%) at this temperature and pressure. For desorption, if we consider the temperature is 65 °C and pressure is 10% of the saturation pressure, the adsorption amount at this condition is 11.03% and 6.99%. So, at these conditions, the amount of water refrigerant available for vaporization at the evaporator in case of our sample and silica gel should be 0% and 3.03% respectively. So, again, our sample cannot produce any cold energy and replace silica gel as adsorbent for adsorption chiller.

4.2.5 Synthesized 13-X Zeolite

Temp: 25 °C

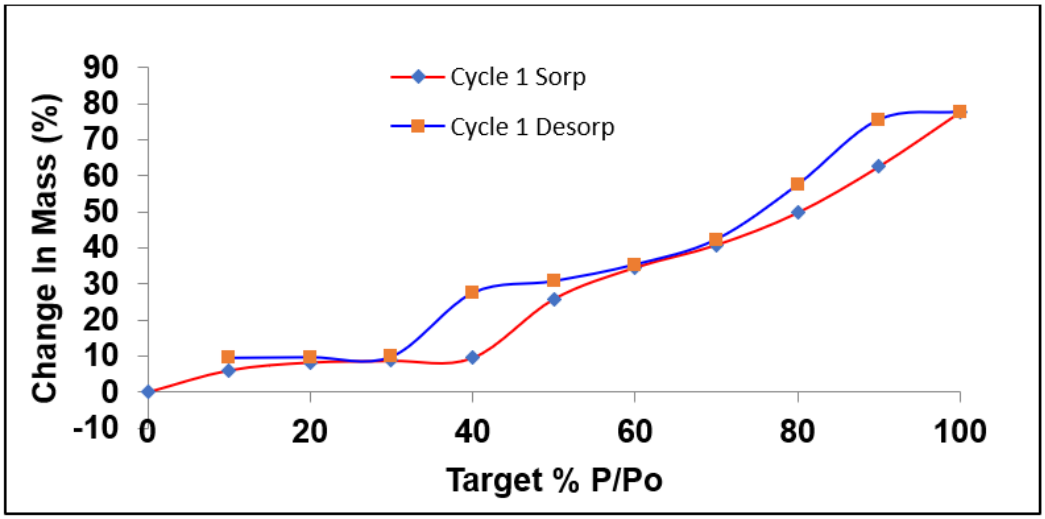

Figure-66: Adsorption Isotherm for Synthesized 13-X Zeolite (25 °C)

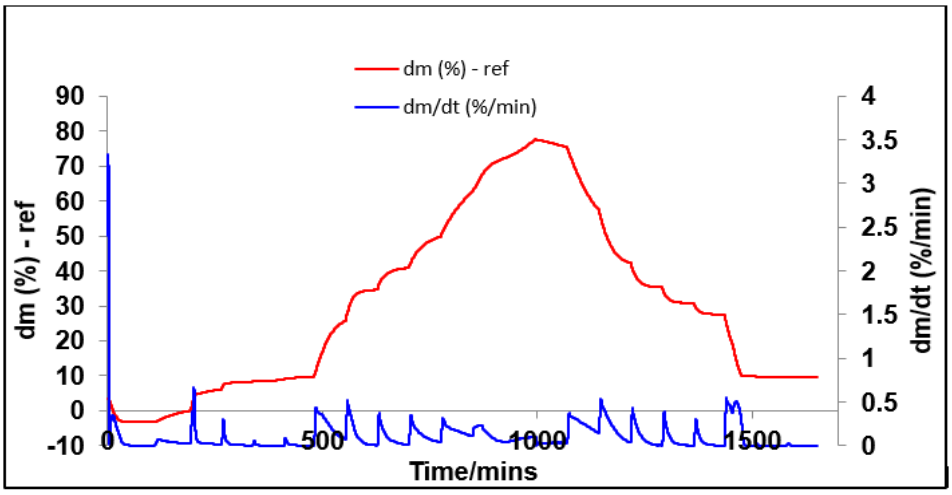

Figure-67: Adsorption Kinetics for Synthesized 13-X Zeolite (25 ^{o}C)

Discussion:

Table-21 (Appendix) represent the data for adsorption capacity of 13-X Zeolite at 25 ^{o}C. For P/P_o=10%, the adsorption capacity is 6.08%. It increases up to 77.64% for P/P_o=100%. This amount of adsorption has been achieved in 60 minutes. The adsorption kinetics (figure-67) suggests that for higher pressure if we increased the duration of adsorption, this sample would have been able to adsorb a little more water vapor. But for lower P/Po (which is actually the working condition for adsorption chiller[61, 62, 64, 65, 69-78]), equilibrium was almost reached in less than 25 minutes.

1. From the shape of the isotherm in figure-66, it can be said that this isotherm resembles type VI isotherm. The flat region indicates monolayer adsorption, followed by a rise (after P/P_o=40%). The adsorption in lower pressure region occurred due to presence of synthesized zeolite. The increase in adsorption in higher pressure region occurred due to capillary condensation in intergranular voids. It seems $NaHCO_3$ also contributed, while hydration played a part probably.
2. It also has significant hysteresis issue. The hysteresis initially reaches the highest point, then keeps decreasing until P/P_o=60%. Then, it increases again, followed by a decrease to close at P/P_o=30%.

Temp: 35 °C

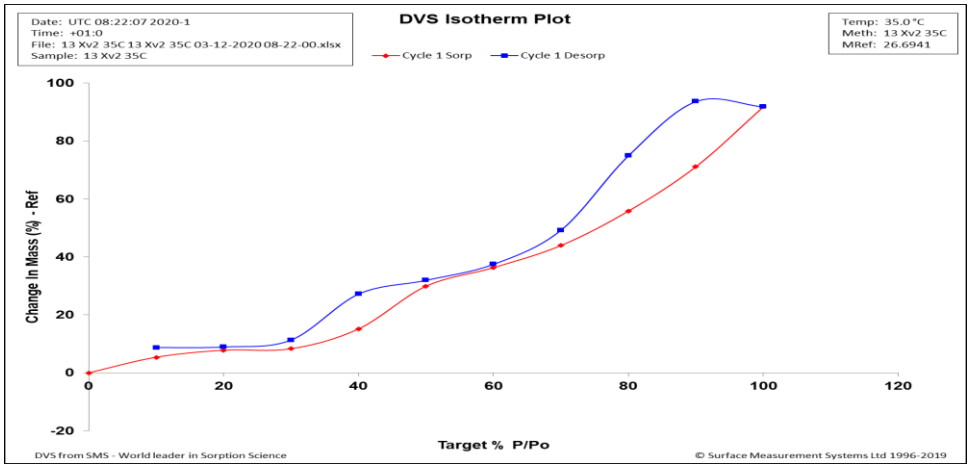

Figure-68: Adsorption Isotherm for Synthesized 13-X Zeolite (35 °C)

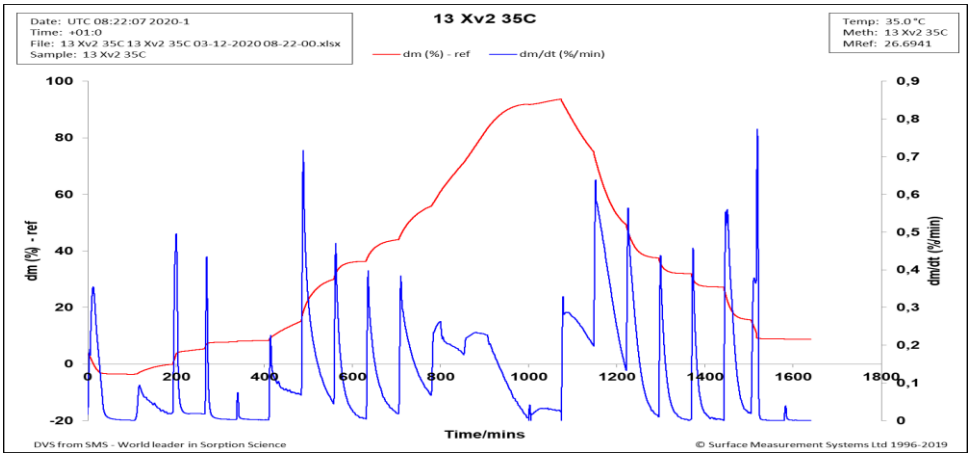

Figure-69: Adsorption Kinetics for Synthesized 13-X Zeolite (35 °C)

Discussion:

Table-22 (Appendix) represents the data for adsorption capacity of 13-X Zeolite at 35 °C. For P/P_o=10%, the adsorption capacity is 5.39%. It increases up to 91.88% for P/P_o=100%. This amount of adsorption has been achieved in 60 minutes. The adsorption kinetics (figure-69) suggests that for higher pressure if we increased the duration of adsorption, this sample would have been able to adsorb a little more water vapor. But for lower P/Po (which is actually the working condition for adsorption chiller [61, 62, 64, 65, 69-78]), equilibrium was almost reached in less than 25 minutes.

1. From the shape of the isotherm in figure-68, it can be said that it resembles a type VI isotherm. The flat region indicates monolayer adsorption, followed by a rise (after P/P_o=30%). The adsorption in lower pressure region occurred due to presence of synthesized zeolite. The increase in adsorption in higher pressure region occurred due to capillary condensation in intergranular voids. It seems $NaHCO_3$ also contributed, while hydration played a part probably.
2. It also has significant hysteresis issue. The hysteresis initially reaches the highest point, then keeps decreasing until P/P_o=60%. Then, it increases again, followed by a decrease up to P/P_o=20%. Then it increases again a little.

Temp: 45 °C

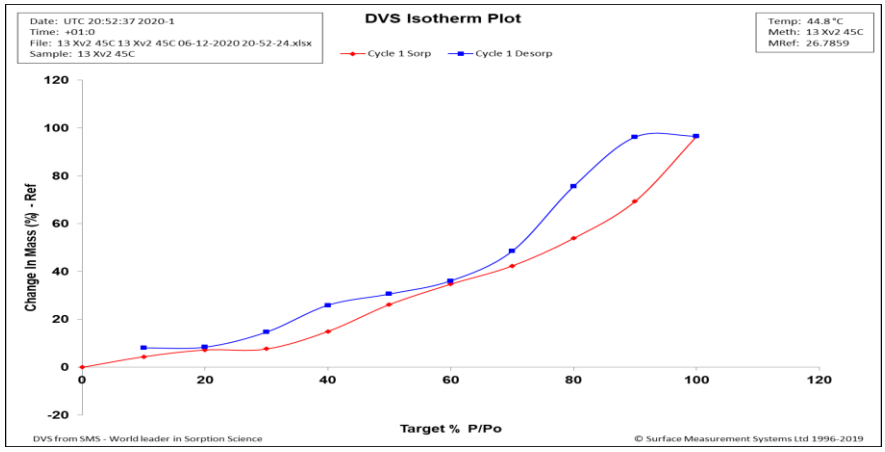

Figure-70: Adsorption Isotherm for Synthesized 13-X Zeolite (45 °C)

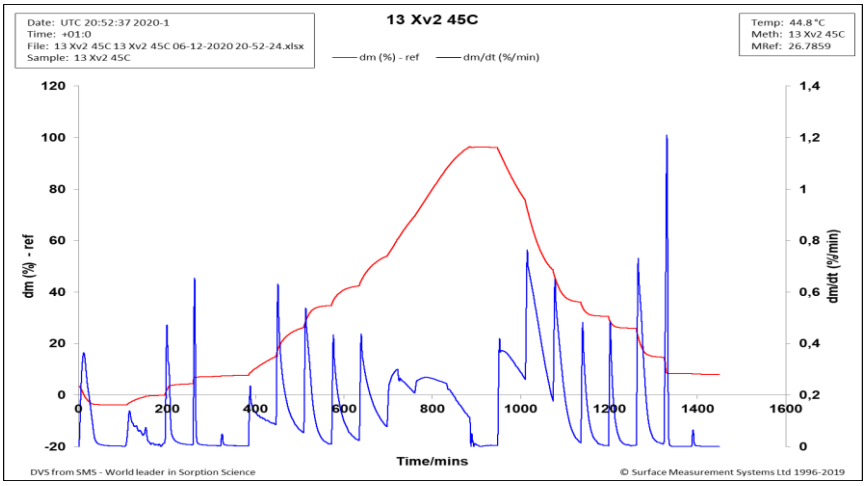

Figure-71: Adsorption Kinetics for Synthesized 13-X Zeolite (45 °C)

Discussion:

Table-23 (Appendix) represents the data for adsorption capacity of 13-X Zeolite at 45 °C. For P/P_o=10%, the adsorption capacity is 4.41%. It increases up to 96.53% for P/P_o=100%. This amount of adsorption was achieved in 60 minutes. The adsorption kinetics suggests (figure-71) that for higher pressure if we increased the duration of adsorption, this sample would have been able to adsorb a little more water vapor. But for lower P/Po (which is actually the working condition for adsorption chiller [61, 62, 64, 65, 69-78]), equilibrium was almost reached in less than 25 minutes.

1. From the shape of the isotherm in figure-70, it can be said that it is a type **VI** isotherm. The flat region indicates monolayer adsorption, followed by a rise (after P/P_o=30). The adsorption in lower pressure region occurred due to presence of synthesized zeolite. The increase in adsorption in higher pressure region occurred due to capillary condensation in intergranular voids. It seems $NaHCO_3$ also contributed, while hydration played a part probably.
2. It also has significant hysteresis issue. The hysteresis initially reaches the highest point, then keeps decreasing until P/P_o=60%. Then, it increases again, followed by a decrease up to P/P_o=20%. Then it increases again a little.

Temp: 55 °C

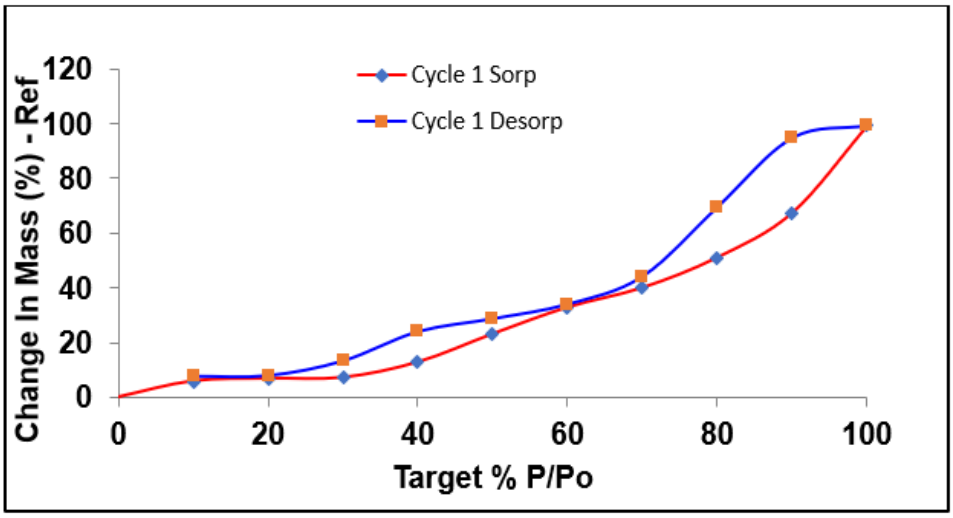

Figure-72: Adsorption Isotherm for Synthesized 13-X Zeolite (55 °C)

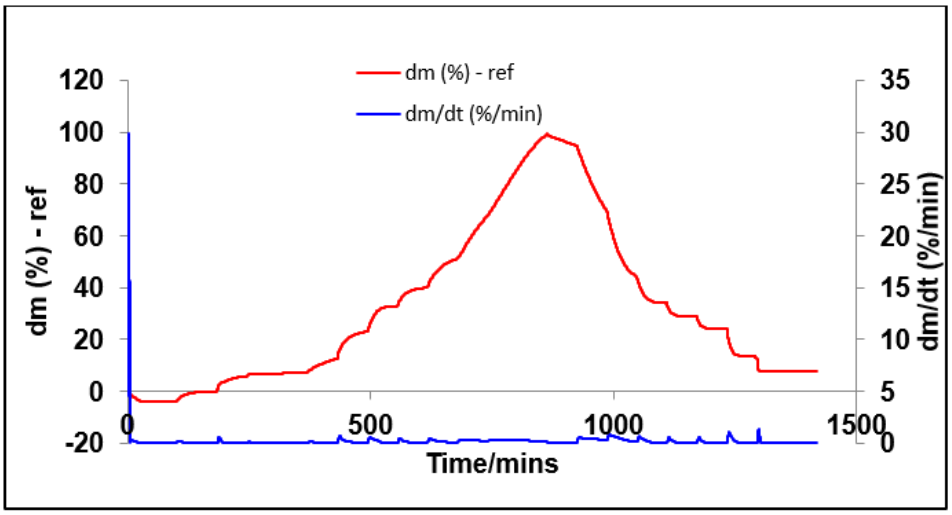

Figure-73: Adsorption kinetics for Synthesized 13-X Zeolite (55 °C)

Discussion:

Table-24 (Appendix) represents the data for adsorption capacity of 13-X Zeolite at 55 °C. For P/P_o=10%, the adsorption capacity is 5.86%. It increases up to 99.26% for P/P_o=100%. This amount of adsorption was achieved in 60 minutes. The adsorption kinetics (figure-73) suggests that for higher pressure if we increased the duration of adsorption, this sample would have been able to adsorb a little more water vapor. But for lower P/Po (which is actually the working condition for adsorption chiller [61, 62, 64, 65, 69-78]), equilibrium was almost reached in less than 20 minutes.

1. From the shape of the isotherm in figure-72, it can be said that it is a type **VI** isotherm. The flat region indicates monolayer adsorption, followed by a rise (after P/P_o=30%). The adsorption in lower pressure region occurred due to presence of synthesized zeolite. The increase in adsorption in higher pressure region occurred due to capillary condensation in intergranular voids. It seems $NaHCO_3$ also contributed, while hydration played a part probably.

2. It also has significant hysteresis issue. The hysteresis initially reaches the highest point, then keeps decreasing until P/P_o=60% (closes). Then, it increases again, followed by a decrease up to P/P_o=20%.

Temp: 65 °C

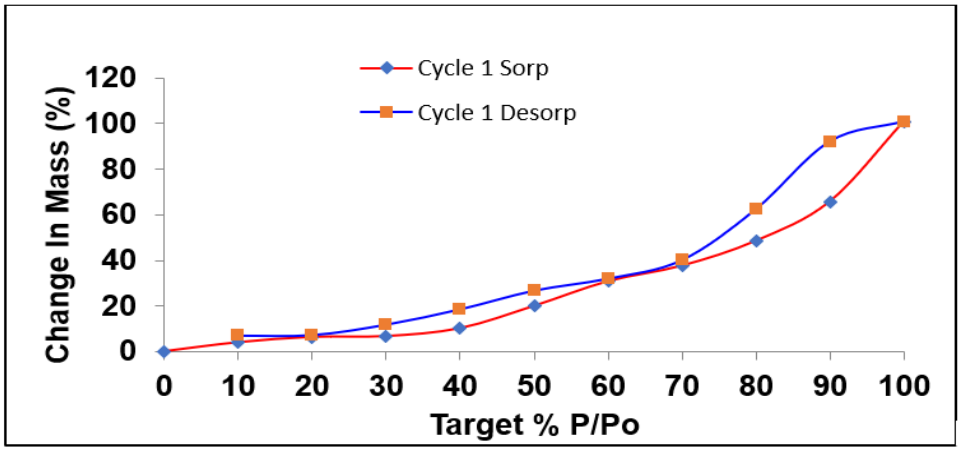

Figure-74: Adsorption Isotherm for Synthesized 13-X Zeolite (65 °C)

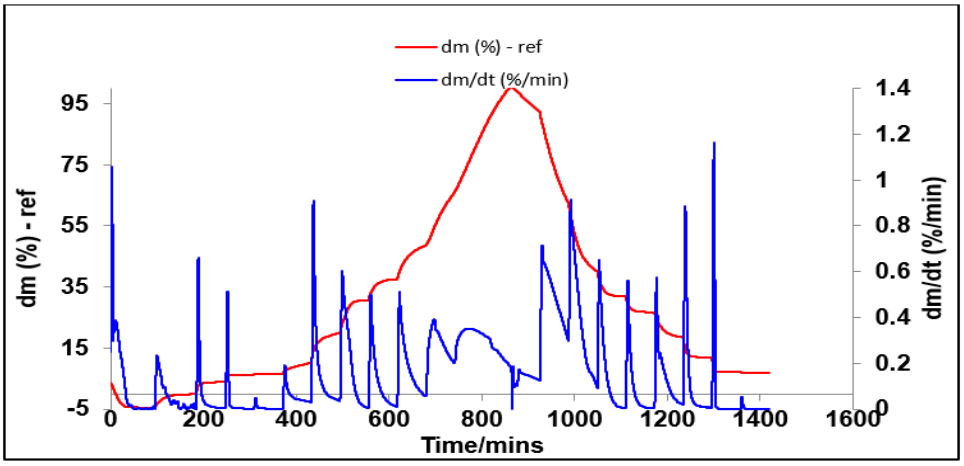

Figure-75: Adsorption Kinetics for Synthesized 13-X Zeolite (65 °C)

Discussion:

Table-25 (Appendix) represents the data for adsorption capacity of 13-X Zeolite at 65 °C. For P/P_o=10%, the adsorption capacity is 3.9%. It increases up to 100.9% for P/P_o=100%. This amount of adsorption was achieved in 60 minutes. The adsorption kinetics suggests (figure-75) that for higher pressure if we increased the duration of adsorption, this sample would have been able to adsorb a little more water vapor. But for lower P/Po (which is actually the working condition for adsorption chiller [61, 62, 64, 65, 69-78]), equilibrium was almost reached in less than 20 minutes.

1. From the shape of the isotherm in figure 73, it can be said that it is a type **VI** isotherm. The flat region indicates monolayer adsorption, followed by a rise (after P/P_o=30%). The adsorption in lower pressure region occurred due to presence of synthesized zeolite. The increase in adsorption in higher pressure region occurred due to capillary condensation in intergranular voids. It seems $NaHCO_3$ also contributed, while hydration played a part probably.

2. It also has significant hysteresis issue. The hysteresis initially reaches the highest point, then keeps decreasing until P/P_o=60% (closes at this point). Then, it increases again, followed by a decrease up to P/P_o=20% (closes at this point). Then it increases again a little.

Overall Discussion

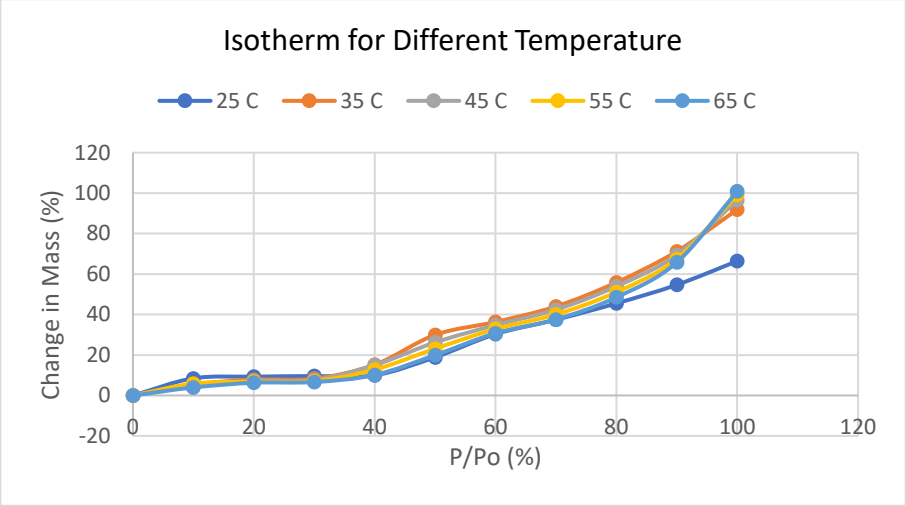

Figure-76: Adsorption Isotherm at Different Temperature (Synthesized 13-X Zeolite)

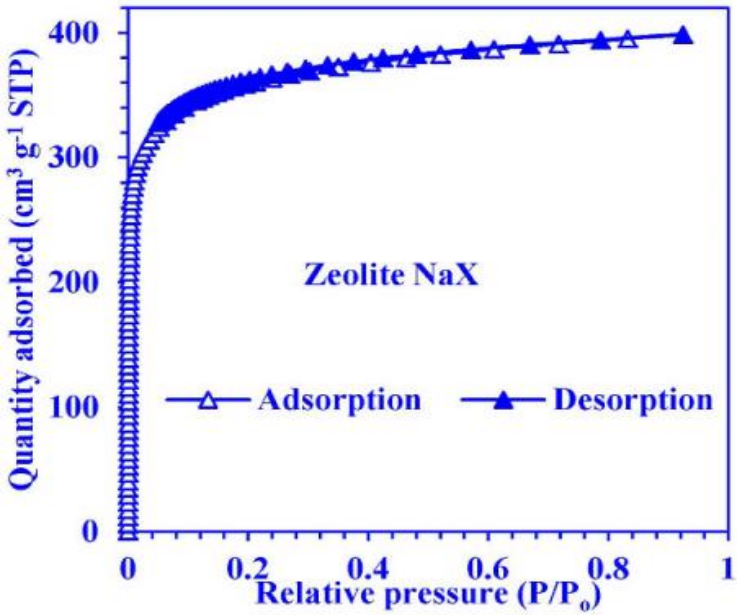

Figure-77: Adsorption Isotherm at 25 ºC Temperature (Commercial 13-X Zeolite) [83]

The above figure-76 shows that the isotherm at different temperature (for respective saturation pressure). It seems, the shape of the isotherms is similar, but it does not represent any particular trend regarding the amount of adsorption in case of isosteric change in pressure and temperature. As already mentioned, the shape looks like type VI, although the usual shape for commercial Na-X zeolite is Type I(figure-54) and the adsorption capacity is also very high at lower P/Po compared to the synthesized zeolite. For commercial zeolite and synthesized zeolite, the adsorption capacity at 25 ºC and P/Po=20% is 34% and 8.27% respectively. XRD and surface analysis suggest that there are presences of other non-porous crystalline phases and amorphous phases, which explain the reason for having a different type of isotherm and lower adsorption capacity. Also, we can say that only a little amount of raw material converted to zeolite.

If we look at the adsorption kinetics (figure-67), we can observe that the sample mass actually increased at P/P_o=0% (almost 4 %) at 25 ^oC. It almost remained constant with increasing temperature. But there was no vapor flow according to the method. It happened due to the fact that temperature was only applied in the sample carrier only and that affected the mass.

Potential Use in Adsorption Chiller: The performance of adsorption refrigeration system is determined by COP and SCP. These two parameters largely depend on how the adsorbent-adsorbate working pair performs, such as how quickly the adsorbent can adsorb and desorb the refrigerant and at what amount under the working condition (pressure and temperature) [1,53].

For this sample, the adsorption occurred for 60 minutes. But, if we look at adsorption kinetics for our sample in figure-67, 69 and 71, we can say that it actually took less than 25 minutes to reach equilibrium at lower P/P_o. In fact, for higher temperature, it was less than 20 minutes (figure-73 and -75). For silica gel it was around 25 minutes. It implies, for this sample adsorption refrigeration cycle time will be similar or less, compared to silica gel.

As I previously explained, based on these research works I am considering two different working conditions for this sample also.

First, for adsorption, if we consider 25 ^oC temperature and 30% of saturation pressure (for water at 25 ^oC), we can observe that silica gel (14.37 %) adsorbed much more water vapor than this sample (8.73%) at this temperature and pressure. For desorption, if we consider the temperature is 65 ^oC and pressure is 10% of the saturation pressure, the adsorption amount at this condition is 7% and 6.99% for our sample and silica gel respectively. So, at these conditions, the amount of water refrigerant available for vaporization at the evaporator in case of our sample and silica gel should be 1.73% and 7.38% respectively. So, our sample can definitely produce some cold energy, but it cannot replace silica gel as adsorbent for adsorption chiller. For such working condition, silica gel has the potential to produce almost 4.3 times more cold energy than our samples.

Second, for adsorption, if we consider 25 ^oC temperature and 20% of saturation pressure (for water at 25 ^oC), we can observe that silica gel (10.02 %) adsorbed much more water vapor than this sample (8.27%) at this temperature and pressure. For desorption, if we consider the temperature is 65 ^oC and pressure is 10% of the saturation pressure, the adsorption amount at this condition is 7% and 6.99%. So, at this condition, the amount of water refrigerant available for vaporization at the evaporator in case of our sample and silica gel should be 1.27% and 3.03% respectively. So, again, our sample can produce some cold energy, but it cannot replace silica gel as adsorbent for adsorption chiller. For such working condition, silica gel has the potential to produce almost 2.4 times more cold energy than our samples.

5.0. Conclusion

XRD analysis substantiated that the targeted compound such as Na-A zeolite and 13-X zeolite were produced successfully from the fly ash by the applied hydrothermal treatment. But the presence of other non-porous crystalline phases and amorphous phases is evident as well. In the respective samples, Na-A zeolite (12 h), Na-A zeolite (24h) and 13X zeolite constitute 66%, 47% and 60% of the total crystalline phase and the rest of the crystalline phases constitute 34%, 53% and 40% respectively. The impregnation of K_2CO_3 did not totally happen in the desired manner and ended up developing other phases. Also, the conversion percentage was low and for 13X zeolite, it is very low. But, comparing the adsorption isotherm of fly ash and synthesized materials, we can say that the applied treatments increased the water adsorption capacity of the materials.

Considering the usual operating condition in adsorption chiller, it has been found that our synthesized Na-A zeolite samples cannot produce any cold energy, whereas the synthesized 13-X zeolite has some potential to create some cold energy. But it cannot replace silica gel (which is used commercially) as adsorbent in adsorption chiller.

Different approaches can be taken to improve the adsorption and desorption performances of these synthesized materials so that they can be suitable for adsorption chiller. Also, they might be used other purposes such as water desiccant and CO_2 capture. But all these things will require further studies to check the feasibility.

Reference

1. Wang, R., Wang, L., & Wu, J. (April 2014). Adsorption Refrigeration Technology: Theory and Application. John Wiley & Sons, Singapore Pte. Ltd.
   DOI:10.1002/9781118197448
2. Cooling, IEA.
   https://www.iea.org/reports/cooling.
   Last Visited: 23.01.2021
3. The Future of Cooling, IEA.
   https://www.iea.org/reports/the-future-of-cooling.
   Last Visited: 23.01.2021
4. Explore energy data by category, indicator, country or region, IEA.
   https://www.iea.org/data-and-statistics?country=WORLD&fuel=Electricity%20and%20heat&indicator=ElecGenByFuel Last Visited: 23.01.2021
5. WU, J,W. (2012). A study of silica gel adsorption desalination system. Thesis Report, School of Mechanical Engineering, Univetsity of Adelaide, Australia.
   https://digital.library.adelaide.edu.au/dspace/bitstream/2440/82463/8/02whole.pdf.
   Last Visited: 23.01.2021
6. Desalination and energy consumption, Energy Central.
   https://energycentral.com/c/ec/desalination-and-energy-consumption#:~:text=The%20amount%20of%20energy%20consumed,to%20one%20jumbo%20jet's%20power.&text=Billions%20of%20gallons%20of%20water,kwh)%20per%20every%20thousand%20gallons.
   Last Visited: 23.01.2021
7. Desalinated water affects the energy equation in the Middle East, IEA.
   https://www.iea.org/commentaries/desalinated-water-affects-the-energy-equation-in-the-middle-east.
   Last Visited: 23.01.2021
8. Jia, X., Klemeš, J. J., Varbanov, P. S., & Alwi, S. R. W. (January 2019). Analyzing the Energy Consumption, GHG Emission, and Cost of Seawater Desalination in China. Energies, 12(463).
   https://doi.org/10.3390/en12030463.
9. Wolak, E., & Kraszewski, S. (October 2016). An overview of adsorptive processes in refrigeration systems. 1st International Conference on the Sustainable Energy and Environment Development (SEED), 10, Article 00104.
   https://doi.org/10.1051/e3sconf/20161000104.
10. Webb, P. A. (January 2003). Introduction to Chemical Adsorption Analytical Techniques and their Applications to Catalysis. MIC Technical Publications.
    https://www.micromeritics.com/Repository/Files/intro_to_chemical_adsorption.pdf
    Last Visited: 23.01.2021
11. Britannica, T. Editors of Encyclopaedia (2013, August 6). Adsorption. Encyclopedia Britannica..

https://www.britannica.com/science/adsorption.
Last Visited: 23.01.2021

12. Physical Adsorption vs. Chemisorption.
http://www.separationprocesses.com/Adsorption/AD_Chp01b.htm
Last Visited: 23.01.2021
13. Application of adsorption, eMedicalPrep.
https://www.emedicalprep.com/study-material/chemistry/surface-chemistry/application-of-adsorption/#:~:text=(2)%20In%20Gas%20masks%20%3A,moisture%20present%20in%20the%20air.
Last Visited: 23.01.2021
14. Figueiredo, J. L., Pereira, M. F. R., Freitas M. M. A. & Orfao, J. J. M. (1999). Modification of the surface chemistry of activated carbons. Carbon (Elsevier), 37(9), 1379–1389.
https://doi.org/10.1016/S0008-6223(98)00333-9.
15. Introducing arenes (aromatic hydrocarbons), Chemguide.
https://www.chemguide.co.uk/organicprops/arenes/background.html.
Last Visited: 23.01.2021
16. Jeirani, Z., Niu, C. H., & Soltan, J. (December 2016). Adsorption of emerging pollutants on activated carbon. Reviews in Chemical Engineering, 33(5).
DOI: https://doi.org/10.1515/revce-2016-0027.
17. Lee, T., Ooi, C. H., Othman, R., & Yeoh, F. Y. (April 2014). Activated carbon fiber - The hybrid of carbon fiber and activated carbon. Reviews on Advanced Materials Science, 36(2), 118-136.
18. Hamza, T. A., Sherif, A. H., & Abdalla, E. A. (June 2017). A novel approach to reinforce provisional material using silica gel powder. Stomatological Disease and Science, 1, 3-7.
https://doi.org/10.20517/2573-0002.2016.12.
19. Spherical silica and irregular silica: what differences, Interchim.
https://blog.interchim.com/spherical-irregular-silica-differences/.
Last Visited: 23.01.2021
20. Christy, A. A. (July 2014). The Nature of Silanol Groups on the Surfaces of Silica, Modified Silica and Some Silica Based Materials. Advanced Materials Research, 998-999, 3-10.
https://doi.org/10.4028/www.scientific.net/AMR.998-999.3
21. Zeolite Structure, Lenntech.
https://www.lenntech.pl/zeolites-structure-types.htm#:~:text=Zeolites%20are%20three%2Ddimensional%2C%20microporous,other%20through%20shared%20oxygen%20atoms.
Last Visited: 23.01.2021
22. Moshoeshoe, M., Tabbiruka, M. S. N., & Obuseng, V. (2017). A Review of the Chemistry, Structure, Properties and Applications of Zeolites. American Journal of Materials Science, 7(5), 196-221.
doi:10.5923/j.materials.20170705.12.
23. Julbe A., Drobek M. (2016) Zeolite A Type. In: Drioli E., Giorno L. (eds) Encyclopedia of Membranes. Springer, Berlin, Heidelberg.

https://doi.org/10.1007/978-3-662-44324-8_604

24. Ríos, C. A., Williams, C. D., & Castellanos, O. M. (November 2012). Crystallization of low silica Na-A and Na-X zeolites from transformation of kaolin and obsidian by alkaline fusion. Ingeniería y Competitividad, 14, No. 1, 9 – 22.
25. Fruijtier-Pölloth, C. (March 2009). The safety of synthetic zeolites used in detergents. Arch Toxicol, 83, 23–35. https://doi.org/10.1007/s00204-008-0327-5.
26. Julbe A., Drobek M. (2014) Zeolite X: Type. In: Drioli E., Giorno L. (eds) Encyclopedia of Membranes. Springer, Berlin, Heidelberg. https://doi.org/10.1007/978-3-642-40872-4_607-1.
27. Georgiev, D., Bogdanov, B., Markovska, I., & Hristov, Y. (2013). A Study on the Synthesis and Structure of Zeolite NaX. Journal of Chemical Technology and Metallurgy, 48 (2), 168-173.
28. Hu, T., Gao, W., Liu, X., Zhang, y., & Meng, C. (October 2017). Synthesis of zeolites Na-A and Na-X from tablet compressed and calcinated coal fly ash. Royal Society Open Science, 4(10), 170921. https://doi.org/10.1098/rsos.170921.
29. Tu, W., Zhang, Y., Bai, J., & Liu, W. (October 2014). Synthesis of zeolite 13X from coal fly ashes and properties of the zeolite products. Applied Mechanics and Materials, 675-677, 724-727. https://doi.org/10.4028/www.scientific.net/AMM.675-677.724.
30. What is a MOF (metal organic framework)? https://www.nanowerk.com/mof-metal-organic-framework.php. Last Visited: 23.01.2021
31. Tan, K., Nijem, N., Gao, Y., Zuluaga, S., Li, J., Thonhauser, T., & Chabal, Y. J. (October 2014). Water interactions in metal organic frameworks. CrystEngComm, 17, 247-260. https://doi.org/10.1039/C4CE01406E.
32. Mourabet, M., Boujaady, H.E., Rhilassi, A. E., Ramdane, H., Bennani-Ziatni, M., Hamri, R. E., & Taitai, A. (September 2011). Defluoridation of water using Brushite: Equilibrium, kinetic and thermodynamic studies. Desalination, 278 (1-3), 1-9. https://doi.org/10.1016/j.desal.2011.05.068.
33. Bénard, P., & Chahine, R. (2008). Solid-State Hydrogen Storage, Carbon nanostructures for hydrogen storage, 261-287. Woodhead Publishing Series in Electronic and Optical Materials. https://doi.org/10.1533/9781845694944.3.261.
34. Swenson, H., & Stadie, N. P. (March 2019). Langmuir's Theory of Adsorption: A Centennial Review. Langmuir, 35 (16), 5409–5426. https://doi.org/10.1021/acs.langmuir.9b00154
35. Singh, A.K. (2016). Engineered Nanoparticles, Nanoparticle Ecotoxicology, 343-450. Academic Press. https://doi.org/10.1016/B978-0-12-801406-6.00008-X.
36. Adsorption at the solid/gas interface. http://www.zzm.umcs.lublin.pl/Wyklad/FGF-Ang/4A.F.G.F.Ads.S-G.%20Interface.pdf Last Visited: 23.01.2021

37. Sing, K. S. W., & Williams, R. T. (December 2004). Physisorption Hysteresis Loops and the Characterization of Nanoporous Materials. Adsorption Science & Technology, 22(10), 773–782. https://doi.org/10.1260/0263617053499032

38. BET Surface Area Analysis of Nanoparticles, Chemistry (LibreTexts). https://chem.libretexts.org/Bookshelves/Analytical_Chemistry/Book%3A_Physical_Methods_in_Chemistry_and_Nano_Science_(Barron)/02%3A_Physical_and_Thermal_Analysis/2.03%3A_BET_Surface_Area_Analysis_of_Nanoparticles
Last Visited: 23.01.2021

39. Ambroz, F., Macdonald, T. J., Martis, V., & Parkin, I. P. (August 2018). Evaluation of the BET Theory for the Characterization of Meso and Microporous MOFs. Small Methods, 2 (11). https://doi.org/10.1002/smtd.201800173.

40. Bashir, H., & Orouji, S. (2015). A new isotherm for multilayer gas adsorption on heterogeneous solid surfaces. Theoretical Chemistry Accounts 134, Article number 1594. https://doi.org/10.1007/s00214-014-1594-2.

41. Hysteresis, Sciencedirect. https://www.sciencedirect.com/topics/chemical-engineering/hysteresis
Last Visited: 23.01.2021

42. Yahia, M. B., Torkia, Y. B., Knani, S., Hachicha, M. A., Khalfaoui, M., & Lamine, A. B. (April 2013). Models for Type VI Adsorption Isotherms from a Statistical Mechanical Formulation. Adsorption Science & Technology, 31 (4), 341–357. https://doi.org/10.1260%2F0263-6174.31.4.341

43. Sotomayor, F. J., Cychosz, K. A., & Thommes, M, (2018). Characterization of Micro/Mesoporous Materials by Physisorption: Concepts and Case Studies. Accounts of Materials & Surface Research.

44. Burtch, N. C., Jasuja, H., & Walton, K.S., (September 2014). Water Stability and Adsorption in Metal–Organic Frameworks. Chem. Rev., 114, 20, 10575–10612. https://doi.org/10.1021/cr5002589.

45. Capillary Condensation, Sciencedirect. https://www.sciencedirect.com/topics/chemistry/capillary-condensation
Last Visited: 23.01.2021

46. Yurdakal, S., Garlisi,C., Özcan, L., Bellardita, m., & Palmisano, G. (2019). Heterogeneous Photocatalysis, (Photo)catalyst Characterization Techniques: Adsorption Isotherms and BET, SEM, FTIR, UV–Vis, Photoluminescence, and Electrochemical Characterizations. Elsevier. https://doi.org/10.1016/B978-0-444-64015-4.00004-3.

47. Capillary condensation and hysteresis in gas phase adsorption, Separation Processes Laboratory, ETH Zurich. https://spl.ethz.ch/research/fundamentals/hysteresis.html#:~:text=In%20materials%20containing%20a%20portion,is%20illustrated%20in%20Figure%201.
Last Visited: 23.01.2021

48. Xu, L., Zhang, J., Ding, J., Liu, T., Shi, G., Li, X., Dang, W., Cheng, Y., & Guo, R. (January 2020). Pore Structure and Fractal Characteristics of Different Shale Lithofacies in the Dalong Formation in the Western Area of the Lower Yangtze Platform. Minerals, 10 (1), 72. https://www.mdpi.com/2075-163X/10/1/72#.

49. Thommes, M., Kaneko, K., Neimark, A., Olivier, J.P., Rodriguez-Reinoso, F., Rouquerol, J., & Sing, K. (2015). Physisorption of gases, with special reference to the evaluation of surface area and pore size distribution (IUPAC Technical Report). Pure Appl. Chem. 2015; 87(9-10): 1051–1069. https://doi.org/10.1515/pac-2014-1117.

50. Elsheniti, M. B., Elsamni, O. A., Al-dadah, R. K., Mahmoud, S., Elsayed, E., & Saleh, K. (2018). Adsorption Refrigeration Technologies. IntechOpen, Sustainable Air Conditioning Systems, Edition: 1, Chapter: 4, 71-95. DOI: 10.5772/intechopen.73167.

51. Jones, E., Qadir, M., Vliet, M. T. H. V., Smakhtin, V., & Kang, S. (March 2019). The state of desalination and brine production: A global outlook. Science of The Total Environment, 657, 1343-1356. https://doi.org/10.1016/j.scitotenv.2018.12.076.

52. As Water Scarcity Increases, Desalination Plants Are on the Rise, YaleEnvironment360. https://e360.yale.edu/features/as-water-scarcity-increases-desalination-plants-are-on-the-rise#:~:text=In%20its%20first%20phase%2C%20it,to%20%242%2C000%20per%20acre%2Dfoot. Last Visited: 23/04/2021

53. Astinaa, I. M., Zidni, M. I., Hasugian, H. R., & Darmanto, P. S. (2018) "Experiment of adsorption refrigeration system with working pairs of difluoromethane and activated carbon modified by sulfuric and nitric acids", AIP Conference Proceedings, 1984 (1). https://doi.org/10.1063/1.5046599.

54. Wang, X., & Chua, H.T. (December 2007). Two bed silica gel–water adsorption chillers: An effectual lumped parameter model. International Journal of Refrigeration, 30 (8), 1417–1426. https://doi.org/10.1016/j.ijrefrig.2007.03.010.

55. Chang,W.S., Wang, C.C., & Shieh, C.C. (July 2015). Design and performance of a solar-powered heating and cooling system using silica gel-water adsorption chiller. Applied Thermal Engineering, 29(10), 2100–2105. https://doi.org/10.1016/j.applthermaleng.2008.10.021.

56. Deshmukh, H., Maiya, M.P., & Murthy, S.S. (May 2015). Continuous vapour adsorption cooling system with three adsorber beds. Applied Thermal Engineering, 82, 380–389. https://doi.org/10.1016/j.applthermaleng.2015.01.013.

57. Wang, D. C., Xia Z. Z., & Wu, J. Y. (March 2006). Design and performance prediction of a novel zeolite–water adsorption air conditioner. Energy Conversion and Management, 47 (5), 590–610. https://doi.org/10.1016/j.enconman.2005.05.011.

58. Sitorus, T.B., Napitupulu, F.H., & Ambarita, H. (2017). A Study on Adsorption Refrigerator Driven by Solar Collector Using Indonesian Activated Carbon. Journal of Engineering and Technological Sciences, 49, No. 5.

https://doi.org/10.5614/j.eng.technol.sci.2017.49.5.7.

59. Tu, W., Zhang, Y., Bai, J., & Liu, W. (October 2014). Synthesis of Zeolite 13X from Coal Fly Ashes and Properties of the Zeolite Products. Applied Mechanics and Materials, 675-677, 724–727. https://doi.org/10.4028/www.scientific.net/amm.675-677.724

60. Panitchakarn, P., Laosiripojana, N., Umpikul, N. V., & Pavasant, P. (2014). Synthesis of high-purity Na-A and Na-X zeolite from coal fly ash. Journal of the Air & Waste Management Association, 64 (5), 586-596. https://doi.org/10.1080/10962247.2013.859184.

61. Ambarita, H., & Kawai, H. (March 2016). Experimental study on solar-powered adsorption refrigeration cycle with activated alumina and activated carbon as adsorbent. Case Studies in Thermal Engineering, 7, 36–46. https://doi.org/10.1016/j.csite.2016.01.006.

62. Wang, X., He, Z., & Chua, H. T. (April 2015). Performance simulation of multi-bed silica gel-water adsorption chillers. Elsevier, International Journal of Refrigeration, 52, 32-41. https://doi.org/10.1016/j.ijrefrig.2014.12.016.

63. Amber, I., & Atta, A. (October 2011). Design, Construction and Testing of a Solar Adsorption Refrigerator Using Synthesised Zeolite A and Water as Adsorbent/Adsorbate Pair. Advanced Materials Research, 367, 495-500· https://doi.org/10.4028/www.scientific.net/AMR.367.495.

64. Sayfikar, M., & Behbahani-nia, A. (March 2013). Study of the performance of a solar adsorption cooling system. Energy Equipment and Systems, 1 (1), 75-90. https://dx.doi.org/10.22059/ees.2013.2741.

65. Brites, G., Costa, J., & Costa, V.. Sustainable Refrigeration Based on The Solar Adsorption Cycle. https://inovenergy.inovcluster.pt/media/29412/SUSTAINABLE_REFRIGERATION_BASED_ON_THE_SOLAR_ADSORPTION_CYCLE.pdf Last Visited: 14/04/2021.

66. Omisanya, N. O., Folayan, C. O., Aku, S. Y., & Adefila, S. S. (2012). Performance of a zeolite – water adsorption refrigerator. Advances in Applied Science Research, 3 (6), 3737-3745.

67. Sztekler, K., Kalawa, W., Nowak, W., Mika, L., Gradziel, S., Krzywanski, J., & Radomska, E. (November 2020). Experimental Study of Three-Bed Adsorption Chiller with Desalination Function. Energies, 13 (21), 5827. https://doi.org/10.3390/en13215827.

68. Wang, D.C., Xia Z.Z. , & Wu, J.Y. (March 2006). Design and performance prediction of a novel zeolite–water adsorption air conditioner. Energy Conversion and Management, 47 (5), 590–610. https://doi.org/10.1016/j.enconman.2005.05.011.

69. Uyun, A. S., Akisawa, A., Miyazaki, T., Ueda, Y., & Kashiwagi, T. (October 2009). Numerical analysis of an advanced three-bed mass recovery adsorption refrigeration cycle. Elsevier, Applied Thermal Engineering, 29, (14–15), 2876-2884. https://doi.org/10.1016/j.applthermaleng.2009.02.008

70. Saha, B. B., Koyama, S., Lee, J. B., Kuwahara, K., Alam, K. C. A., Hamamoto, Y., Akiswa, A., & Kashiwagi, T. (August 2003). Performance evaluation of a low-temperature waste heat driven multi-bed adsorption chiller. Elsevier, International Journal of Multi phase Flow, 29(8), 1249–1263.

https://doi.org/10.1016/S0301-9322(03)00103-4

71. Sharafian, A., Mehr, S. M. N., Huttema, W., & Bahrami, M. (April 2016). Effects of different adsorber bed designs on in-situ water uptake rate measurements of AQSOA FAM-Z02 for vehicle air conditioning applications. Elsevier, Applied Thermal Engineering, 98, 568-574.

https://doi.org/10.1016/j.applthermaleng.2015.12.060

72. Khanam, M., Jribi, S., Miyazaki, T., Saha B. B., & Koyama, S. (June 2018). Energy Analysis and Performance Evaluation of the Adsorption Refrigeration System. Energies, 11 (6), 1499. https://doi.org/10.3390/en11061499

73. Sitorus, T. B., Napitupulu, F. H., & Ambarita, H. (2017). A Study on Adsorption Refrigerator Driven by Solar Collector Using Indonesian Activated Carbon. J. Eng. Technol. Sci., 49 (5), 657-670.

74. Sharafian, A., Dan, P. C., Huttema, W., & Bahrami, M. (May 2016). Performance analysis of a novel expansion valve and control valves designed for a waste heat-driven two-adsorber bed adsorption cooling system. Elsevier, Applied Thermal Engineering, 100, 1119-1129.

https://doi.org/10.1016/j.applthermaleng.2016.02.118

75. Myat, A., Choon, N. K., Thu, K., & Kim, Y. D. (February 2013). Experimental investigation on the optimal performance of Zeolite–water adsorption chiller. Elsevier, Applied Energy, 102, 582-590.

https://doi.org/10.1016/j.apenergy.2012.08.005

76. Tchernev, D. (March 1999). A waste driven automotive air conditioning system. ISHPC 99, Munich, 65-70.

77. Schawe, D. (2001). Theoretical and experimental investigations of an adsorption heat pump with heat transfer between two adsorbers. Thesis, Process and Biotechnology, Faculty of Energy, University of Stuttgart.
http://dx.doi.org/10.18419/opus-1518

78. Trindade M. V. (July 2015). Modelling and optimization of an adsorption cooling system for automotive applications. PhD Dissertation, Doctoral Program of Energy Technology, Universidad Politécnica De Valencia.

79. DVS Vacuum-Surface Measurement System (Device brochure)
https://www.surfacemeasurementsystems.com/wpcontent/uploads/2017/08/DVS_Vacuum.pdf
Last Visited: 14/04/2021

80. Xray Powder Pattern Generated for Na-X, Hydrated, Database of Zeolite Structures.
https://europe.iza-structure.org/IZA-SC/pow_pat.php?STC=FAU&ID=FAU_2.
Last Visited: 17/04/2021.

81. Xray Powder Pattern Generated for Na-A, Hydrated, Database of Zeolite Structures. https://europe.iza-structure.org/IZA-SC/pow_pat.php?STC=LTA&ID=LTA_0. Last Visited: 17/04/2021.

82. Rahmati, M., & Modarress, H. (July 2012). The effects of structural parameters of zeolite on the adsorption of hydrogen: a molecular simulation study. Molecular Simulation, 38, (13). http://dx.doi.org/10.1080/08927022.2012.685941

83. Sharma, P., Song, J. S., Han, M., & Cho, C. H. (March 2016). GIS-NaP1 zeolite microspheres as potential water adsorption material: Influence of initial silica concentration on adsorptive and physical/topological properties. Scientific Reports, Volume 6, Issue 1. https://doi.org/10.1038/srep22734.

84. Waszkiewicz, S., Saidani-Scott, H., & Tierney, M.. Analysis of Adsorption Refrigeration System Using Zeolite and Methanol. Department of Mechanical Engineering, University of Bristol, UK. http://hpc.01.free.fr/papers/vol2/hpc01_91.pdf. Last Visited: 1/05/2021

85. Valdés, M. G., Pérez-Cordoves, A.I., & Díaz-García, M.E. (January 2006). Zeolites and zeolite – based materials in analytical chemistry. Trends in Analytical Chemistry, 25(1), 24 – 30. https://doi.org/10.1016/j.trac.2005.04.016.

86. Nakano, T., Mizukane, T., & Nozue, Y. (2010). Insulating state of Na clusters and their metallic transition in low-silica X zeolite. Journal of Physics and Chemistry of Solids, 71 (4), 650– 653. https://doi.org/10.1016/j.jpcs.2009.12.059.

87. Duan, T.C., Nakano, T., & Nozue, Y. (2007). Evidence for ferromagnetism in rubidium clusters incorporated into zeolite A. Journal of Magnetism and Magnetic Materials 310 (2), 1013–1015. https://doi.org/10.1016/j.jmmm.2006.10.219.

Appendix:

1. Tables:

Table 4: Isotherm Data for Silica Gel (25 °C)

% P/Po	Sorption	Desorption	Hysteresis
0.0	0.00		
10.0	5.28	7.02	1.74
20.0	10.02	13.37	3.35
30.0	14.37	23.27	8.90
40.0	18.96	28.86	9.90
50.0	23.09	30.63	7.53
60.0	27.48	31.88	4.41
70.0	31.38	32.87	1.49
80.0	33.32	33.67	0.35
90.0	34.18	34.24	0.06
100.0	33.25	34.25	

Table 5: Isotherm Data for Silica Gel (35 °C)

% P/Po	Sorption	Desorption	Hysteresis
0,0	0,00		
10,0	5,19	5,47	0,29
20,0	8,51	9,00	0,48
30,0	11,68	13,76	2,08
40,0	16,59	23,95	7,36
50,0	20,35	28,61	8,25
60,0	23,93	30,31	6,38
70,0	27,42	31,41	3,99
80,0	30,48	32,28	1,80
90,0	32,56	32,97	0,42
100,0	33,53	33,53	

Table 6: Isotherm Data for Silica Gel (45 °C)

% P/Po	Sorption	Desorption	Hysteresis
0.0	0.00		
10.0	5.96	6.35	0.39
20.0	11.82	13.22	1.40
30.0	16.14	21.60	5.47
40.0	20.69	28.73	8.04
50.0	25.28	30.76	5.48
60.0	29.53	32.02	2.49
70.0	32.46	32.98	0.52
80.0	33.57	33.73	0.16
90.0	34.08	34.23	0.15
100.0	33.78	33.78	

Table 7: Isotherm Data for Silica Gel (55 °C)

% P/Po	Sorption	Desorption	Hysteresis
0.0	0.00		
10.0	6.98	7.35	0.38
20.0	11.05	11.62	0.56
30.0	15.16	17.73	2.57
40.0	19.59	26.70	7.10
50.0	24.18	29.93	5.74
60.0	28.55	31.37	2.82
70.0	31.75	32.44	0.69
80.0	33.03	33.22	0.19
90.0	33.74	33.76	0.02
100.0	33.82	33.82	

Table 8: Isotherm Data for Silica Gel (65 °C)

% P/Po	Sorption	Desorption	Hysteresis
0,0	0,00		
10,0	6,47	6,99	0,52
20,0	10,72	11,01	0,30
30,0	14,77	16,32	1,55
40,0	19,15	25,09	5,94
50,0	23,73	29,50	5,77
60,0	28,12	31,05	2,93
70,0	31,44	32,18	0,74
80,0	32,80	32,98	0,18
90,0	33,53	33,54	0,01
100,0	33,69	33,69	

Table 9: Isotherm Data for Fly Ash (25 °C)

% P/Po	Sorption	Desorption	Hysteresis
0.0	-0.0002		
10.0	0.2166	0.2546	0.0380
20.0	0.1342	0.1609	0.0268
30.0	0.1012	0.1286	0.0274
40.0	0.0766	0.1160	0.0394
50.0	0.0626	0.1061	0.0436
60.0	0.0479	0.0807	0.0327
70.0	0.0193	0.0517	0.0324
80.0	-0.0285	0.0215	0.0499
90.0	-0.0486	-0.0261	0.0224
100.0	-0.0582	-0.0582	

Table 10: Isotherm Data for Fly Ash (65 °C)

% P/Po	Sorption	Desorption	Hysteresis
0.0	0.0000		
10.0	0.0827	0.1445	0.0618
20.0	0.0656	0.1266	0.0610
30.0	0.0625	0.1175	0.0551
40.0	0.0740	0.1069	0.0329
50.0	0.0586	0.1171	0.0586
60.0	0.0418	0.0898	0.0480
70.0	0.0146	0.0615	0.0469
80.0	-0.0039	0.0233	0.0272
90.0	-0.0292	-0.0320	-0.0028
100.0	-0.0929	-0.0929	

Table 11: Isotherm Data for Synthesized Na-A Zeolite (12 h) (25 °C)

% P/Po	Sorption	Desorption	Hysteresis
0.0	-0.01		
10.0	0.49	1.99	1.50
20.0	1.16	2.51	1.35
30.0	1.66	2.96	1.29
40.0	2.11	3.41	1.30
50.0	2.48	3.79	1.31
60.0	3.11	5.18	2.07
70.0	4.67	6.12	1.45
80.0	6.50	7.48	0.98
90.0	8.96	10.00	1.03
100.0	12.09	12.09	

Table 12: Isotherm Data for Synthesized Na-A Zeolite (12 h) (35 °C)

% P/Po	Sorption	Desorption	Hysteresis
0.0	-0.01		
10.0	1.48	3.05	1.58
20.0	2.28	3.73	1.45
30.0	2.99	4.35	1.36
40.0	3.48	4.79	1.32
50.0	4.01	5.43	1.42
60.0	4.84	7.16	2.32
70.0	7.14	8.40	1.27
80.0	9.29	10.52	1.23
90.0	13.09	15.62	2.54
100.0	16.70	16.70	

Table 13: Isotherm Data for Synthesized Na-A Zeolite (12 h) (45 °C)

% P/Po	Sorption	Desorption	Hysteresis
0.0	-0.01		
10.0	1.94	3.62	1.69
20.0	2.96	4.57	1.61
30.0	3.53	5.06	1.53
40.0	4.02	5.50	1.48
50.0	4.54	5.98	1.44
60.0	5.20	7.26	2.06
70.0	7.01	8.98	1.97
80.0	9.85	11.07	1.22
90.0	13.96	16.69	2.73
100.0	20.65	20.65	

Table 14: Isotherm Data for Synthesized Na-A Zeolite (12 h) (55 °C)

% P/Po	Sorption	Desorption	Hysteresis
0.0	-0.01		
10.0	6.83	8.58	1.76
20.0	7.71	9.36	1.66
30.0	8.37	9.93	1.56
40.0	8.91	10.42	1.50
50.0	9.46	10.91	1.44
60.0	10.06	11.64	1.58
70.0	11.36	14.27	2.91
80.0	15.30	16.64	1.34
90.0	19.93	23.29	3.36
100.0	29.45	29.45	

Table 15: Isotherm Data for Synthesized Na-A Zeolite (12 h) (65 °C)

% P/Po	Sorption	Desorption	Hysteresis
0.0	0.00		
10.0	8.71	9.68	0.97
20.0	9.63	10.59	0.96
30.0	10.25	11.21	0.96
40.0	10.74	11.73	1.00
50.0	11.17	12.22	1.04
60.0	11.59	12.80	1.20
70.0	12.10	14.53	2.43
80.0	16.90	18.00	1.10
90.0	22.02	24.19	2.16
100.0	33.07	33.07	

Table 16: Isotherm Data for Synthesized Na-A Zeolite (24 h) (25 °C)

% P/Po	Sorption	Desorption	Hysteresis
0.0	0.00		
10.0	3.28	6.58	3.30
20.0	3.90	7.29	3.39
30.0	4.35	7.80	3.44
40.0	4.79	8.31	3.52
50.0	5.17	8.85	3.69
60.0	5.89	12.77	6.88
70.0	10.80	16.98	6.18
80.0	18.46	22.86	4.40
90.0	25.67	32.11	6.44
100.0	34.57	34.57	

Table 17: Isotherm Data for Synthesized Na-A Zeolite (24 h) (35 °C)

% P/Po	Sorption	Desorption	Hysteresis
0.0	0.00		
10.0	4.97	8.92	3.96
20.0	5.63	9.82	4.18
30.0	6.18	10.43	4.25
40.0	6.65	10.92	4.27
50.0	7.17	11.48	4.31
60.0	7.95	12.98	5.03
70.0	13.96	21.04	7.08
80.0	24.08	28.91	4.84
90.0	33.27	41.46	8.20
100.0	42.81	42.81	

Table 18: Isotherm Data for Synthesized Na-A Zeolite (24 h) (45 °C)

% P/Po	Sorption	Desorption	Hysteresis
0.0	0.00		
10.0	6.16	10.04	3.88
20.0	7.05	11.17	4.12
30.0	7.62	11.81	4.19
40.0	8.14	12.32	4.18
50.0	8.72	12.83	4.11
60.0	9.49	13.55	4.06
70.0	12.47	22.83	10.35
80.0	25.73	32.08	6.34
90.0	35.58	46.83	11.25
100.0	50.02	50.02	

Table 19: Isotherm Data for Synthesized Na-A Zeolite (24 h) (55 °C)

% P/Po	Sorption	Desorption	Hysteresis
0.0	0.00		
10.0	6.37	10.36	3.99
20.0	7.18	11.24	4.06
30.0	7.84	11.86	4.03
40.0	8.45	12.40	3.95
50.0	9.11	12.93	3.81
60.0	9.96	13.62	3.66
70.0	11.86	22.00	10.14
80.0	25.46	32.65	7.19
90.0	37.39	49.64	12.25
100.0	54.51	54.51	

Table 20: Isotherm Data for Synthesized Na-A Zeolite (24 h) (65 °C)

% P/Po	Sorption	Desorption	Hysteresis
0.0	0.00		
10.0	9.66	11.03	1.37
20.0	10.47	12.01	1.54
30.0	10.98	12.60	1.62
40.0	11.40	13.08	1.68
50.0	11.78	13.54	1.76
60.0	12.19	14.14	1.95
70.0	12.83	15.45	2.62
80.0	20.04	32.53	12.49
90.0	35.77	52.17	16.41
100.0	59.33	59.33	

Table 21: Isotherm Data for Synthesized 13-X Zeolite (25 °C)

% P/Po	Sorption	Desorption	Hysteresis
0.0	0.00		
10.0	6.08	9.55	3.47
20.0	8.27	9.73	1.45
30.0	8.73	9.90	1.18
40.0	9.51	27.52	18.01
50.0	25.84	30.78	4.94
60.0	34.59	35.37	0.78
70.0	40.85	42.31	1.46
80.0	49.78	57.39	7.61
90.0	62.56	75.40	12.84
100.0	77.64	77.64	

Table 22: Isotherm Data for Synthesized 13-X Zeolite (35 °C)

P/Po %	Sorption	Desorption	Hysteresis
0.0	0.00		
10.0	5.39	8.75	3.36
20.0	7.83	8.97	1.14
30.0	8.32	11.37	3.05
40.0	15.18	27.24	12.06
50.0	29.93	31.99	2.06
60.0	36.34	37.52	1.17
70.0	43.99	49.30	5.31
80.0	55.87	75.02	19.14
90.0	71.21	93.71	22.50
100.0	91.88	91.88	

Table 23: Isotherm Data for Synthesized 13-X Zeolite (45 °C)

% P/Po	Sorption	Desorption	Hysteresis
0.0	0.00		
10.0	4.41	8.08	3.67
20.0	7.27	8.40	1.13
30.0	7.67	14.68	7.01
40.0	15.00	25.93	10.93
50.0	26.23	30.59	4.37
60.0	34.77	36.12	1.35
70.0	42.39	48.54	6.15
80.0	53.95	75.59	21.64
90.0	69.42	96.16	26.75
100.0	96.53	96.53	

Table 24: Isotherm Data for Synthesized 13-X Zeolite (55 ºC)

% P/Po	Sorption	Desorption	Hysteresis
0.0	0.00		
10.0	5.86	7.73	1.88
20.0	6.76	7.97	1.21
30.0	7.14	13.33	6.18
40.0	12.77	24.02	11.26
50.0	23.10	28.73	5.63
60.0	32.85	34.03	1.17
70.0	40.02	44.18	4.16
80.0	51.10	69.51	18.41
90.0	67.47	94.78	27.31
100.0	99.26	99.26	

Table 25: Isotherm Data for Synthesized 13-X Zeolite (65 ºC)

% P/Po	Sorption	Desorption	Hysteresis
0.0	0.0		
10.0	3.9	7.0	3.0
20.0	6.3	7.2	0.9
30.0	6.6	11.8	5.2
40.0	10.1	18.5	8.4
50.0	19.9	26.7	6.8
60.0	30.7	32.0	1.2
70.0	37.6	40.1	2.5
80.0	48.5	62.4	13.9
90.0	65.8	92.1	26.4
100.0	100.9	100.9	

2. Figures:

(A) Temp: 25ºC (Higher Activation Temperature (250 ºC), Longer Activation and Adsorption Duration)

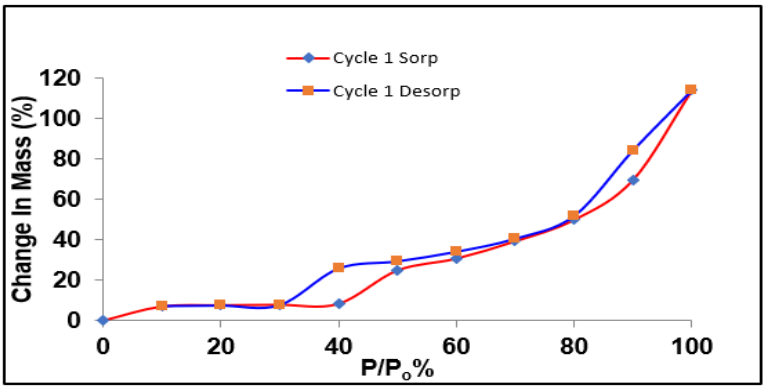

Figure-78: Adsorption Isotherm for Synthesized 13-X Zeolite (25 °C)

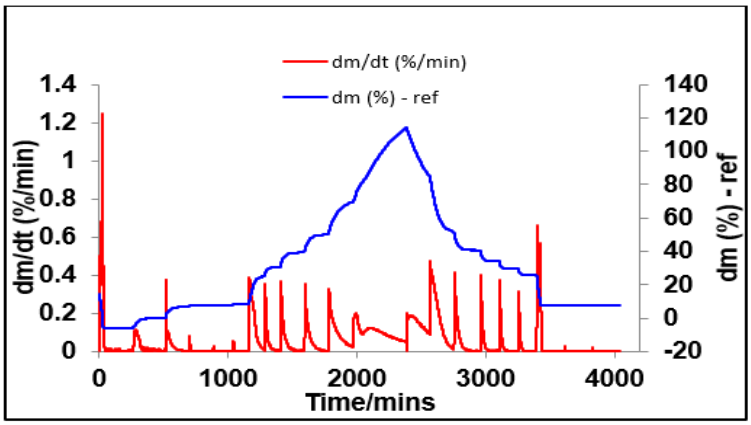

Figure-79: Adsorption Kinetics for Synthesized 13-X Zeolite (25 °C)